NOAA Technical Report NESDIS 131

The GOES-14 Science Test:
Imager and Sounder Radiance and Product Validations

Washington, D.C.
August 2010

U.S. DEPARTMENT OF COMMERCE
National Oceanic and Atmospheric Administration
National Environmental Satellite, Data, and Information Service

NOAA TECHNICAL REPORTS

National Environmental Satellite, Data, and Information Service

The National Environmental Satellite, Data, and Information Service (NESDIS) manages the Nation's civil Earth-observing satellite systems, as well as global national data bases for meteorology, oceanography, geophysics, and solar-terrestrial sciences. From these sources, it develops and disseminates environmental data and information products critical to the protection of life and property, national defense, the national economy, energy development and distribution, global food supplies, and the development of natural resources.

Publication in the NOAA Technical Report series does not preclude later publication in scientific journals in expanded or modified form. The NESDIS series of NOAA Technical Reports is a continuation of the former NESS and EDIS series of NOAA Technical Reports and the NESC and EDS series of Environmental Science Services Administration (ESSA) Technical Reports.

An electronic copy of this report may be obtained at http://www.star.nesdis.noaa.gov/star/corp_pubs.php

A limited number of copies of earlier reports are available by contacting Susan Devine, NOAA/NESDIS, E/RA, 5200 Auth Road, Room 701, Camp Springs, Maryland 20746, (301) 763-8127 x136. Copies can also be ordered from the National Technical Information Service (NTIS), U.S. Department of Commerce, Sills Bldg., 5285 Port Royal Road, Springfield, VA 22161, (703) 487-4650 (prices on request for paper copies or microfiche, please refer to PB number when ordering). A partial listing of more recent reports appears below:

NESDIS 100 The Resolving Power of a Single Exact-Repeat Altimetric Satellite or a Coordinated Constellation of Satellites: The Definitive Answer and Data Compression. Chang-Kou Tai, April 2001.

NESDIS 101 Evolution of the Weather Satellite Program in the U.S. Department of Commerce - A Brief Outline. P. Krishna Rao, July 2001.

NESDIS 102 NOAA Operational Sounding Products From Advanced-TOVS Polar Orbiting Environmental Satellites. Anthony L. Reale, August 2001.

NESDIS 103 GOES-11 Imager and Sounder Radiance and Product Validations for the GOES-11 Science Test. Jaime M. Daniels and Timothy J. Schmit, August 2001.

NESDIS 104 Summary of the NOAA/NESDIS Workshop on Development of a Coordinated Coral Reef Research and Monitoring Program. Jill E. Meyer and H. Lee Dantzler, August 2001.

NESDIS 105 Validation of SSM/I and AMSU Derived Tropical Rainfall Potential (TRaP) During the 2001 Atlantic Hurricane Season. Ralph Ferraro, Paul Pellegrino, Sheldon Kusselson, Michael Turk, and Stan Kidder, August 2002.

NESDIS 106 Calibration of the Advanced Microwave Sounding Unit-A Radiometers for NOAA-N and NOAA-N=. Tsan Mo, September 2002.

NESDIS 107 NOAA Operational Sounding Products for Advanced-TOVS: 2002. Anthony L. Reale, Michael W. Chalfant, Americo S. Allergrino, Franklin H. Tilley, Michael P. Ferguson, and Michael E. Pettey, December 2002.

NESDIS 108 Analytic Formulas for the Aliasing of Sea Level Sampled by a Single Exact-Repeat Altimetric Satellite or a Coordinated Constellation of Satellites. Chang-Kou Tai, November 2002.

NOAA Technical Report NESDIS 131

The GOES-14 Science Test: Imager and Sounder Radiance and Product Validations

Donald W. Hillger
NOAA/NESDIS/STAR
Colorado State University
Foothills Campus
Fort Collins, CO 80523

Timothy J. Schmit
NOAA/NESDIS/STAR
University of Wisconsin
Space Science and Engineering Center
Madison, WI 53706

Washington, DC
August 2010

U.S. DEPARTMENT OF COMMERCE
Gary Locke, Secretary

National Oceanic and Atmospheric Administration
Dr. Jane Lubchenco, Under Secretary of Commerce for Oceans and Atmosphere
and NOAA Administrator

National Environmental Satellite, Data, and Information Service
Mary Kicza, Assistant Administrator

The GOES-14 Science Test:
Imager and Sounder Radiance and Product Validations

Editors:

Donald W. Hillger[1] and Timothy J. Schmit[3]

Other Contributors:

Americo Allegrino[6], A. Scott Bachmeier[4], Andrew Bailey[6], Eric Brunning[10], Hyre Bysal[13], Lawrence Carey[15], Jaime M. Daniels[5], Mathew M. Gunshor[4], Jay Hanna[12], Andy Harris[10], Michael P. Hiatt[2], Seiichiro Kigawa[16], John A. Knaff[1], Jun Li[4], Daniel T. Lindsey[1], Eileen M. Maturi[9], Wen Meng[11], Kevin Micke[2], Jon Mittaz[10], James P. Nelson III[4], Walt Petersen[14], Gordana Rancic[6], Dale G. Reinke[2], Christopher C. Schmidt[4], Anthony J. Schreiner[4], Christopher Schultz[15], Elise Schultz[15], Dustin Sheffler[12], Dave Stettner[4], William Straka[4], Chris Velden[4], Gary S. Wade[3], Steve Wanzong[4], Dave Watson[2], Crystal Woodard[15], Xiangqian (Fred) Wu[7], and Fangfang Yu[8]

Affiliations:

[1]StAR/RAMMB (SaTellite Applications and Research/Regional and Mesoscale Meteorology Branch)
[2]CIRA (Cooperative Institute for Research in the Atmosphere)
Colorado State University, Fort Collins

[3]StAR/ASPB (SaTellite Applications and Research/Advanced Satellite Products Branch)
[4]CIMSS (Cooperative Institute for Meteorological Satellite Studies)
University of Wisconsin, Madison

[5]StAR/OPDB (SaTellite Applications and Research/Operational Products Development Branch)
[6]I.M. Systems Group, Inc. (IMSG), Rockville, Maryland

[7]StAR/SPB (SaTellite Applications and Research/Sensor Physics Branch)
[8]ERT, Inc., Annapolis Junction, MD

[9]StAR/SOCD (SaTellite Applications and Research/Satellite Oceanography and Climatology Branch)
[10]CICS (Cooperative Institute for Climate Studies)
University of Maryland, College Park
[11]Dell Perot Systems (DPS)

[12]NOAA/NESDIS Satellite Analysis Branch (SAB)

[13]NOAA/NESDIS Office of Satellite Operations (OSO)

[14]NASA/MSFC (Marshall Space Flight Center), Earth Sciences Office
[15]University of Alabama, Huntsville

[16]Meteorological Satellite Center, Japan Meteorological Agency

TABLE OF CONTENTS

Executive Summary of the GOES-14 NOAA Science Test 1

1. Introduction 2

1.1. GOALS FOR THE GOES-14 SCIENCE TEST 3

2. Satellite Schedules and Sectors 5

3. Changes to the GOES Imager from GOES-8 through GOES-14 11

4. GOES Data Quality 13

4.1. FIRST IMAGES 13
4.1.1. Visible 13
4.1.2. Infrared (IR) 15
4.1.3. Sounder 17
4.2. SPECTRAL RESPONSE FUNCTIONS (SRFS) 19
4.2.1. Imager 19
4.2.2. Sounder 19
4.3. RANDOM NOISE ESTIMATES 20
4.3.1. Imager 20
4.3.2. Sounder 25
4.4. STRIPING DUE TO MULTIPLE DETECTORS 29
4.4.1. Imager 29
4.4.2. Sounder 30
4.5. IMAGER-TO-IMAGER COMPARISON 32
4.6. IMAGER-TO-POLAR-ORBITER COMPARISONS 37
4.7. STRAY LIGHT ANALYSIS 43
4.8. INSTRUMENT PERFORMANCE MONITORING 45
4.8.1. Telemetry Monitoring 45
4.8.2. IR Calibration Coefficients Monitoring 46
4.8.3. Monitoring of Space-look (SPLK) Statistics 47
4.8.4. Monitoring Blackbody (BB) Scan Statistics 48
4.8.5. Initial Post-launch Calibration for the Imager Visible Band 49
4.9. FINER SPATIAL RESOLUTION GOES-14 IMAGER BAND-6 50

5. Product Validation 50

5.1. TOTAL PRECIPITABLE WATER (TPW) FROM THE SOUNDER 51
5.1.1. Validation of Precipitable Water (PW) Retrievals from the GOES-14 Sounder 51
5.2. LIFTED INDEX (LI) FROM THE SOUNDER 58
5.3. CLOUD PARAMETERS FROM THE SOUNDER AND IMAGER 59
5.4. ATMOSPHERIC MOTION VECTORS (AMVS) FROM THE IMAGER 62
5.5. CLEAR SKY BRIGHTNESS TEMPERATURE (CSBT) FROM THE IMAGER 65
5.6. SEA SURFACE TEMPERATURE (SST) FROM THE IMAGER 67
5.6.1. SST Generation 67
5.6.2. SST Validation 68
5.7. FIRE DETECTION 70
5.8. VOLCANIC ASH DETECTION 72

5.9. TOTAL COLUMN OZONE 73
5.10. GOES SURFACE AND INSOLATION PRODUCT (GSIP) 75

6. Other Accomplishments with GOES-14 76

6.1. GOES-14 IMAGER VISIBLE (BAND-1) SPECTRAL RESPONSE 76
6.2. LUNAR CALIBRATION 79
6.3. IMPROVED IMAGE NAVIGATION AND REGISTRATION (INR) WITH GOES-14 79
6.4. SPECIAL 1-MINUTE SCANS 80
6.5. SPATIAL LINE-SHIFTED OVER-SAMPLING TEST 80

7. Coordination with University of Alabama/Huntsville 80

7.1. DEEP CONVECTION: EXAMPLE CASE STUDIES 81
7.1.1. Marginal Lightning and Severe Weather: 2 December 2009 81
7.1.2. Severe Convection: 8-9 December 2009 84
7.2. WINTER STORM EVENTS 86
7.2.1. Washington DC, 19 December 2009 86
7.2.2. Oklahoma, 24 December 2009 87
7.3. SRSO FOR LIGHTNING SUMMARY 88

8. Coordination with Snow Study for Canadian Olympics 89

9. Overall Recommendations Regarding this and Future GOES Science Tests 89

Acknowledgments 90

References/Bibliography 91

Appendix A: Results from the Line-shifted Over-sampling Test 93

A1. SCIENTIFIC OBJECTIVES/GOALS 93
A2. HISTORY 93
A3. CONCEPT 93
A4. TESTING ACTIVITIES 94
A4.1. Data Acquisition 94
A4.2. Data Distribution 94
A4.3. Image Motion Estimation 94
A5. SUMMARY AND PROPOSALS FOR GOES-15 95

Appendix B: Web Sites Related to the GOES-14 Science Test 101

Appendix C: Acronyms Used in this Report 102

LIST OF TABLES

Table 2.1: Summary of Test Schedules for the GOES-14 Science Test 6
Table 2.2: Daily Implementation of GOES-14 Science Test Schedules 7
Table 3.1: GOES Imager band nominal wavelengths (GOES-8 through 15) 11
Table 3.2: GOES Imager band nominal spatial resolution (GOES-12 through 15) 11
Table 4.1: GOES-14 Imager Noise Levels 21
Table 4.2: Summary of the Noise for GOES-8 through GOES-14 Imager Bands 21
Table 4.3: Summary of the noise (in temperature units) for GOES-8 through GOES-14 Imager IR bands. The specification (SPEC) noise levels are also listed 23
Table 4.4: GOES-14 Sounder Noise Levels 25
Table 4.5: Summary of the Noise for GOES-8 through GOES-14 Sounder Bands 26
Table 4.6: GOES-14 Sounder NEdR compared to those from GOES-8 through GOES-13 and the specification noise values. 28
Table 4.7: GOES-14 Sounder NEdT compared to those from GOES-8 through GOES-13. 29
Table 4.8: GOES-14 Imager Detector-to-Detector Striping 30
Table 4.9: GOES-14 Sounder Detector-to-Detector Striping 30
Table 4.10: Comparison of GOES-14 Imager to Infrared Atmospheric Sounding Interferometer (IASI) using the CIMSS-method. The bias is the mean of the absolute values of the differences. .. 38
Table 4.11: Brightness temperature (Tb) biases between GOES-14 Imager and AIRS/IASI for the daytime collocated pixels and the double difference between AIRS and IASI through GOES-14 Imager daytime collocation data using the GSICS-method. The Tb biases between GOES-14 and IASI over the nighttime (9:30 pm) collocated pixels are also compared. The Tb biases were based on the collocated pixels acquired after 24 November 2009. Standard deviations are given in parentheses. 40
Table 4.12: GOES-14 Sounder IR vs. IASI brightness temperature difference at nighttime, compared to those of GOES-11/12 Sounder using the GSICS-method. The data in the parentheses are the standard deviation of the Tb difference at the collocation pixels. 42
Table 4.13: Telemetry variables. 46
Table 5.1: Verification statistics for GOES-12 and GOES-14 retrieved precipitable water, first guess (GFS) precipitable water, and radiosonde observations of precipitable water for the period 30 November 2009 to 4 January 2010. 52
Table 5.2: Verification statistics for GOES-14 vs. RAOB Match Verification Statistics NHEM winds (m/s): 30 November 2009 – 16 January 2010 64
Table 5.3: Verification statistics for GOES-12 and GOES-14, collocated (0.1 deg, 25 hPa) RAOB Match Verification Statistics for NHEM winds (m/s): 30 November 2009 – 16 January 2010 65
Table 7.1: Summary of significant case study dates for MSFC GOES-14 SRSO 81

Table A1: GOES-14 Over-sampling Test Frame Definitions. Note that frame time intervals between two sequences are *not constant.* 97

LIST OF FIGURES

Figure 1.1: GOES-O spacecraft decal 3
Figure 3.1: The GOES-14 Imager weighting functions. 12
Figure 3.2: The GOES-14 Sounder weighting functions. 12
Figure 4.1: The first visible (0.63 μm) image from the GOES-14 Imager occurred on 27 July 2009 starting at 1730 UTC. 13
Figure 4.2: A GOES-14 close-up view centered over central California showed marine fog and stratus adjacent to the Pacific Coast, with cumulus clouds developing inland over the higher terrain of the Sierra Nevada. 14
Figure 4.3: GOES-14 full-disk image for "water vapor" band (band-3, 6.5 μm) from 17 August 2009 starting at 1732 UTC. 15
Figure 4.4: GOES-14 Imager bands (top) and the corresponding GOES-12 Imager bands (bottom). Both sets of images are shown in their native projections. 16
Figure 4.5: The visible (band-19) image from the GOES-14 Sounder shows data from 28 July 2009. The west and east 'saw-tooth' edges are due to the geometry of collecting the pixels. 17
Figure 4.6: The first IR Sounder images for GOES-14 from 18 August 2009 (top) compared to GOES-12 (bottom). Both sets of images have been remapped to a common projection. Note the less noisy Sounder band-15 (4.6 μm). 18
Figure 4.7: The four GOES-14 Imager IR band SRFs super-imposed over the calculated high-resolution earth-emitted U.S. Standard Atmosphere spectrum. Absorption due to carbon dioxide (CO_2), water vapor (H_2O), and other gases are evident in the high-spectral resolution earth-emitted spectrum. 19
Figure 4.8: The eighteen GOES-14 Sounder IR band SRFs (Rev A.) super-imposed over the calculated high-resolution earth-emitted U.S. Standard Atmosphere spectrum. 20
Figure 4.9: Variance of pre-clamp and post-clamp space-look scan count for GOES-14, compared with those for GOES-11/12/13. 22
Figure 4.10: Time-series of the variance of GOES-14 Imager pre-clamp and post-clamp space-look scan at three temporal scales. Top: 2-day period with 8 detector data, middle: 10-day period with 8 detector data, and bottom: mean values from 30 November 2009 through 19 January 2010. 23
Figure 4.11: GOES-14 Imager NEdT calculated at 300 K temperature, except band-3 at 230 K, compared to the specifications. 24
Figure 4.12: GOES-14 Sounder noise values (space-look count variance) compared to those from GOES-11/12/13. 27
Figure 4.13: GOES-14 Sounder band-11 image, for a time of less striping (upper panel), and more striping (lower panel). 32
Figure 4.14: Two-dimensional smoothed histogram of GOES-12 band-2 pixel temperatures (K) vs. GOES-14 band-2 pixel temperatures. 34
Figure 4.15: Two-dimensional smoothed histogram of GOES-12 band-3 pixel temperatures (K) vs. GOES-14 band-3 pixel temperatures (K). 34
Figure 4.16: Two-dimensional smoothed histogram of GOES-12 band-4 pixel temperatures (K) vs. GOES-14 band-4 pixel temperatures (K). 35
Figure 4.17: Two-dimensional smoothed histogram of GOES-12 band-6 pixel temperatures (K) vs. GOES-14 band-6 pixel temperatures (K). 35

Figure 4.18: Two-dimensional smoothed histogram of GOES-11 band-2 pixel temperatures (K) vs. GOES-14 band-2 pixel temperatures (K). 36
Figure 4.19: Two-dimensional smoothed histogram of GOES-11 band-3 pixel temperatures (K) vs. GOES-14 band-3 pixel temperatures (K). 36
Figure 4.20: Two-dimensional smoothed histogram of GOES-11 band-4 pixel temperatures (K) vs. GOES-14 band-4 pixel temperatures (K). 37
Figure 4.21: Spectral response function of GOES-14 Imager (top) and Sounder (bottom), together with the AIRS/IASI spectra. 39
Figure 4.22: GOES-14 Imager and AIRS/IASI inter-calibration for the daytime. 40
Figure 4.23: The Tb bias between GOES-14 and IASI Tb bias over the nighttime (9:30 pm) collocated pixels using the GSICS-method. 41
Figure 4.24: Mean and standard deviation of GOES-11/12/14 Sounder brightness temperature difference from nighttime IASI data in December 2009 using the GSICS-method. 43
Figure 4.25: GOES-12 and GOES-14 Imager (top), and GOES-14 band-2 (bottom), from 21 September 2009. Note the large stray radiation from the sun. 44
Figure 4.26: Monitoring of GOES-14 Imager and Sounder PRT temperature data. The top panels are 2 consecutive day observation data, the middle ones are for 10-day data, and the bottom panel shows the mean of the 8 detectors over the PLT period, from 30 November 2009 through 19 January 2010. 46
Figure 4.27: Monitoring of the first-order gain and the bias values for the GOES-14 Sounder band-8 (11.03 µm). A sudden disruption of the slope values can be observed around 1800 UTC in the two-day observation panel for the GOES-14 Sounder data. 47
Figure 4.28: Monitoring of mean filtered pre-clamp space-look data for GOES-14 Imager band-3 (6.5 µm). The zero values happen periodically for the two detectors at the same time period every day. 48
Figure 4.31: Improved Imager spatial resolution at 13.3 µm for GOES-14 (right) compared to GOES-12 (left) from 26 August 2009. 50
Figure 5.1: Time series of Root Mean Square Error (RMSE) between GOES-12 and GOES-14 retrieved precipitable water and radiosonde observation of precipitable water over the period 30 November 2006 to 4 January 2010. 53
Figure 5.2: Time series of bias (GOES-radiosonde) between GOES-12 and GOES-14 retrieved precipitable water and radiosonde observation of precipitable water over the period 30 November 2009 to 4 January 2010. 54
Figure 5.3: Time series of correlation between GOES-12 and GOES-14 retrieved precipitable water and radiosonde observation of precipitable water over the period 30 November 2009 to 4 January 2010. 55
Figure 5.4: Time series of the number of collocations between GOES-12 and GOES-14 retrieved precipitable water and radiosonde observation of precipitable water over the period 30 November 2009 to 4 January 2010. 56
Figure 5.5: GOES-14 (top) and GOES-11/12 (bottom) retrieved TPW (mm) from the Sounder displayed as an image. The data are from 0000 UTC on 4 December 2009. Measurements from radiosondes are overlaid as white text; cloudy FOVs are denoted as shades of gray. 57
Figure 5.6: GOES-14 Sounder TPW from two retrieval algorithms (i.e., Ma (upper-panel) and Li (lower-panel). Both images are from 14 December 2009. 58
Figure 5.7: GOES-14 (top) and GOES-12 (lower) retrieved Lifted Index (LI) from the Sounder displayed as an image. The data are from 1746 UTC on 14 December 2009. 59

Figure 5.8: GOES-14 Imager cloud-top pressure from 11 November 2009 starting at 1745 UTC..... 60
Figure 5.9: GOES-14 Sounder cloud-top pressure from 11 November 2009 starting at 1745 UTC. The Sounder data have been remapped into the GOES-14 Imager projection. 60
Figure 5.10: GOES-12 cloud-top pressure from the Sounder from 1746 UTC on 10 September 2009.. 61
Figure 5.11: GOES-14 cloud-top pressure from the Sounder from the nominal 1746 UTC on 10 September 2009. 61
Figure 5.12: GOES-14 Sounder visible image from the nominal 1746 UTC on 10 September 2009..... 62
Figure 5.13: GOES-14 NHEM cloud drift AMV on 7 January 2010 at 1045 UTC. 63
Figure 5.14: GOES-14 NHEM water vapor AMV on 7 January 2010 at 1045 UTC. 63
Figure 5.15: GOES-11 (top), GOES-12 (middle) and GOES-14 (bottom) Imager Clear-Sky Brightness Temperature cloud mask from 1400 UTC on 6 January 2010. Each image is shown in the GOES-14 satellite projection. 66
Figure 5.16: GOES-14 north sector band-2 (upper-left); GOES-14 north sector band-4 (upper-right); GOES-14 south sector band-2 (lower-left); GOES-14 south sector band-4 (lower-right). 67
Figure 5.17: GOES-14 SST imagery (Hourly SST composite with applied 98% clear sky probability (left) and hourly composite clear sky probability). 68
Figure 5.18: GOES-12 SST daytime and nighttime retrievals vs. buoys. 69
Figure 5.19: GOES-14 SST daytime and nighttime retrievals vs. buoys. 70
Figure 5.20: GOES Imager 3.9 µm images from GOES-11 (left), GOES-14 (center) and GOES-12 (right). Each satellite is shown in its native perspective. 71
Figure 5.21: GOES Imager 3.9 µm time series from GOES-11, GOES-12 and GOES-14. 72
Figure 5.22: GOES-11, GOES-14, and GOES-12 10.7 µm IR and 6.7/6.5 µm water vapor images. 73
Figure 5.23: Example of GOES-12 Imager Total Column Ozone on 14 January 2010 at 1200 UTC. ... 74
Figure 5.24: Example of GOES-14 Imager Total Column Ozone on 14 January 2010 at 1200 UTC. The image is displayed in the GOES-12 perspective. 74
Figure 5.25: GOES-12 Imager downwelling surface insolation on 1 December 2009 beginning at 1745 UTC..... 75
Figure 5.26: GOES-14 Imager downwelling surface insolation on 1 December 2009 beginning at 1745 UTC..... 76
Figure 6.1: GOES-12 (blue) and GOES-14 (red) Imager visible (approximately 0.65 or 0.63 µm) band SRFs, with a representative spectrum for grass over-plotted (green). 77
Figure 6.2: Comparison of the visible (0.65 µm) imagery from GOES-12 and GOES-14 (0.63 µm) on 1 September 2009 demonstrates how certain features, such as surface vegetation, are more evident with the GOES-14 visible data. 78
Figure 6.3: GOES-14 Imager visible (0.65 µm) band image of the moon from 9 August 2009 for a scan that started at 2053 UTC. 79
Figure 7.1: PPI from ARMOR at 2103 UTC on 2 December 2009 at 0.7° elevation. Reflectivity (upper-left), radial velocity (upper-right), differential reflectivity (lower-left) and specific differential phase (lower-right) are all shown. The cell that prompted the tornado warning is highlighted by the red arrow. Cells just to the south of the tornado-warned storm briefly produced lightning about 2130 UTC (yellow arrows). 82
Figure 7.2: Dual Doppler Analysis using the WSR 88D radar at Hytop AL (KHTX) and UA Huntsville's ARMOR radar (2103 UTC). Shown are reflectivity (shaded) and ground-relative wind vectors. The cell that prompted the tornado warning is highlighted by the red arrow. Cells just to the south of the tornado-warned storm are producing lightning. Only very slight rotation is evident in the hook region of the dual-Doppler analysis. 82

Figure 7.3: Total lightning measurements using the North Alabama Lightning Mapping Array for 2 December 2009 at 2130-2140 UTC. Vertical lines in the top panel represent lightning flashes, while the lower three panels represent the distribution of VHF sources in the XY (lower-right), XZ (middle) and YZ (lower-right) directions. Cooler colors represent flashes that occur earlier, while warmer colors show flashes that occur later in the period. Not unexpectedly, the source heights in this storm are relatively low in altitude. 83
Figure 7.4: ARMOR image 2116 UTC at 3.4° elevation. Displayed are: reflectivity (CZ, upper-left), specific differential phase (KD, upper-middle), visible GOES-14 with lightning Flash Extent Density (FED, upper-right) at 2116 UTC, differential reflectivity (CD, lower-left), correlation coefficient (RH, lower-middle), and visible GOES-14 with FED at 2118 UTC (lower-right). A large drop core is identified in the dual-polarization data 50 km east of the radar along the apex of the bowed reflectivity feature. 84
Figure 7.5: As in previous figure, but 2121 UTC for ARMOR image, 2120 UTC for specific differential phase, and 2121 UTC for lightning FED. 85

Figure A1: Frame Coverage of Over-sampling Testing. The first frame is 1150 km (east-west) by 250 km (north-south). The second frame is 1150 km by 500 km, offset from the first frame by 2 km (one-half pixel) in the north-south direction. The third frame is 1150 km by 250 km, with its north-south start address equal to the stop address of the first frame. 96
Figure A2: Composite image generation on over-sampling testing. Blue and red dots indicate the center of the pixel Field-Of-View that is shown by rose-colored squares. The second frame is offset from the first and third frame by 2 km (one-half pixel) in the north-south direction. 97
Figure A3: Comparison of Over-sampled Images to Normal Images. Top: The rivers and bays located in Glen Canyon National Recreation Area, Utah and Arizona can be seen clearly in the over-sampled image. Clouds: The over-sampled images also show clear cloud features in all IR bands. Remarkable noise appears in the over-sampled image of band-3 since the striping of this band is enhanced by the filters. An additional filter can reduce the striping noise. Band-1 (visible band) is the only reference that shows cloud contents in the scene. 98
Figure A4: Image Motion Evaluation of Land Features. The land features of the rivers and bays around Glen Canyon National Recreation Area were used to evaluate image motion errors. The top images show the area used for the evaluation. The red squares of the top images indicate the size of pattern matching (i.e., 17 by 17 pixels on the over-sampled image.) The algorithm that is used for the pattern matching is the cross-correlation method with elliptical fitting of a matching surface. The bottom chart illustrates the histogram of the motion speed. The motion speed of the over-sampled image (blue line) is distributed with an average of 0.5 m/s and a standard deviation of 0.31 m/s, while the motion speed of the normal image (red line) shows an average of 1.2 m/s and a standard deviation of 0.84 m/s. 99
Figure A5: NOAA-17 and GOES-14 Images. NOAA-17 flew over the area GOES-14 observed in the over-sampling testing, 15 minutes later. 100

Executive Summary of the GOES-14 NOAA Science Test

The Science Test for GOES-14 produced several results and conclusions:

- GOES-14 Imager and Sounder data were collected during the five-week NOAA Science Test that took place during December 2009 while the satellite was stationed at 105ºW longitude. Additional pre-Science Test data, such as the first visible and IR images, were collected during the summer and fall of 2009.

- Improved (4 km) resolution of the 13.3 µm band required changes to the GVAR (GOES VARiable) format.

- Imager and Sounder data were collected for a host of schedules, including rapid scan imagery. GVAR datastream were stored at several locations for future needs.

- A GOES Sounder calibration issue, which could be caused by a loose lens or optical element, with respect to averaging calibration slopes was identified.

- Initial Infrared Atmospheric Sounding Interferometer (IASI) and Atmospheric Infrared Sounder (AIRS) high-spectral resolution inter-calibrations with both the Imager and Sounder were verified for good radiometric accuracy.

- Many level 2 products were generated (retrievals, atmospheric motion vectors, clouds, Clear Sky Brightness Temperature (CSBT), Lifted Index, Sea Surface Temperature (SST), total column ozone, etc.) and validated.

- Many GOES-14 images and examples were posted on the Web in near real-time.

Changes were implemented with the GOES-14 compared to previous GOES Imagers:

- The detector size of the Imager 13.3 µm band (band-6) was changed from 8 km to 4 km by incorporating two detectors instead of one. The GVAR format was modified.

- In order to operate the instruments (Imager and Sounder) during the eclipse periods and Keep-Out-Zone (KOZ) periods, improved spacecraft batteries and partial-image frames were utilized. Improved instrument performance means there will no longer be the required health and safety related KOZ outages.

- Colder patch (detector) temperatures were noted due to the new spacecraft design. In general, Imager and Sounder data from GOES-14 (and GOES-13) are improved considerably in quality (noise level) to that from GOES-8 through GOES-12.

- In addition, the image navigation and registration with GOES-14 (and GOES-13) are much improved, especially in comparison to GOES-8 through GOES-12. The improved satellite and instrument performance will allow more earth-scene data to be scanned during the four hours around satellite midnight.

1. Introduction

The latest Geostationary Operational Environmental Satellite (GOES), GOES-O, was launched on 27 June 2009, and reached geostationary orbit at 89.5°W on 8 July 2009 to become GOES-14. It was later moved to 104.5ºW for the Science Test and eventual storage. While the XRS (X-Ray Sensor) is operating on GOES-14, the Imager and Sounder await operational use. GOES-14 was the second of the three GOES-N/O/P series spacecraft, with GOES-P launched in March 2010.

The National Oceanic and Atmospheric Administration (NOAA)/National Environmental Satellite, Data, and Information Service (NESDIS) conducted a five-week GOES-14 Science Test that began 30 November 2009 and ended officially on 4 January 2010. The first two weeks of the Science Test schedule were integrated within the National Aeronautics and Space Administration (NASA) GOES-14 Post-Launch Test (PLT) schedule. An additional three weeks of the Science Test were performed under NOAA/NESDIS control.

GOES-14 has an Imager and Sounder similar to those on GOES-8/12, but GOES-14, like GOES-13, is on a different spacecraft bus. The new bus allows improvements both to navigation and registration, as well as the radiometrics. Due to larger spacecraft batteries, the GOES-N/O/P system is able to supply data through the eclipse periods, thereby addressing one of the major limitations of eclipse and related outages. Outages due to Keep Out Zones (KOZ) are also minimized. In terms of radiometric improvements, a colder patch (detector) temperature results in the GOES-13/14 instruments (Imager and Sounder) being less noisy. In addition, there is a potential reduction in detector-to-detector striping to be achieved through increasing the Imager scan-mirror dwell time on the blackbody from 0.2 s to 2 s. Finally, the navigation was improved due to the new spacecraft bus and the use of star trackers (as opposed to the previous method of edge-of-earth sensors). In general, the navigation accuracy (at nadir) improves from between 4-6 km with previous Imagers to less than 2 km with those on the GOES-N/O/P satellites.

Figure 1.1: GOES-O spacecraft decal

This report describes the NOAA/NESDIS Science Test portion only. In addition, the Imager and Sounder are covered, while the solar/space instruments are not. System performance and operational testing of the spacecraft and instrumentation was performed as part of the PLT. During the Science Test, GOES-14 was operated in a special test mode, where the default schedule involved routine emulation of either GOES-East or GOES-West operations. Numerous other scan schedules and sectors were constructed and used for both the Imager and the Sounder. GOES-14 was then placed into storage mode on 19 January 2010. Current plans call for GOES-14 to remain in storage until after GOES-13 has become operational. At the time of the GOES-14 Science Test, GOES-12 was operating in the GOES-East position, and GOES-11 was operating in the GOES-West position.

1.1. Goals for the GOES-14 Science Test

First goal: To assess the quality of the GOES-14 radiance data. This evaluation was accomplished through comparison to data from other satellites or by calculating the signal-to-noise ratio compared to specifications, as well as assessing the striping in the imagery due to multiple detectors.

Second goal: To generate products from the GOES-14 data stream and compare to those produced from other satellites. These products included several Imager and Sounder products: land skin temperatures, temperature/moisture retrievals, total precipitable water, lifted index, cloud-top pressure, atmospheric motion vectors, and sea surface temperatures. Validation of these products was accomplished through comparisons to products generated from other satellites or through comparisons to radiosondes and ground-based instruments.

Third goal: To collect nearly-continuous rapid-scan imagery of interesting weather cases at temporal resolutions as fine as every 30 seconds, a capability of rapid-scan imagery from GOES-R that is not implemented operationally on the current GOES. The rapid-scan data may augment radar and lightning data, collected at special networks, to investigate the potential for improving severe weather forecasts.

Fourth goal: To monitor the impact of any instrument changes. Changes included the increased spatial resolution (from 8 km to 4 km) for the Imager 13.3 μm band (band-6) on GOES-14. Other improvements which began with GOES-13 include: better navigation, improved calibration and the capabilities of the GOES-N series to operate through eclipse, when the satellite is in the shadow of the earth, as well as to minimize outages due to Keep Out Zones (KOZ), when the sun can potentially contaminate imagery by being within the field of view of the instruments (Imager and Sounder).

Finally, the GOES-14 Imager and Sounder data were received via direct downlink at the following sites: (1) CIRA, Colorado State University, Fort Collins CO; (2) Space Science and Engineering Center (SSEC), University of Wisconsin-Madison, Madison WI; and (3) NOAA/NESDIS, Suitland/Camp Springs MD. Each site ingested, archived, and made the data available on its own internal network in McIDAS (Man computer Interactive Data Access System) format, as well as to other sites as needed. The NOAA-NESDIS Regional and Mesoscale Meteorology Branch (RAMMB) at CIRA also made the GOES-14 imagery available over the internet via RAMSDIS Online. Image and product loops were also made available on the CIMSS Web site. See Appendix A for the appropriate URLs for these and many other GOES-14 related Web sites.

This report documents results from these various activities undertaken by NOAA/NESDIS and its Cooperative Institutes during this test period. Organizations which participated in these GOES-14 Science Test activities included the: NOAA/NESDIS SaTellite Applications and Research (StAR); NOAA/NESDIS Office of Satellite Data Processing and Distribution (OSDPD); Cooperative Institute for Meteorological Satellite Studies (CIMSS); Cooperative Institute for Research in the Atmosphere (CIRA); NOAA/NESDIS Satellite Analysis Branch (SAB), and NASA/MSFC. The GOES-14 NOAA Science Test was co-lead by D. Hillger and T. Schmit, both of NOAA/NEDSIS STAR.

NOAA Technical Reports similar to this one were produced for both the **GOES-11** (Daniels et al. 2001), **GOES-12** (Hillger et al. 2003), and **GOES-13** (Hillger and Schmit, 2007 and 2009) Science Tests. The reference/bibliography section contains other articles related to the GOES-14 Science Test.

2. Satellite Schedules and Sectors

A total of nine schedules involving numerous predefined Imager and Sounder sectors were constructed for the GOES-14 Science Test. The choice of Imager and Sounder sectors was a result of input from the various research and development groups participating in the Science Test. Most of these schedules are similar to those run during the GOES-13 Science Test (Hillger and Schmit 2006).

Thanks to dedicated support provided by the NOAA/NESDIS/Satellite Operations Control Center (SOCC) and the Office of Satellite Operations (OSO), a significant amount of flexibility existed with respect to switching and activating the schedules on a daily basis. The ease with which the schedules could be activated was important for capturing significant weather phenomena of varying scales and locations during the Science Test period.

A brief summary of the nine schedules is provided in Table 2.1. The C5RTN and C4RTN schedules, emulating GOES-East or GOES-West operations respectively, were the default schedules if no other schedule was requested at the cutoff of 1 hour before the 1630 UTC daily schedule change time. For the Sounder, the default schedules were also emulated normal GOES-East and GOES-West operations.

The C1CON schedule was mainly for emulating GOES-R Advanced Baseline Imager (ABI) data, where five-minute images will be routine over CONUS. The C2SRSO and C3SRSO schedules, with images at 1-minute and 30-second intervals respectively, were prepared to provide the ability to call up Super Rapid Scan Operations (SRSO) during the test period. The C6FD schedule allowed continuous 30-minute interval full-disk imaging of the entire hemisphere. The C7MOON and "C8" schedules provided specialized datasets of the moon, and for line-shifted over-sampling of Imager data to emulate the higher spatial resolution of the GOES-R ABI, respectively. Finally, the C59RTN schedule contained partial-image frames that will be available to users during Keep-Out-Zones, to avoid solar contamination radiances and the detrimental effect on image products.

The daily implementation of the various schedules during the entire Science Test is presented in Table 2.2. The GOES-14 daily call-up began on 30 November 2009 and continued through 4 January 2010. GOES-14 continued to collect imagery for more than two weeks, through 19 January 2010, before the GOES-14 Imager and Sounder were turned off.

Table 2.1: Summary of Test Schedules for the GOES-14 Science Test

Test Schedule Name	Imager	Sounder	Purpose
C1CON	Continuous 5-minute CONUS sector	26-minute CONUS sector every 30 minutes	Test navigation, ABI-like (temporal) CONUS scans
C2SRSO	Continuous 1-minute rapid-scan (with center point specified for storm analysis)	26-minute CONUS sector every 30 minutes	Test navigation, ABI-like (temporal) mesoscale scans
C3SRSO	Continuous 30-second rapid-scan (with center point at one of three locations: Huntsville AL, Norman OK, or Washington DC)[1]	26-minute CONUS sector every 30 minutes	Coordination with lightning detection arrays in Huntsville AL, Norman OK, and Washington DC areas
C4RTN	Emulates GOES-West routine operations	Emulates GOES-West routine operations	Radiance and product comparisons
C5RTN	Emulates GOES-East routine operations	Emulates GOES-East routine operations	Radiance and product comparisons
C6FD	Continuous 30-minute full disk (including off-earth measurements)	Sectors on both east and west limbs every hour (including off-earth measurements)[2]	Imagery for noise, striping, etc.
C7MOON (depends on moon availability)	Capture moon off edge of earth (when possible) for calibration purposes	Inserted into GOES-East routine operations	Test ABI lunar calibration concepts
"C8" (inserted into C5 GOES-East routine schedule)	Emulates 2 km ABI resolution through spatial over-sampling (19 minutes for a small sector per specific line-shifted scan strategy)	Emulates GOES-East routine operations	ABI-like higher-resolution data emulation
C59RTN (modified C5 GOES-East routine schedule)	Partial-image frames[3] testing (such frames will be available during semi-annual satellite-eclipse/keep-out-zone periods)	Emulates GOES-East routine operations	AWIPS testing and product generation

[1] Including the Hazardous Weather Testbed in North Alabama (centered at Huntsville AL, 34.72°N -86.65°E), the Oklahoma Lightning Mapping Array (centered at Norman OK, 35.28°N -97.92°E), and the Washington DC lightning mapping array (centered over Falls Church VA, 38.89°N -77.17°E).
[2] Limb sectors similar to GOES Sounder scans during previous GOES Science Tests.
[3] Partial-image frames include the following: CONUS and CONUS replacement, Northern HEMI and Northern HEMI replacement, Southern HEMI and Southern HEMI replacement, and Northern HEMI-extended and Northern HEMI-extended replacement.

Table 2.2: Daily Implementation of GOES-14 Science Test Schedules (Daily starting time: 1630 UTC)

Starting Date [Julian Day] (Day of Week)	Test Schedule Name	Imager	Sounder	Purpose
Start of 5-week Science Test				
November 30 [334] (Monday)	C5RTN	Emulates GOES-East routine operations	Emulates GOES-East routine operations	Some final changes in software at Satellite Operations were still being implemented
December 01 [335] (Tuesday)	C6FD	Continuous 30-minute full disk (including off-earth measurements)	Sectors on both east and west limbs every hour (including off-earth measurements)	Imagery for noise, striping, etc.
December 02 [336] (Wednesday)	C2SRSO	Continuous 1-minute rapid-scan (centered at 34.7°N / 85.6°W, 1 degree E of Huntsville AL)	26-minute CONUS sector every 30 minutes	Significant weather event over SE U.S.
December 03 [337] (Thursday)	"C8" (inserted into C5 schedule)	Emulates GOES-East routine operations (with special scans inserted)	Emulates GOES-East routine operations	Radiance and product comparisons (plus ABI-like higher-resolution data emulation)
December 04 [338] (Friday)	C1CON	Continuous 5-minute CONUS sector	26-minute CONUS sector every 30 minutes	ABI-like (temporal) CONUS scans
December 05 [339] (Saturday)	C2SRSO	Continuous 1-minute rapid-scan (centered at 28.59°N / 80.65°W, Kennedy Space Center)	26-minute CONUS sector every 30 minutes	Coordination with lightning mapping array over KSC
December 06 [340] (Sunday)	C5RTN	Emulates GOES-East routine operations	Emulates GOES-East routine operations	Radiance and product comparisons
December 07 [341] (Monday)	C4RTN	Emulates GOES-West routine operations	Emulates GOES-West routine operations	Radiance and product comparisons

December 08 [342] (Tuesday)	C2SRSO	Continuous 1-minute rapid-scan (centered at 34.7°N / 86.6°W, Huntsville AL)	26-minute CONUS sector every 30 minutes	Coordinate with lightning detection array in Huntsville AL
December 09 [343] (Wednesday)	C1CON	Continuous 5-minute CONUS sector	26-minute CONUS sector every 30 minutes	ABI-like (temporal) CONUS scans
December 10 [344] (Thursday)	C4RTN	Emulates GOES-West routine operations	Emulates GOES-East routine operations	Radiance and product comparisons
December 11 [345] (Friday)	C1CON	Continuous 5-minute CONUS sector	26-minute CONUS sector every 30 minutes	ABI-like (temporal) CONUS scans
December 12 [346] (Saturday)	C4RTN	Emulates GOES-West routine operations	Emulates GOES-West routine operations	Radiance and product comparisons
December 13 [347] (Sunday)	C4RTN	Emulates GOES-West routine operations	Emulates GOES-West routine operations	Radiance and product comparisons
December 14 [348] (Monday)	C5RTN	Emulates GOES-East routine operations	Emulates GOES-East routine operations	Radiance and product comparisons
December 15 [349] (Tuesday)	C5RTN	Emulates GOES-East routine operations	Emulates GOES-East routine operations	Radiance and product comparisons
December 16 [350] (Wednesday)	C5RTN	Emulates GOES-East routine operations	Emulates GOES-East routine operations	Radiance and product comparisons
December 17 [351] (Thursday)	C59RTN	Partial-image frames testing (modified C5 GOES-East routine schedule)	Emulates GOES-East routine operations	AWIPS testing and product generation
December 18 [352] (Friday)	C2SRSO	Continuous 1-minute rapid-scan (centered at 32°N / 82°W, on the Georgia coast)	26-minute CONUS sector every 30 minutes	Significant weather event over SE U.S.
December 19 [353] (Saturday)	C2SRSO	Continuous 1-minute rapid-scan (centered at 39°N / 77°W, Washington DC)	26-minute CONUS sector every 30 minutes	Significant East Coast snowstorm

December 20 [354] (Sunday)	C2SRSO	Continuous 1-minute rapid-scan (centered at 50°N / 123°W, Whistler BC, Canada)	26-minute CONUS sector every 30 minutes	Mountain snow study for 2010 Olympics
December 21 [355] (Monday)	C4RTN	Emulates GOES-West routine operations	Emulates GOES-West routine operations	Radiance and product comparisons
December 22 [356] (Tuesday)	C4RTN	Emulates GOES-West routine operations	Emulates GOES-West routine operations	Radiance and product comparisons
December 23 [357] (Wednesday)	C4RTN	Emulates GOES-West routine operations	Emulates GOES-West routine operations	Radiance and product comparisons
December 24 [358] (Thursday)	C2SRSO	Continuous 1-minute rapid-scan (centered at 35.1°N / 89.8°W, Memphis TN)	26-minute CONUS sector every 30 minutes	Large weather system over central U.S.
December 25 [359] (Friday)	C1CON	Continuous 5-minute CONUS sector	26-minute CONUS sector every 30 minutes	ABI-like (temporal) CONUS scans
December 26 [360] (Saturday)	C1CON	Continuous 5-minute CONUS sector	26-minute CONUS sector every 30 minutes	ABI-like (temporal) CONUS scans
December 27 [361] (Sunday)	C1CON	Continuous 5-minute CONUS sector	26-minute CONUS sector every 30 minutes	ABI-like (temporal) CONUS scans
December 28 [362] (Monday)	C6FD	Continuous 30-minute full disk (including off-earth measurements)	Sectors on both east and west limbs every hour (including off-earth measurements)	Imagery for noise, striping, etc.
December 29 [363] (Tuesday)	C5RTN	Emulates GOES-East routine operations	Emulates GOES-East routine operations	Radiance and product comparisons
December 30 [364] (Wednesday)	C1CON	Continuous 5-minute CONUS sector	26-minute CONUS sector every 30 minutes	ABI-like (temporal) CONUS scans
December 31 [365] (Thursday)	C4RTN	Emulates GOES-West routine operations	Emulates GOES-West routine operations	Radiance and product comparisons
January 01 [001] (Friday)	C4RTN	Emulates GOES-West routine operations	Emulates GOES-West routine operations	Radiance and product comparisons

January 02 [002] (Saturday)	C4RTN	Emulates GOES-West routine operations	Emulates GOES-West routine operations	Radiance and product comparisons
January 03 [003] (Sunday)	C4RTN	Emulates GOES-West routine operations	Emulates GOES-West routine operations	Radiance and product comparisons
January 04 [004] (Monday)	C7MOON[1]	Capture moon off edge of earth (when possible) for calibration purposes	Inserted into GOES-East routine operations	Test ABI lunar calibration concepts
End of 5-week Science Test				
Starting January 05 [005] through January 19 [019]	C5RTN or C4RTN	Emulates GOES-East or **west** routine operations	Emulates GOES-East or **west** routine operations	GOES-14 operated in this schedule until it was put into storage mode

[1] Additional (and better) moon images were taken on 10 August 2009 [Julian Day 222].

3. Changes to the GOES Imager from GOES-8 through GOES-14

The differences in spectral bands between the two versions of the GOES Imager (Schmit et al. 2002a) are explained in Table 3.1. Each version has five bands. The Imager on GOES-8 through GOES-11 contains bands 1 through 5. The Imagers on GOES-12, 13, 14, and 15 contain bands 1 through 4 and band-6.

Table 3.1: GOES Imager band nominal wavelengths (GOES-8 through 15)

GOES Imager Band	Wavelength Range (µm)	Central Wavelength (µm)	Meteorological Objective
1	0.53 to 0.75	0.65 (GOES-8/12) 0.63 (GOES-13/15)	Cloud cover and surface features during the day
2	3.8 to 4.0	3.9	Low cloud/fog and fire detection
3	6.5 to 7.0 5.8 to 7.3	6.75 (GOES-8/11) 6.48 (GOES-12/15)	Upper-level water vapor
4	10.2 to 11.2	10.7	Surface or cloud-top temperature
5	11.5 to 12.5	12.0 (GOES-8/11)	Surface or cloud-top temperature and low-level water vapor
6	12.9 to 13.7	13.3 (GOES-12/14)	CO_2 band: Cloud detection

The differences in the nominal spatial resolution between the more recent GOES Imager are explained in Table 3.2. The east-west over-sampling is not included in the table. The increased resolution of band-6 necessitated a change in the GVAR format, to include an additional block of data associated with two detectors instead of only one detector.

Table 3.2: GOES Imager band nominal spatial resolution (GOES-12 through 15)

GOES Imager Band	Central Wavelength (µm)	Spatial Resolution (km)	Number of Detectors
1	0.65	1	8
2	3.9	4	2
3	6.48	4	2
4	10.7	4	2
6	13.3	8 (GOES-12/13) 4 (GOES-14/15)	1 (GOES-12/13) 2 (GOES-14/15)

Figures 3.1 and 3.2 show the nominal region of the atmosphere sensed by each Imager and Sounder band on GOES-14. Note these are representative of clear-skies and a nadir view.

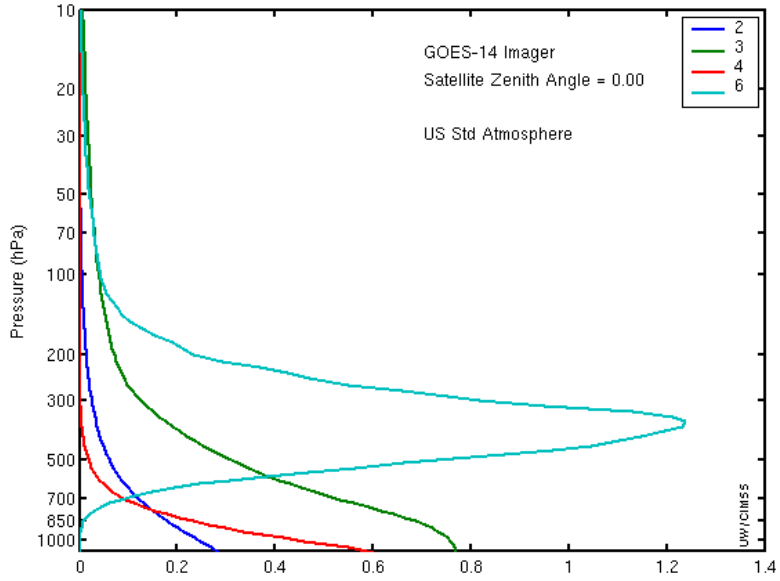

Figure 3.1: The GOES-14 Imager weighting functions.

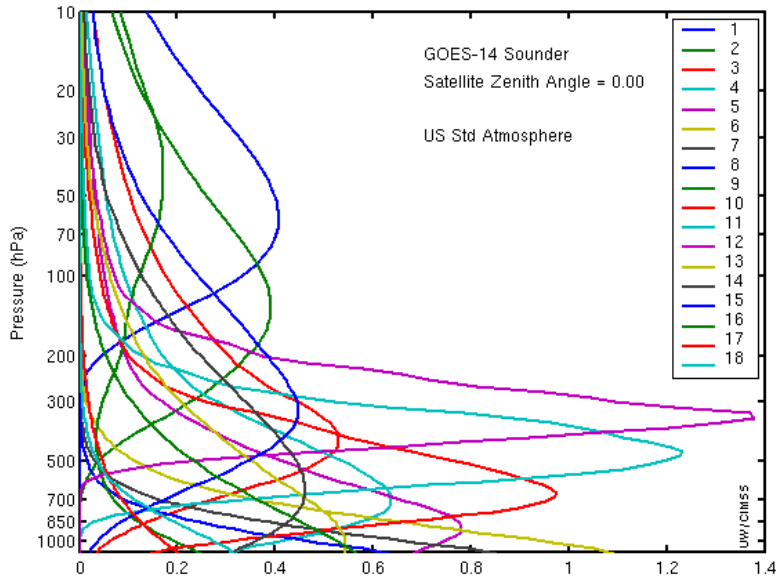

Figure 3.2: The GOES-14 Sounder weighting functions.

4. GOES Data Quality

4.1. First Images

The first step to ensure quality products is to verify the quality of the radiances that are used as inputs to the product generation.

4.1.1. Visible

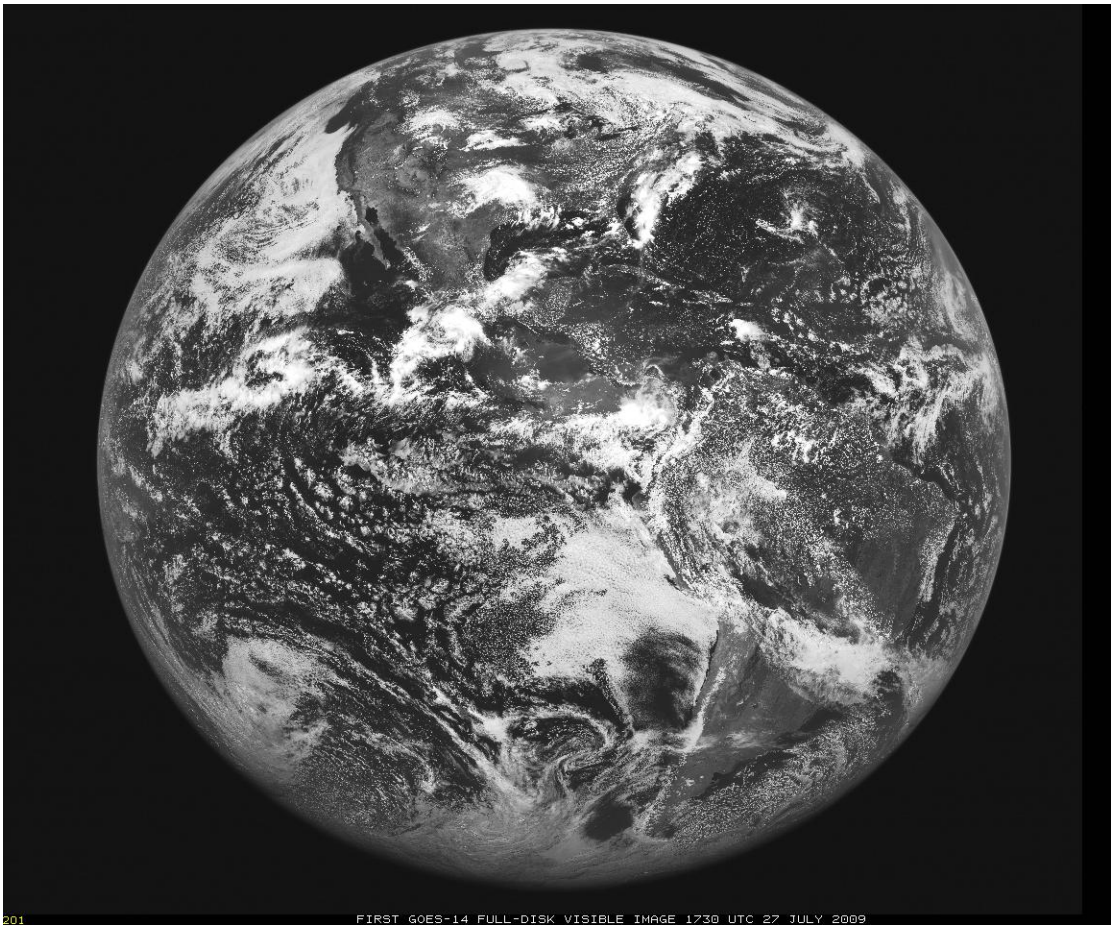

Figure 4.1: The first visible (0.63 µm) image from the GOES-14 Imager occurred on 27 July 2009 starting at 1730 UTC.

Figure 4.2: A GOES-14 close-up view centered over central California showed marine fog and stratus adjacent to the Pacific Coast, with cumulus clouds developing inland over the higher terrain of the Sierra Nevada.

4.1.2. Infrared (IR)

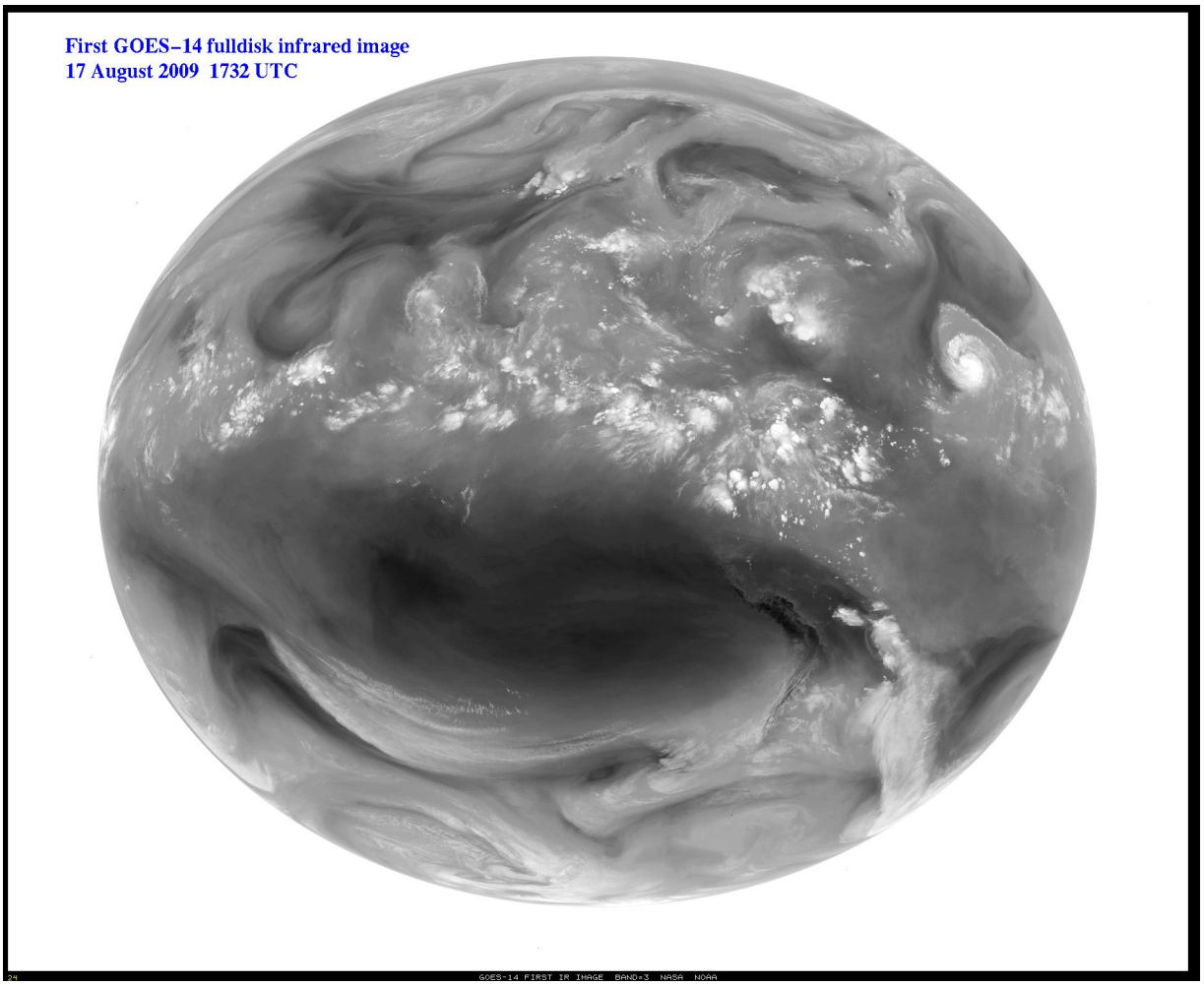

Figure 4.3: GOES-14 full-disk image for "water vapor" band (band-3, 6.5 μm) from 17 August 2009 starting at 1732 UTC.

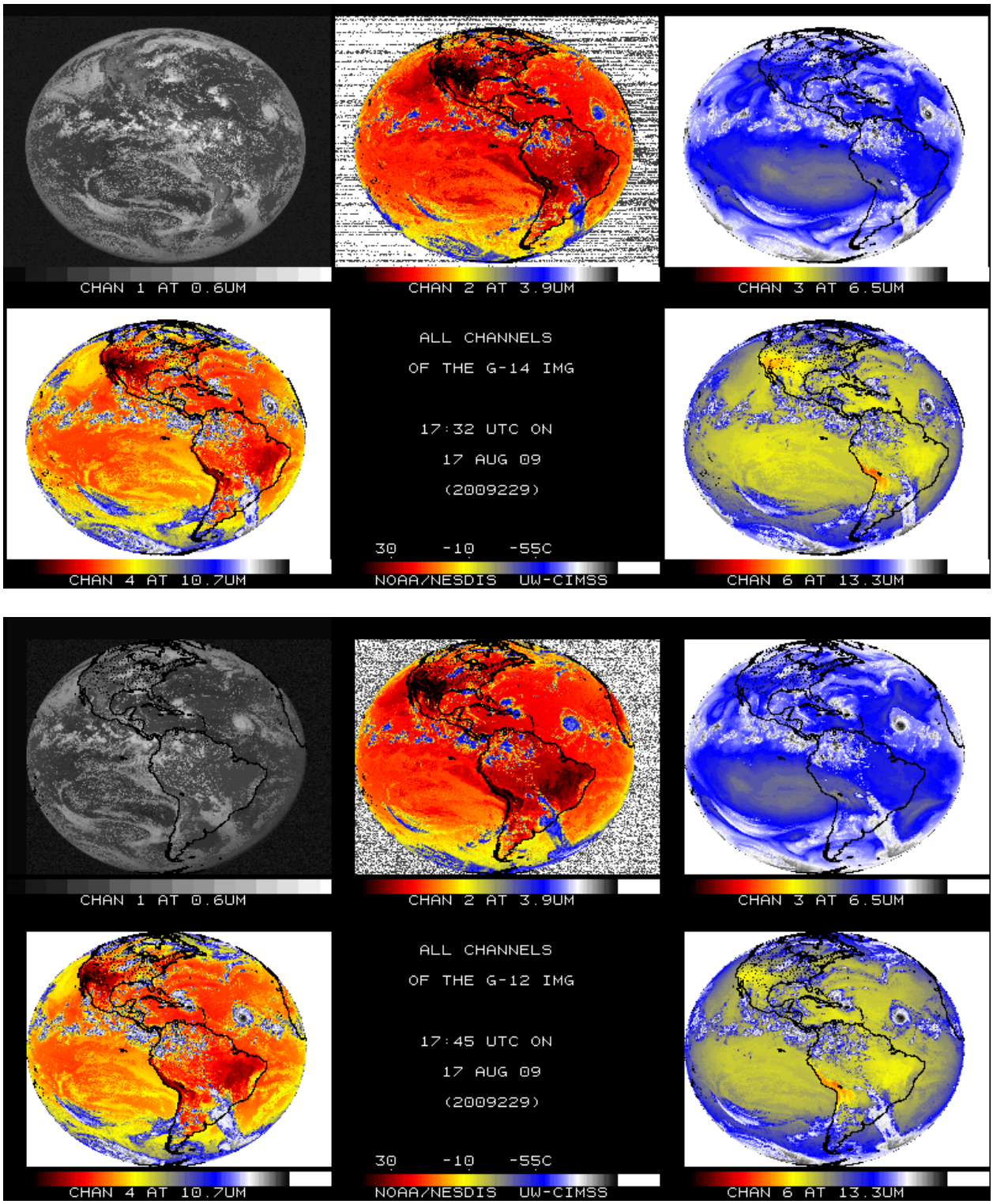

Figure 4.4: GOES-14 Imager bands (top) and the corresponding GOES-12 Imager bands (bottom). Both sets of images are shown in their native projections.

The images in Figure 4.4 have been sub-sampled. The sub-sampling is necessary, in part, due to the fact that the first GOES-14 Imager full disk images were too wide.

4.1.3. Sounder

The first GOES-14 Sounder images showed good qualitative agreement with GOES-12.

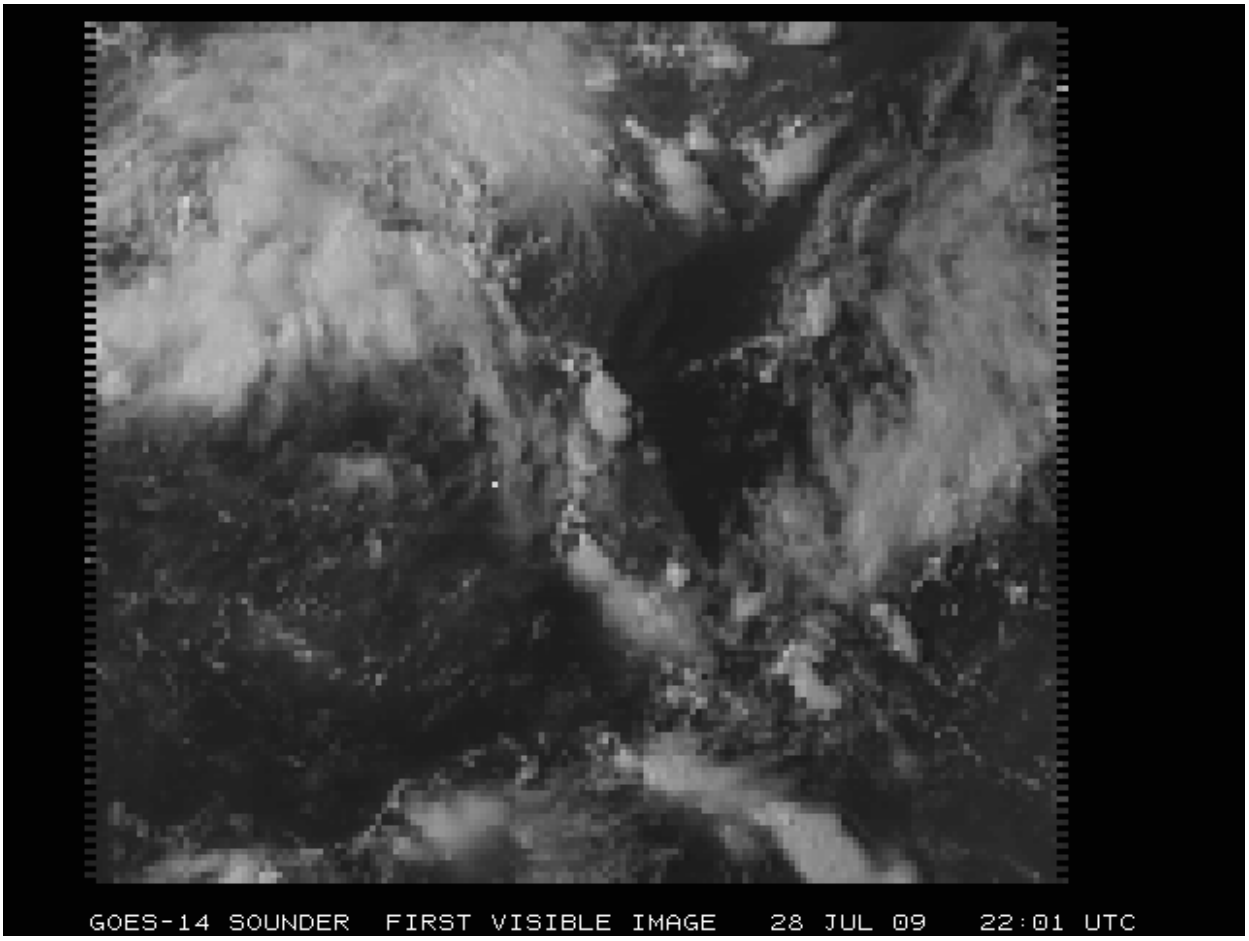

Figure 4.5: The visible (band-19) image from the GOES-14 Sounder shows data from 28 July 2009. The west and east 'saw-tooth' edges are due to the geometry of collecting the pixels.

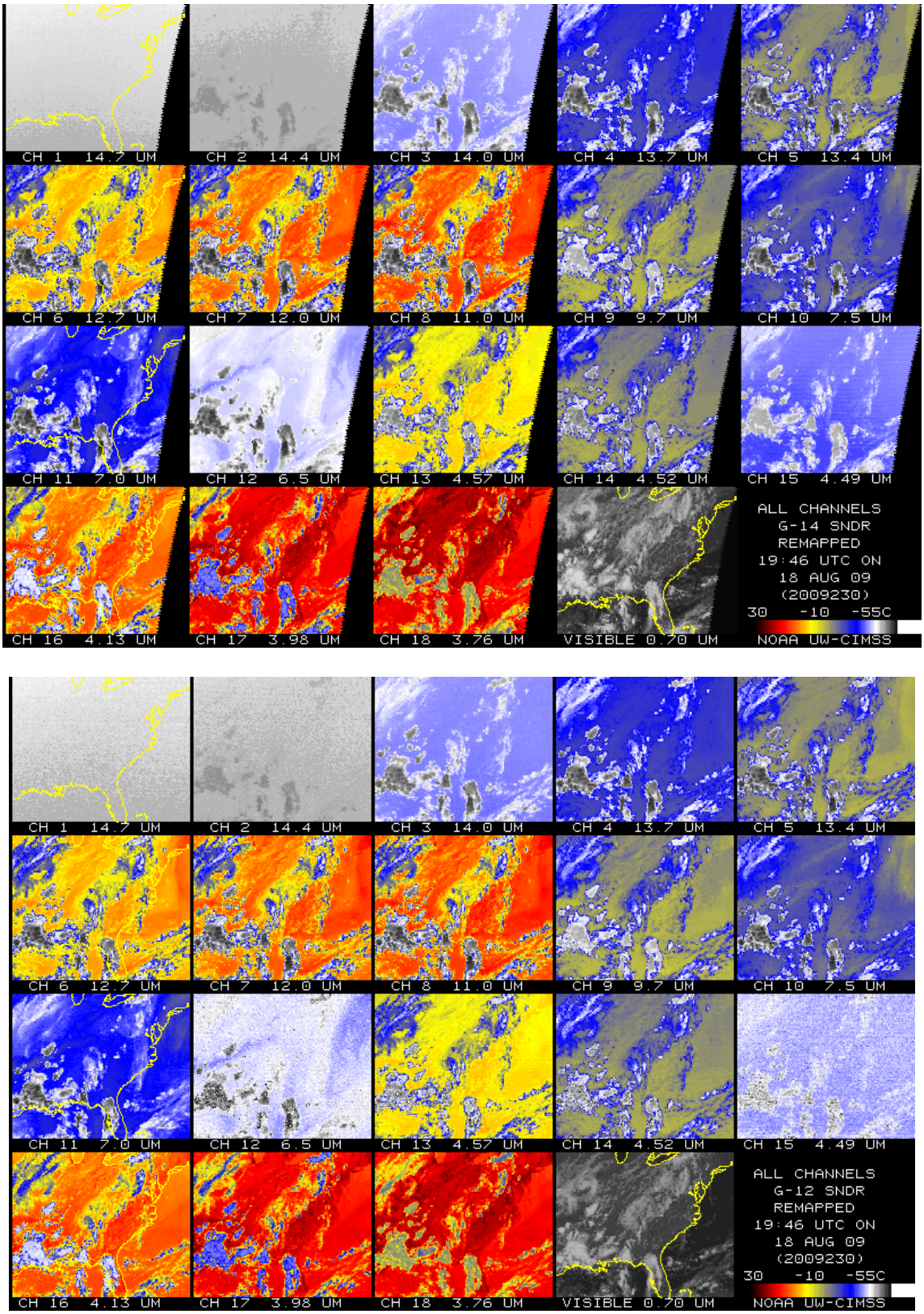

Figure 4.6: The first IR Sounder images for GOES-14 from 18 August 2009 (top) compared to GOES-12 (bottom). Both sets of images have been remapped to a common projection. Note the less noisy Sounder band-15 (4.6 µm).

4.2. Spectral Response Functions (SRFs)

4.2.1. Imager

The GOES spectral response functions (SRFs) for the GOES series Imagers can be found at http://www.oso.noaa.gov/goes/goes-calibration/goes-imager-srfs.htm and are plotted in Figure 4.7. Note that there are currently two versions (Revision D and E) on the GOES-14 Imager SRF. The GOES-14 Imager is spectrally similar to the GOES-12 Imager, in that it has the spectrally-wide 'water vapor' band. Information about the GOES calibration can be found in Weinreb et al. (1997).

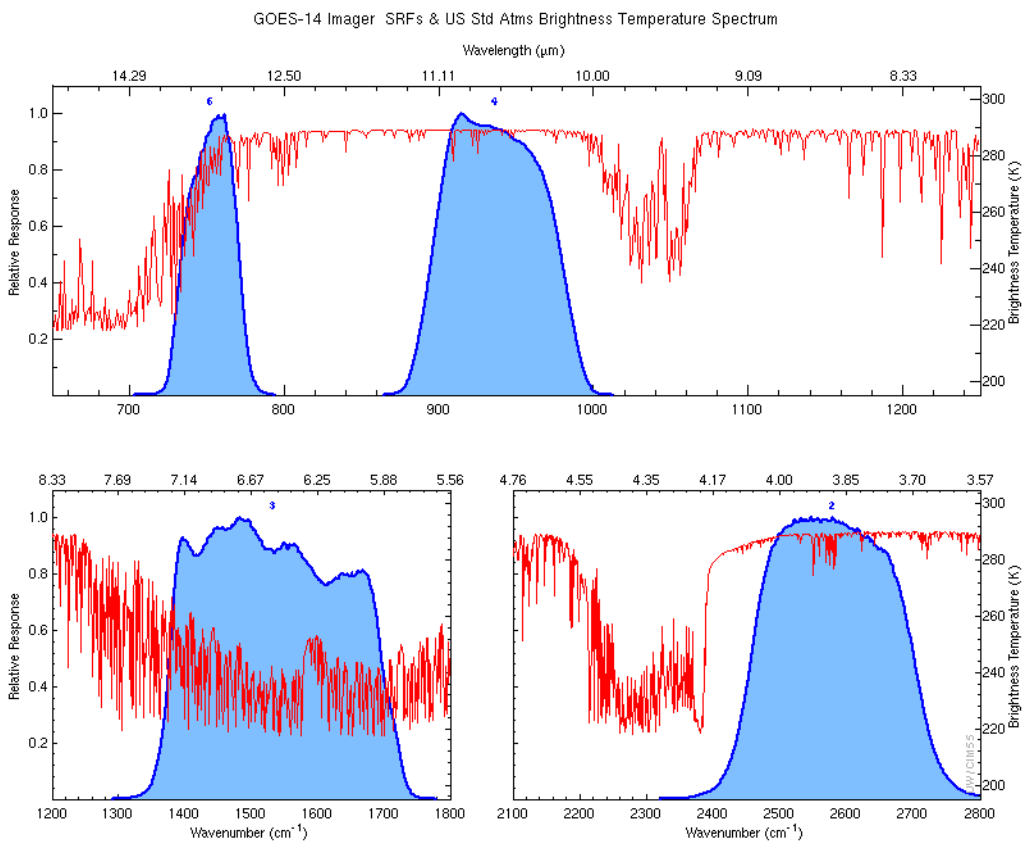

Figure 4.7: The four GOES-14 Imager IR band SRFs super-imposed over the calculated high-resolution earth-emitted U.S. Standard Atmosphere spectrum. Absorption due to carbon dioxide (CO_2), water vapor (H_2O), and other gases are evident in the high-spectral resolution earth-emitted spectrum.

4.2.2. Sounder

The GOES SRFs for the GOES series Sounders can be found at http://www.oso.noaa.gov/goes/goes-calibration/goes-sounder-srfs.htm and are plotted in Figure 4.8. The GOES-14 Sounder also has a Revision F of the SRF. The overall band selection is unchanged from previous GOES Sounders (Schmit et al. 2002b). As before, the carbon dioxide

(CO_2), ozone (O_3), and water vapor (H_2O) absorption bands are indicated in the calculated high-spectral resolution earth-emitted U.S. Standard Atmosphere spectrum. The central wavenumbers (wavelengths) of the spectral bands range from 680 cm^{-1} (14.7 μm) to 2667 cm^{-1} (3.75 μm) (Menzel et al. 1998).

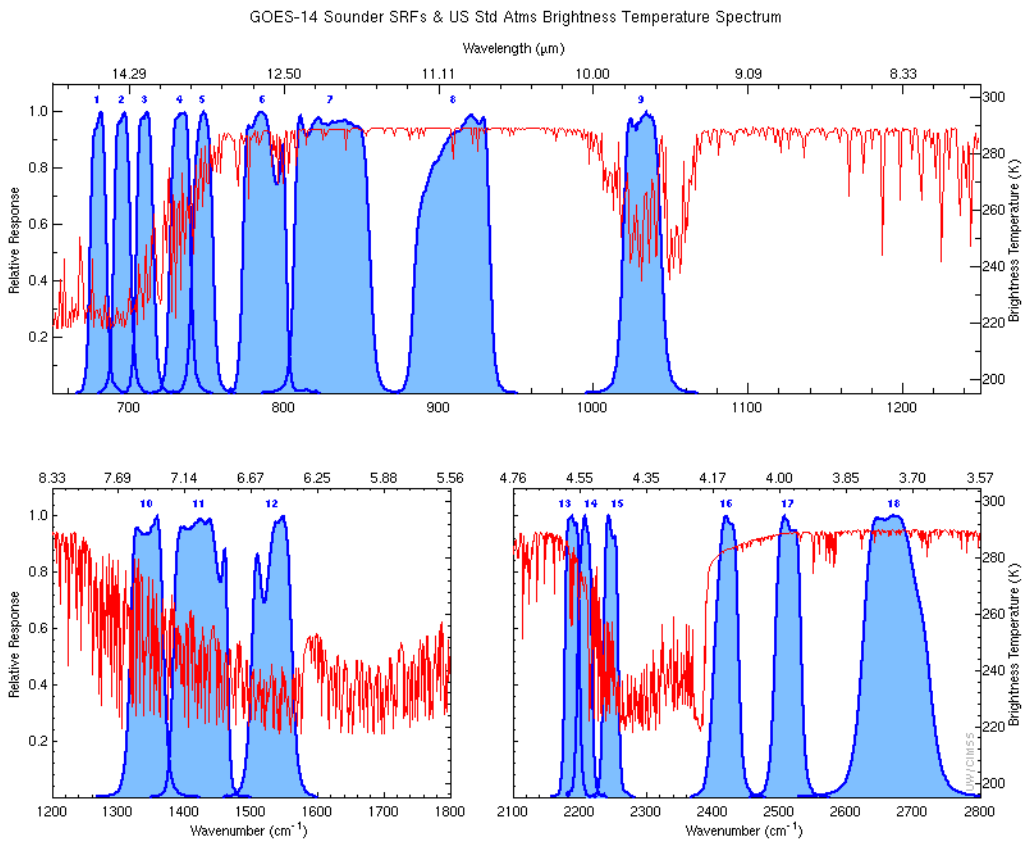

Figure 4.8: The eighteen GOES-14 Sounder IR band SRFs (Rev A.) super-imposed over the calculated high-resolution earth-emitted U.S. Standard Atmosphere spectrum.

4.3. Random Noise Estimates

Band noise estimates for the GOES-14 Imager and Sounder were computed using two different approaches. In the first approach, the band noise levels were determined by calculating the variance (and standard deviation) of radiance values in a space-look scene. The second approach involved performing a spatial structure analysis (Hillger and Vonder Haar, 1988). Both approaches yielded nearly identical band noise estimates. Results of the both approaches are presented below.

4.3.1. Imager

Full-disk images for the Imager provided off-earth space views and allowed noise levels to be determined. Estimated noise levels for the GOES-14 Imager were averaged over time for both

east and west-limb space views for 24 hours of data starting at 1645 UTC on 28 December 2009 and ending at 1615 UTC on 29 December 2009. Results are presented in Table 4.1 in radiance units. The limb-averaged noise levels (second to last column) compared well with those from simpler variance (standard deviation) analysis (last column), the values of which were computed on a much smaller dataset.

Table 4.1: GOES-14 Imager Noise Levels

(In radiance units, from 24 hours of limb/space views on Julian days 362-363).

Imager Band	Central Wavelength (µm)	East Limb	West Limb	Limb Average	Variance Analysis
		mW/(m^2·sr·cm^{-1})			
2	3.9	0.0020	0.0021	**0.0020**	0.0020
3	6.5	0.023	0.024	**0.023**	0.022
4	10.7	0.10	0.10	**0.10**	0.10
6	13.3	0.19	0.19	**0.19**	0.19

A further comparison of the noise levels from the GOES-14 Imager with those from previous GOES Imagers is presented in Table 4.2. In this table the noise levels are given in temperature units. In general, noise levels were much improved over those for older GOES, with both GOES-13 and 14 in particular having lower noise in most bands than GOES-8 through 12.

Keep in mind as well, the decrease in the pixel size for band-6 images (from 4 km to 2 km) on GOES-14 compared to GOES-13 could be expected to result in an increase in noise in that band. But the noise level for GOES-14 band-6 is only slightly higher than it was for GOES-13.

Table 4.2: Summary of the Noise for GOES-8 through GOES-14 Imager Bands

(In temperature units; the Specification (SPEC) values are also listed).

Imager Band	Central Wavelength (µm)	GOES -14	GOES-13	GOES-12	GOES-11	GOES-10	GOES-9	GOES-8	SPEC
		(K @ 300 K, except band-3 @ 230 K)							
2	3.9	**0.053**	0.051	0.13	0.14	0.17	0.08	0.16	1.40
3	6.5 / 6.7	**0.18**	0.14	0.15	0.22	0.09	0.15	0.27	1.00
4	10.7	**0.060**	0.053	0.11	0.08	0.20	0.07	0.12	0.35
5	12.0	**-**	-	-	0.20	0.24	0.14	0.20	0.35
6	13.3	**0.11**	0.061	0.19	-	-	-	-	0.32

Band noise estimates for the GOES-14 Imager **visible** band were also monitored at the GOES-14 Instrument Performance Monitoring (IPM) system with the variance of the pre-clamp and post-clamp space-look count data embedded in the GVAR B11. Figure 4.9 shows the mean pre-clamp and post-clamp space-look count variance of the GOES-14 Imager in December 2009, compared with those of the GOES-13 data in February 2010, and GOES-11 and 12 data in December 2009. As shown in this figure, the visible band noise level is very similar in GOES-13 and GOES-14, which is greatly improved over earlier GOES satellites. Except for the diurnal variations, there is no significant long-term change in space-look variance during the GOES-14 PLT test period (Figure 4.10). Both the pre-clamp and post-clamp space count variance shows that the noise level reaches the peak at night around 1200 UTC. Same with the pre-clamp space-look monitoring, occasional zero values also observed at the pre-clamp space-look variances which are associated with a not-used 9.2-s scan clamp. These zero values do not impact the operational calibration accuracy (Weinreb and Mitchell, 2010).

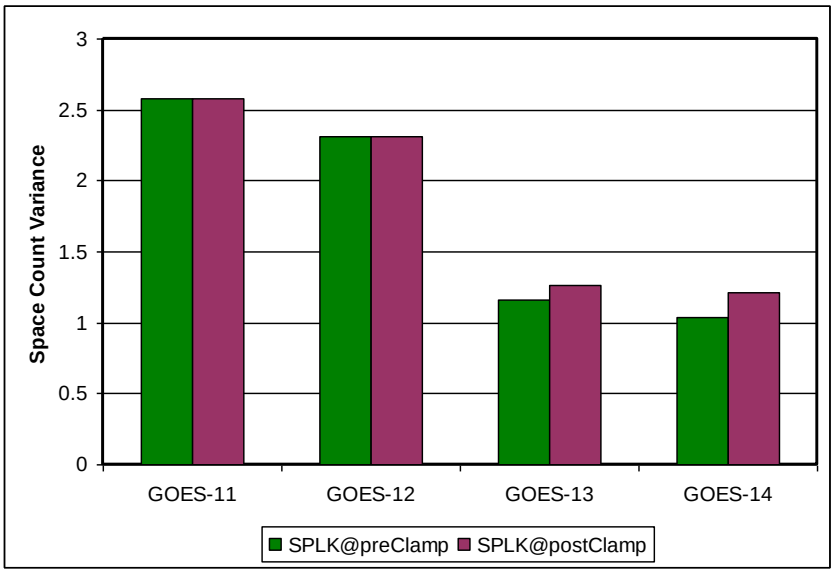

Figure 4.9: Variance of pre-clamp and post-clamp space-look scan count for GOES-14, compared with those for GOES-11/12/13.

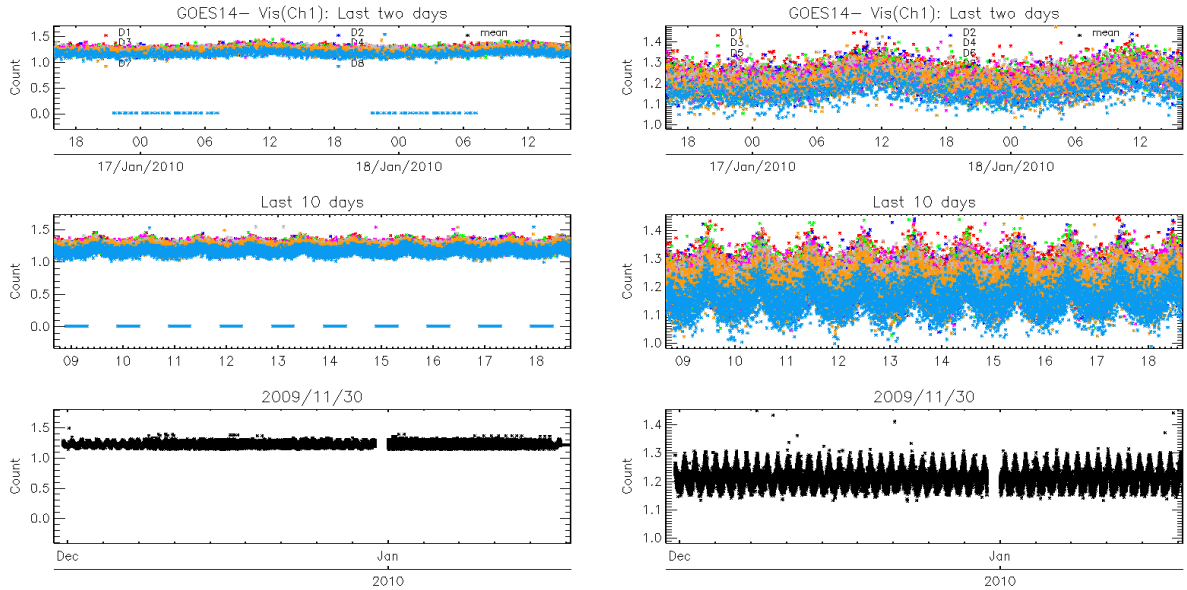

Figure 4.10: Time-series of the variance of GOES-14 Imager pre-clamp and post-clamp space-look scan at three temporal scales. Top: 2-day period with 8 detector data, middle: 10-day period with 8 detector data, and bottom: mean values from 30 November 2009 through 19 January 2010.

The noise in the GOES-14 IR bands was monitored using Noise Equivalent delta Radiance (NEdR) and Noise Equivalent delta Temperature (NEdT) of blackbody scan data with the GOES IPM system (Figure 4.11). GOES-14 Imager IR band noise in temperature units is compared to the rest of the GOES series (GOES-8 through GOES-13) in Table 4.3. GOES-14 seems to have larger noise level for all the IR bands expect for band-2. But all the IR band noise is comparable with the other satellite IR bands which are all within the specifications. There is slight diurnal variation in the NEdT values for each IR band, with the highest values around 1200 UTC. This diurnal variation appears to be unique to GOES-14 and may suggest a loose lens issue.

Table 4.3: Summary of the noise (in temperature units) for GOES-8 through GOES-14 Imager IR bands. The specification (SPEC) noise levels are also listed.

Imager Band	Central wave-length (µm)	GOES-14	GOES-13	GOES-12	GOES-11	GOES-10	GOES-9	GOES-8	SPEC
		K @ 300 K, except band-3 @ 230 K							
2	**3.9**	0.057	0.059	0.102	0.123	0.090	0.094	0.092	1.4
3	**6.5/6.7**	0.197	0.170	0.149	0.265	0.149	0.134	0.160	1.0
4	**10.7**	0.051	0.045	0.073	0.073	0.061	0.055	0.173	0.35
5	**12.0**				0.176	0.112	0.123	0.172	0.35
6	**13.3**	0.106	0.067	0.102					0.32

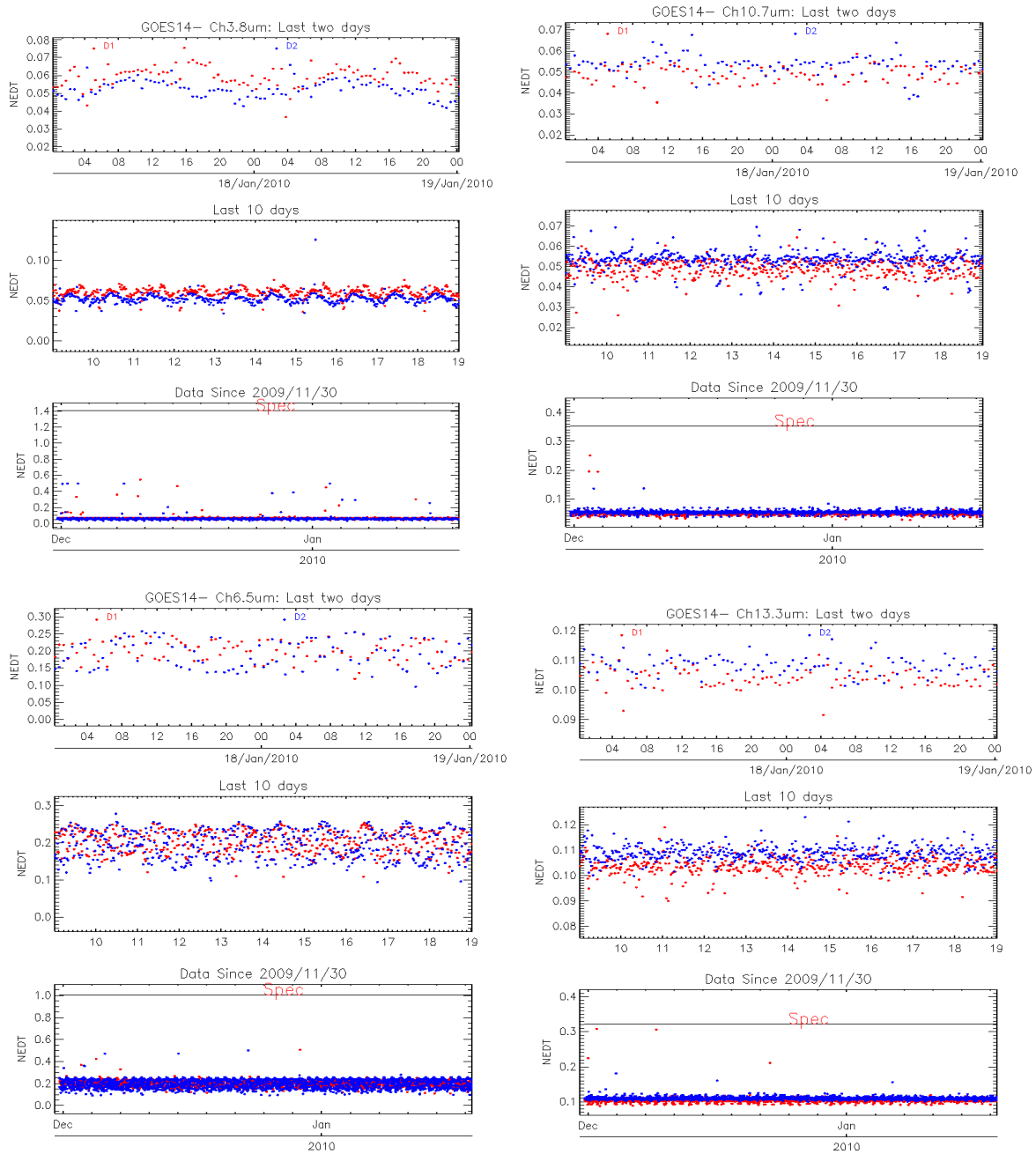

Figure 4.11: GOES-14 Imager NEdT calculated at 300 K temperature, except band-3 at 230 K, compared to the specifications.

4.3.2. Sounder

Special GOES-14 limb-view Sounder sectors allow noise values to be determined by the scatter of radiance values looking at uniform off-earth space views. Noise values were computed for both west-limb and east-limb space-view data and averaged over the time period from 1630 UTC on 28 December 2009 through 1600 UTC on 29 December 2009. The limb-averaged values in Table 4.4 (second to last column) compare well to those from a simpler variance analysis (last column).

Table 4.4: GOES-14 Sounder Noise Levels

(In radiance units, from 24 hours of limb/space views on Julian days 335-336).

Sounder Band	Central Wavelength (µm)	East Limb	West Limb	Limb Average	Variance Analysis
		mW/(m^2·sr·cm^{-1})			
1	14.71	0.29	0.29	**0.29**	0.33
2	14.37	0.24	0.24	**0.24**	0.28
3	14.06	0.21	0.21	**0.21**	0.22
4	13.64	0.16	0.16	**0.16**	0.17
5	13.37	0.15	0.15	**0.15**	0.16
6	12.66	0.075	0.071	**0.073**	0.098
7	12.02	0.056	0.050	**0.053**	0.080
8	11.03	0.072	0.079	**0.076**	0.110
9	9.71	0.066	0.069	**0.068**	0.090
10	7.43	0.038	0.039	**0.039**	0.040
11	7.02	0.024	0.025	**0.025**	0.030
12	6.51	0.028	0.029	**0.029**	0.030
13	4.57	0.0034	0.0035	**0.0035**	0.003
14	4.52	0.0035	0.0035	**0.0035**	0.003
15	4.46	0.0034	0.0033	**0.0033**	0.003
16	4.13	0.0019	0.0020	**0.0019**	0.002
17	3.98	0.0015	0.0016	**0.0016**	0.002
18	3.74	0.00074	0.00074	**0.00074**	0.001

A further comparison of the noise levels for the GOES-14 Sounder with those from previous GOES Sounders is presented in Table 4.5. Noise levels are in general much improved over those for older GOES, with both GOES-13 and 14 in particular having lower noise in most bands than GOES-8 through 12.

Table 4.5: Summary of the Noise for GOES-8 through GOES-14 Sounder Bands

(In radiance units; the Specification (SPEC) values are also listed).

Sounder Band	Central Wavelength (µm)	GOES-14	GOES-13	GOES-12	GOES-11	GOES-10	GOES-9	GOES-8	SPEC
		$mW/(m^2 \cdot sr \cdot cm^{-1})$							
1	14.71	**0.29**	0.32	0.77	0.67	0.71	1.16	1.76	0.66
2	14.37	**0.24**	0.25	0.61	0.51	0.51	0.80	1.21	0.58
3	14.06	**0.21**	0.23	0.45	0.37	0.41	0.56	0.98	0.54
4	13.64	**0.16**	0.18	0.39	0.36	0.41	0.46	0.74	0.45
5	13.37	**0.15**	0.18	0.34	0.34	0.36	0.45	0.68	0.44
6	12.66	**0.073**	0.095	0.14	0.17	0.16	0.19	0.32	0.25
7	12.02	**0.053**	0.086	0.11	0.11	0.09	0.13	0.20	0.16
8	11.03	**0.076**	0.10	0.11	0.14	0.12	0.09	0.13	0.16
9	9.71	**0.068**	0.11	0.14	0.13	0.10	0.11	0.16	0.33
10	7.43	**0.039**	0.081	0.099	0.09	0.07	0.08	0.08	0.16
11	7.02	**0.025**	0.046	0.059	0.06	0.04	0.05	0.07	0.12
12	6.51	**0.029**	0.063	0.11	0.11	0.07	0.09	0.11	0.15
13	4.57	**0.0035**	0.0061	0.0062	0.006	0.007	0.008	0.012	0.013
14	4.52	**0.0035**	0.0064	0.0062	0.007	0.005	0.007	0.010	0.013
15	4.46	**0.0033**	0.0055	0.0066	0.006	0.005	0.006	0.009	0.013
16	4.13	**0.0019**	0.0030	0.0024	0.003	0.003	0.003	0.004	0.008
17	3.98	**0.0016**	0.0026	0.0022	0.003	0.002	0.003	0.004	0.008
18	3.74	**0.00074**	0.0011	0.00094	0.001	0.001	0.001	0.002	0.004

Band noise estimates for the GOES-14 Sounder were also monitored at the GOES-14 IPM system.

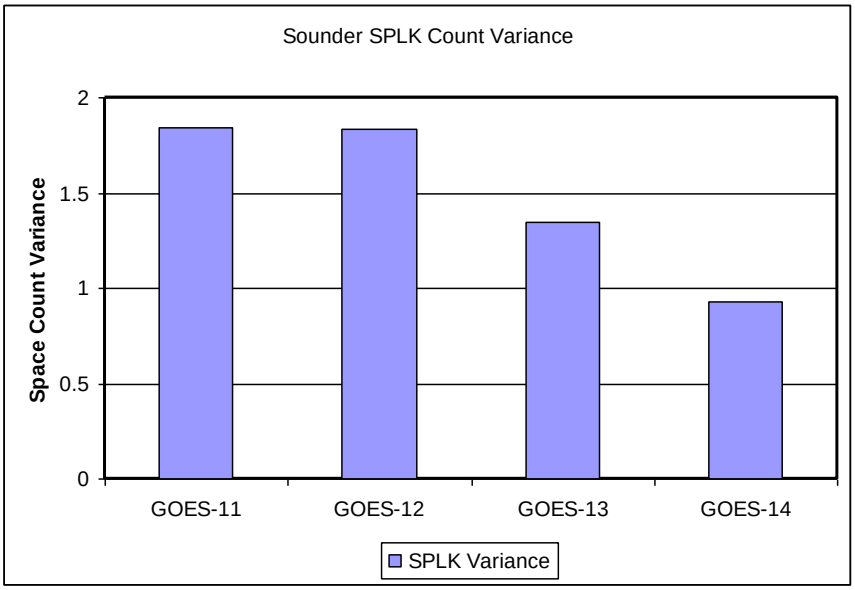

Figure 4.12: GOES-14 Sounder noise values (space-look count variance) compared to those from GOES-11/12/13.

GOES-14 Sounder noise was monitored with NEdR and NEdT at blackbody scan with measured blackbody temperature, and the results are also available at the GOES-14 IPM Web page. Tables 4.6 and 4.7 summarize the noise levels for GOES-8 through GOES-14. The GOES-14 Sounder noise levels are improved compared to previous GOES Sounders.

Table 4.6: GOES-14 Sounder NEdR compared to those from GOES-8 through GOES-13 and the specification noise values.

Sounder Band	Central Wave-length (µm)	GOES-14	GOES-13	GOES-12	GOES-11	GOES-10	GOES-9	GOES-8	SPEC
		mW/(m^2·sr·cm^{-1})							
1	14.71	0.268	0.288	0.326	0.300	0.645	0.563	0.998	0.66
2	14.37	0.221	0.230	0.282	0.247	0.441	0.455	0.755	0.58
3	14.06	0.188	0.211	0.221	0.186	0.347	0.344	0.685	0.54
4	13.64	0.142	0.167	0.200	0.179	0.360	0.294	0.512	0.45
5	13.37	0.141	0.169	0.185	0.175	0.338	0.275	0.495	0.44
6	12.66	0.064	0.080	0.076	0.092	0.147	0.127	0.223	0.25
7	12.02	0.042	0.054	0.056	0.058	0.079	0.080	0.144	0.16
8	11.03	0.044	0.097	0.127	0.137	0.096	0.079	0.129	0.16
9	9.71	0.054	0.127	0.184	0.132	0.120	0.113	0.161	0.33
10	7.43	0.033	0.096	0.129	0.107	0.077	0.716	0.082	0.16
11	7.02	0.020	0.054	0.075	0.070	0.048	0.044	0.071	0.12
12	6.51	0.027	0.076	0.138	0.134	0.091	0.079	0.111	0.15
13	4.57	0.0028	0.0046	0.024	0.0045	0.006	0.006	0.008	0.013
14	4.52	0.0029	0.0049	0.023	0.0056	0.004	0.005	0.008	0.013
15	4.46	0.0025	0.0042	0.025	0.0044	0.004	0.005	0.008	0.013
16	4.13	0.0016	0.0023	0.009	0.0023	0.002	0.002	0.003	0.008
17	3.98	0.0013	0.0020	0.008	0.0021	0.002	0.002	0.002	0.008
18	3.74	<0.0001	<0.0001	0.0033	0.0010	<0.0001	0.001	0.002	0.004

Table 4.7: GOES-14 Sounder NEdT compared to those from GOES-8 through GOES-13.

Sounder Band	Central Wave-length (µm)	GOES -14	GOES -13	GOES -12	GOES -11	GOES -10	GOES -9	GOES-8
		K @ blackbody temperature						
1	14.71	0.158	0.170	0.193	0.178	0.383	0.333	0.591
2	14.37	0.129	0.135	0.165	0.147	0.259	0.267	0.443
3	14.06	0.109	0.123	0.128	0.108	0.201	0.199	0.398
4	13.64	0.082	0.096	0.115	0.103	0.208	0.169	0.295
5	13.37	0.081	0.097	0.106	0.100	0.194	0.158	0.283
6	12.66	0.036	0.046	0.043	0.053	0.084	0.072	0.127
7	12.02	0.024	0.031	0.032	0.033	0.045	0.046	0.082
8	11.03	0.026	0.057	0.074	0.081	0.056	0.047	0.076
9	9.71	0.035	0.082	0.118	0.104	0.077	0.072	0.103
10	7.43	0.034	0.097	0.130	0.108	0.078	0.071	0.082
11	7.02	0.023	0.063	0.088	0.083	0.056	0.052	0.084
12	6.51	0.039	0.112	0.206	0.201	0.135	0.116	0.165
13	4.57	0.023	0.038	0.195	0.038	0.047	0.045	0.084
14	4.52	0.026	0.043	0.205	0.050	0.035	0.046	0.067
15	4.46	0.025	0.042	0.248	0.043	0.037	0.046	0.075
16	4.13	0.027	0.038	0.147	0.040	0.038	0.039	0.056
17	3.98	0.028	0.045	0.186	0.047	0.042	0.054	0.085
18	3.74	<0.001	<0.001	0.119	0.037	<0.001	0.038	0.064

4.4. Striping Due to Multiple Detectors

For the GOES Imager there are two detectors per spectral band, and for the GOES Sounder, there are four detectors for each spectral band. Differences between the measurements in these detectors can cause striping in GOES images. Striping becomes more obvious as random noise decreases, allowing the striping to dominate the random noise. Striping is defined as the difference between the average values for each detector from the average value in all detectors.

4.4.1. Imager

Full-disk images from the Imager provide off-earth space views, allowing both noise levels (reported above) and detector-to-detector striping to be determined in an otherwise constant signal situation. Table 4.8 gives estimates of GOES-14 Imager detector-to-detector striping for a 24 hour period starting at 1645 UTC on 28 December 2009 through 1615 UTC on 29 December 2009. Striping was computed from off-earth space-view measurements on each side of the earth (columns 3 and 4). The limb averages (third to last column) are then determined and compared to the noise level (second to last column). A ratio of striping to noise is also computed (last column). Ratios greater than 1 indicate that the striping is larger than the noise. Because the noise has decreased with the latest GOES series, the striping is more obvious than for earlier GOES, as will be seen in some of the images presented later in this report.

Table 4.8: GOES-14 Imager Detector-to-Detector Striping

(In radiance units, from 24 hours of limb/space views on Julian days 362-363).

Imager Band	Central Wavelength (µm)	East Limb	West Limb	Limb Average	Noise	Striping/Noise Ratio
		mW/(m^2·sr·cm^{-1})				
2	3.9	0.0061	0.0077	**0.0069**	0.0020	**3.5**
3	6.5 / 6.7	0.060	0.074	**0.067**	0.023	**2.9**
4	10.7	0.18	0.090	**0.14**	0.10	**1.4**
6	13.3	0.67	0.24	**0.46**	0.19	**2.4**

4.4.2. Sounder

Detector-to-detector striping for the Sounder is documented in Table 4.9 from measurements taken from the same off-earth space-view sectors used for the noise analysis for the Sounder, 1630 UTC on 1 December 2009 through 1600 UTC on 2 December 2009. The limb-averaged values (third from last column) are compared to the noise levels (second to last column), with the ratio of striping to noise in the last column. Values larger than one (sometimes much larger), indicate that striping is much more significant than noise for several of the Sounder bands. The largest ratios, for the longwave IR bands, do not mean that striping is obvious in the images from these bands, because the inherent signal is also very large in these window bands.

Table 4.9: GOES-14 Sounder Detector-to-Detector Striping

(In radiance units, from 24 hours of limb/space views on Julian days 335-336).

Sounder Band	Central Wavelength (µm)	East Limb	West Limb	Limb Average	Noise	Striping/Noise Ratio
		mW/(m^2·sr·cm^{-1})				
1	14.71	0.51	0.74	**0.63**	0.29	**2.2**
2	14.37	0.47	0.64	**0.56**	0.24	**2.3**
3	14.06	0.71	0.76	**0.74**	0.21	**3.5**
4	13.64	0.78	0.89	**0.84**	0.16	**5.2**
5	13.37	0.79	1.07	**0.93**	0.15	**6.2**
6	12.66	1.11	1.20	**1.16**	0.073	**15.8**
7	12.02	1.03	1.16	**1.10**	0.053	**20.7**
8	11.03	1.17	0.95	**1.06**	0.076	**13.9**
9	9.71	0.50	0.44	**0.47**	0.068	**6.9**
10	7.43	0.19	0.16	**0.18**	0.039	**4.6**
11	7.02	0.12	0.091	**0.11**	0.025	**4.4**
12	6.51	0.041	0.035	**0.038**	0.029	**1.3**
13	4.57	0.012	0.0056	**0.0088**	0.0035	**2.5**

14	4.52	0.0054	0.0024	**0.0039**	0.0035	**1.1**
15	4.46	0.0027	0.0020	**0.0024**	0.0033	**0.7**
16	4.13	0.0075	0.0062	**0.0069**	0.0019	**3.6**
17	3.98	0.0078	0.0057	**0.0068**	0.0016	**4.2**
18	3.74	0.0048	0.0041	**0.0045**	0.00074	**6.1**

The GOES-14 Sounder exhibits discontinuous calibration slopes across many of the daily Housekeeping (HK) times. Outside of the discontinuity itself (which occurs between the pre- and post-Housekeeping blackbody/calibration events), the slopes usually display typical diurnal behavior throughout the rest of the day. Because of these discontinuous slopes, calibration M-mode=1 ('instantaneous' slopes) is used instead of M-mode=3 (diurnal averaging of slopes over multiple days) in Sensor Processing System (SPS) for processing the GOES-14 Sounder frames. It is postulated that the discontinuities are due to a loose lens or optical element.

However, on 14 January 2010 following the slope discontinuity at HK (~1834 UTC), the GOES-14 Sounder continued to display rapid slope changes lasting for a few hours. Other occurrences of rapid slope changes following GOES-14 HK have also been observed, although relatively rarely. Evidence of striping/banding in the GOES-14 Sounder earth-frames after the 14 January 2010 HK is attributable to these post-HK rapid slope changes.

Modified calibration procedures are being investigated to mitigate the effect of rapid slope changes on the radiances.

Figure 4.13 gives examples of GOES-14 band-11 for a time of less striping versus more striping.

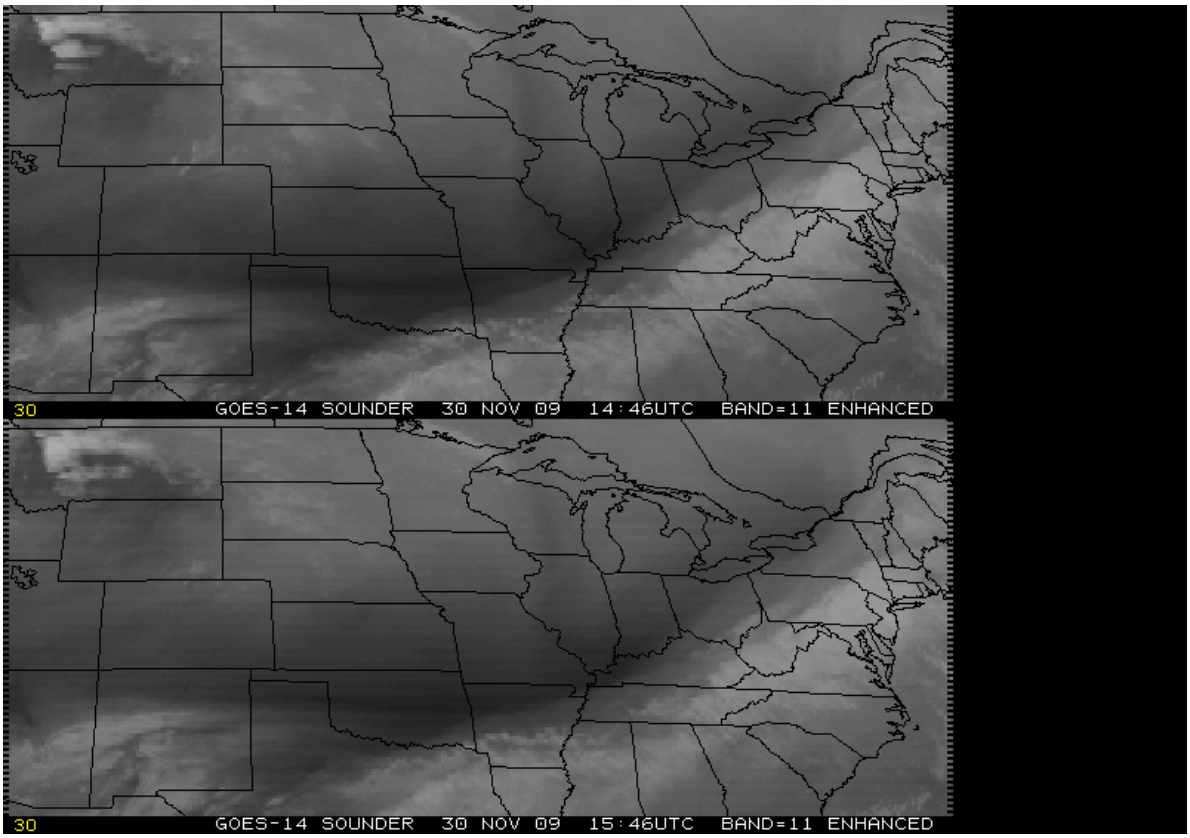

Figure 4.13: GOES-14 Sounder band-11 image, for a time of less striping (upper panel), and more striping (lower panel).

4.5. Imager-to-Imager Comparison

GOES-14 data were evaluated by comparing pixel temperatures of a 10 x 10 pixel box in a Mercator projection centered at 40˚N/90˚W for bands 2, 3, 4, and 6 to a similar domain on the operational GOES-East satellite (GOES-12). Comparisons were also performed with the operational GOES-West satellite (GOES-11) by comparing pixel temperatures of a 10 x 10 pixel box in a Mercator projection centered at 40˚N/120˚W for bands 2, 3, and 4. All results were plotted in a two-dimensional smoothed histogram approach which allows for a better representation of data in dense areas (Eilers and Goeman, 2004). Additionally, numerous statistics were calculated in order to determine the performance of the GOES-14 Imager bands compared to the respective Imager bands on GOES-11 and GOES-12.

GOES-East emulation testing began in SAB on 25 November 2009 and was completed on 19 January 2010. This testing period resulted in sample sizes of nearly 100,000 pixels for all bands tested. Figures 4.14 through 4.17 show two-dimensional smoothed histograms of GOES-12 vs. GOES-14 pixel temperatures taken from a 10 x 10 domain centered at 40˚N/90˚W for bands 2, 3, 4, and 6. The figures feature a dashed line representing the perfect fit line with numerous performance statistics included on the graphs. A nearly perfect correlation ($r > 0.98$) was observed between GOES-12 and GOES-14 pixel temperatures for all tested bands. On bands 2, 3, and 4 no significant biases were detected in the data. Mean Absolute Errors (MAE) were less than or equal to roughly 1 K for bands 3 and 4 and was around 1.7 K for band-2. For band-6 (see

Figure 4.17), SAB did note a modest bias of roughly 1.2 K where GOES-14 pixel temperatures were warmer than corresponding GOES-12 pixel temperatures. MAEs for those pixels was around 1.5 K. The increased spatial resolution of band-6 data on GOES-14 could be the primary reason for the observed differences. Root Mean Square Errors (RMSE) compared favorably to their respective MAEs on bands 3 and 6 while differences of over 0.8 K were noted on bands 2 and 4. RMSEs place more emphasis on large errors (Jolliffe and Stephenson, 2003), suggesting there were several cases of large differences between band-2 and 4 pixels on GOES-12 and GOES-14. These cases were manually investigated and most were determined to be a function of slight navigational errors near cloud edges.

GOES-West emulation testing began in SAB on 22 December 2009 and was completed on 14 January 2010. The shorter testing period resulted in much smaller sample sizes (~40,000 pixels) for bands 2 and 4. Additionally, scripting errors for band-3 data retrieval further limited the sample size (~12,000 pixels). Figures 4.18 through 4.20 show two-dimensional smoothed histograms of GOES-11 vs. GOES-14 pixel temperatures taken from a 10 x 10 domain centered at 40˚N/120˚W for bands 2, 3, and 4. Similar to the previous set of figures, they feature a dashed line representing the perfect fit line with numerous performance statistics included on the graphs. A high correlation ($r > 0.88$) was also observed between GOES-11 and GOES-14 data but it is noted that the correlation coefficients were much lower than what was observed between GOES-12 and GOES-14. For bands 2 and 4 no significant biases (~< 1.2 K) were detected with the data while band-3 did feature a rather large bias of ~2.6 K where GOES-14 pixels were warmer than the corresponding GOES-11 pixels. This rather large bias is mostly due to the different instrument spectral response functions for this band between the two imagers. Also, there is a limited sample size of band-3 data. MAEs were around 3.0 K for bands 2 and 3 and a very large 6 K for band-4. RMSE compared favorably to its respective MAE on band-3 data while the RMSEs for bands 2 and 4 data were nearly double their respective MAEs. This result suggests many large differences were observed between pixel temperatures of GOES-11 and GOES-14.

Since the performance statistics between GOES-11 and GOES-14 data featured much larger errors than what was observed between GOES-12 and GOES-14 data, a manual investigation was conducted to determine the source of the errors. It was determined that many, if not all, of the large errors were due to rather significant navigational differences between GOES-11 and GOES-14 data. An examination of land features surprisingly showed that GOES-11 data featured the superior navigation during these test time periods.

Quantitative testing of GOES-14 while in GOES-East emulation yielded a nearly perfect correlation between pixel temperatures of GOES-12 and GOES-14. Mean errors were generally within 1-2 K with little bias noted with the exception of band-6 data. Part of the observed differences may be explained by the finer horizontal resolution of band-6 data on the GOES-14 Imager. Also, others have compared this band to high-spectral resolution co-located Infrared Atmospheric Sounding Interferometer (IASI) and Atmospheric Infrared Sounder (AIRS) measurements and have shown a smaller bias than from GOES-12.

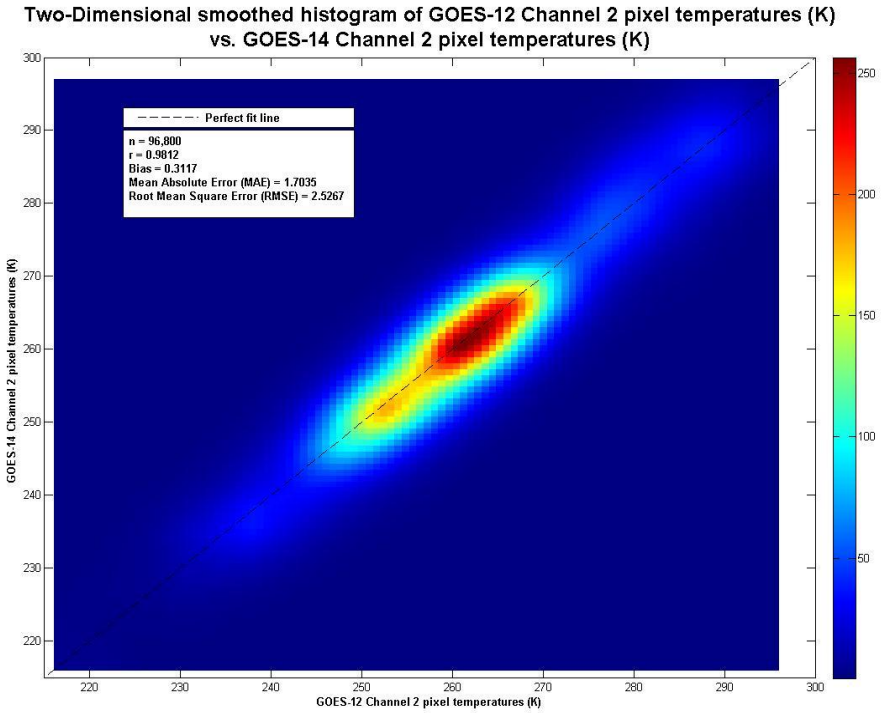

Figure 4.14: Two-dimensional smoothed histogram of GOES-12 band-2 pixel temperatures (K) vs. GOES-14 band-2 pixel temperatures.

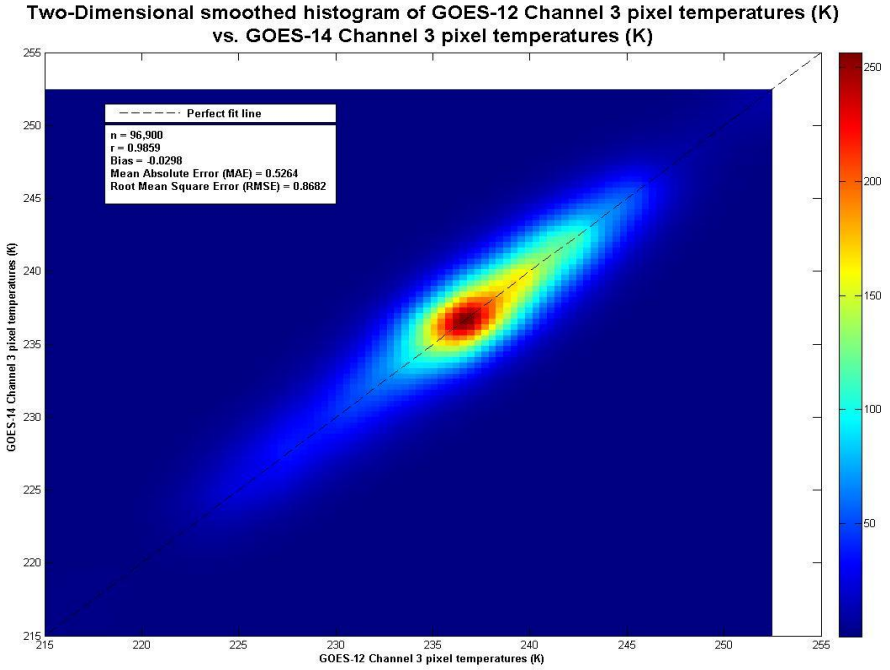

Figure 4.15: Two-dimensional smoothed histogram of GOES-12 band-3 pixel temperatures (K) vs. GOES-14 band-3 pixel temperatures (K).

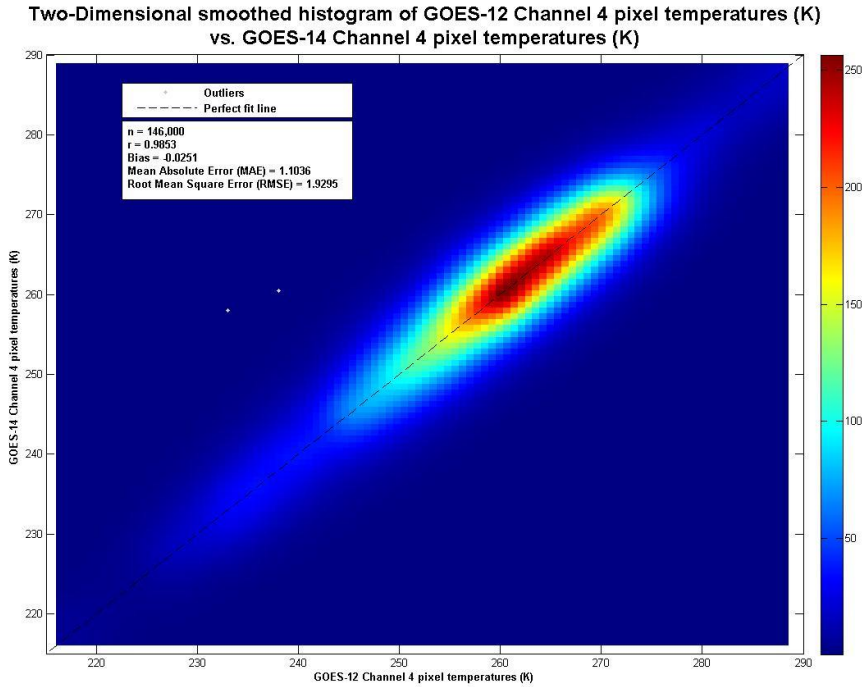

Figure 4.16: Two-dimensional smoothed histogram of GOES-12 band-4 pixel temperatures (K) vs. GOES-14 band-4 pixel temperatures (K).

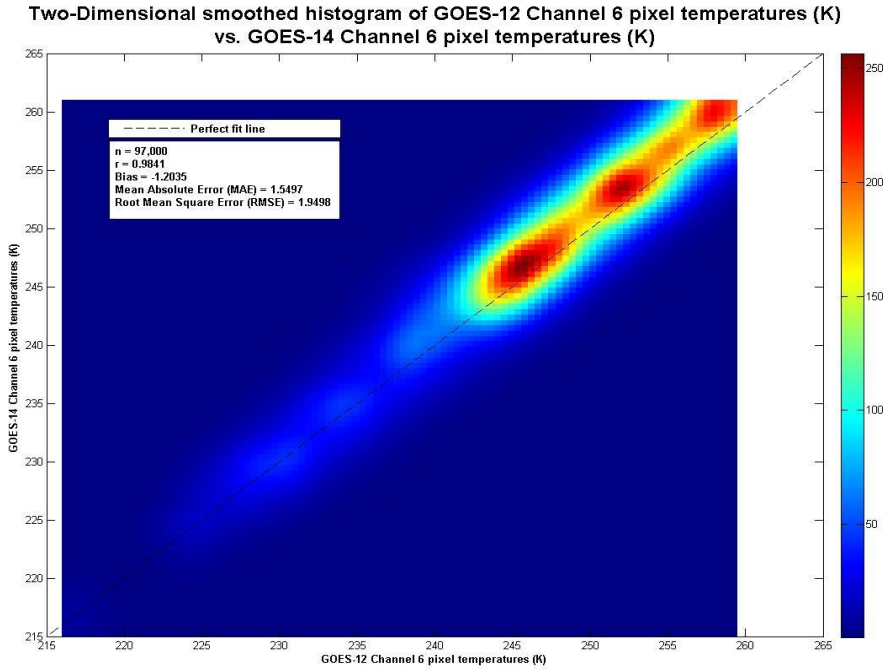

Figure 4.17: Two-dimensional smoothed histogram of GOES-12 band-6 pixel temperatures (K) vs. GOES-14 band-6 pixel temperatures (K).

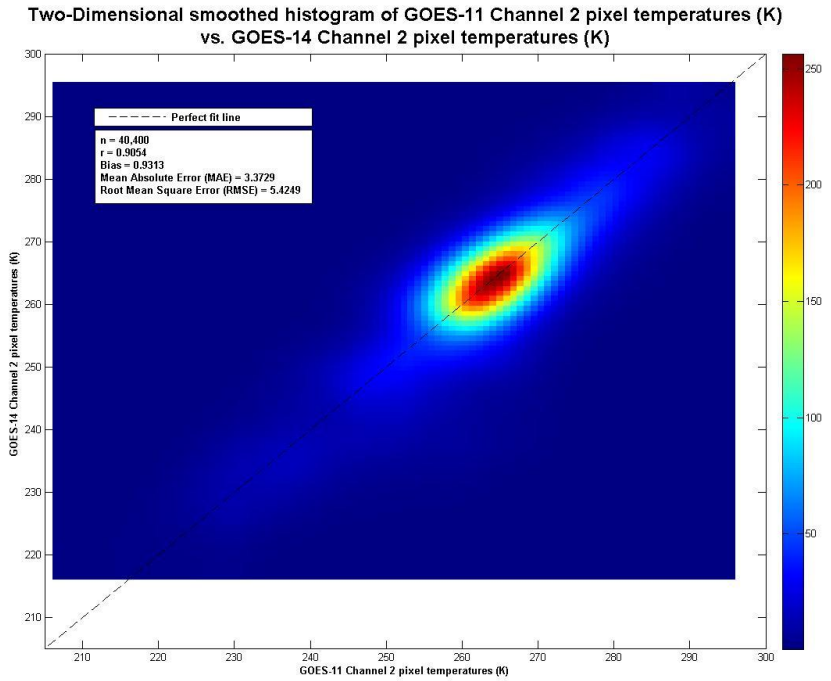

Figure 4.18: Two-dimensional smoothed histogram of GOES-11 band-2 pixel temperatures (K) vs. GOES-14 band-2 pixel temperatures (K).

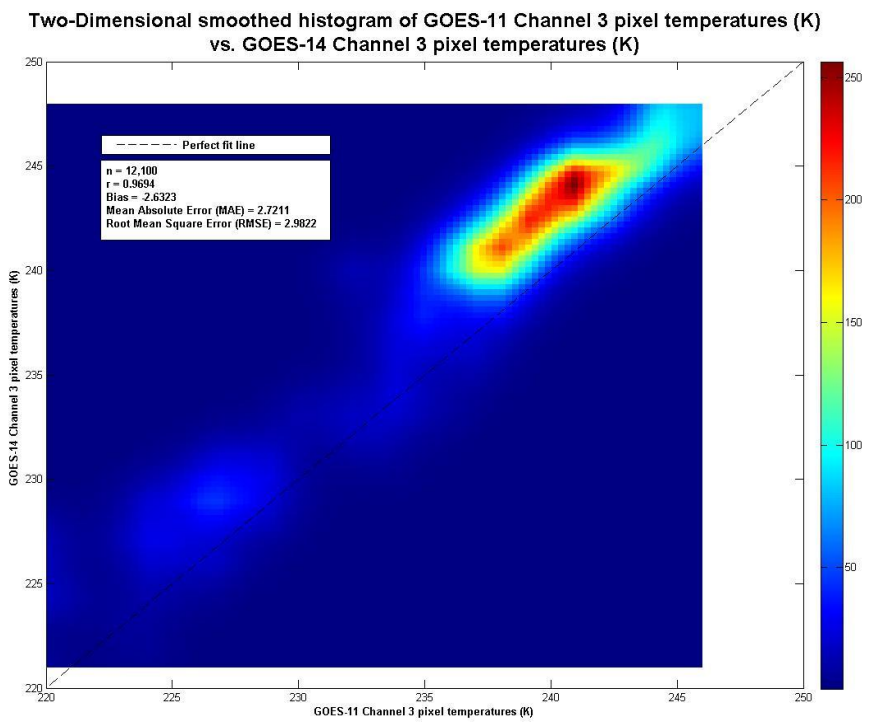

Figure 4.19: Two-dimensional smoothed histogram of GOES-11 band-3 pixel temperatures (K) vs. GOES-14 band-3 pixel temperatures (K).

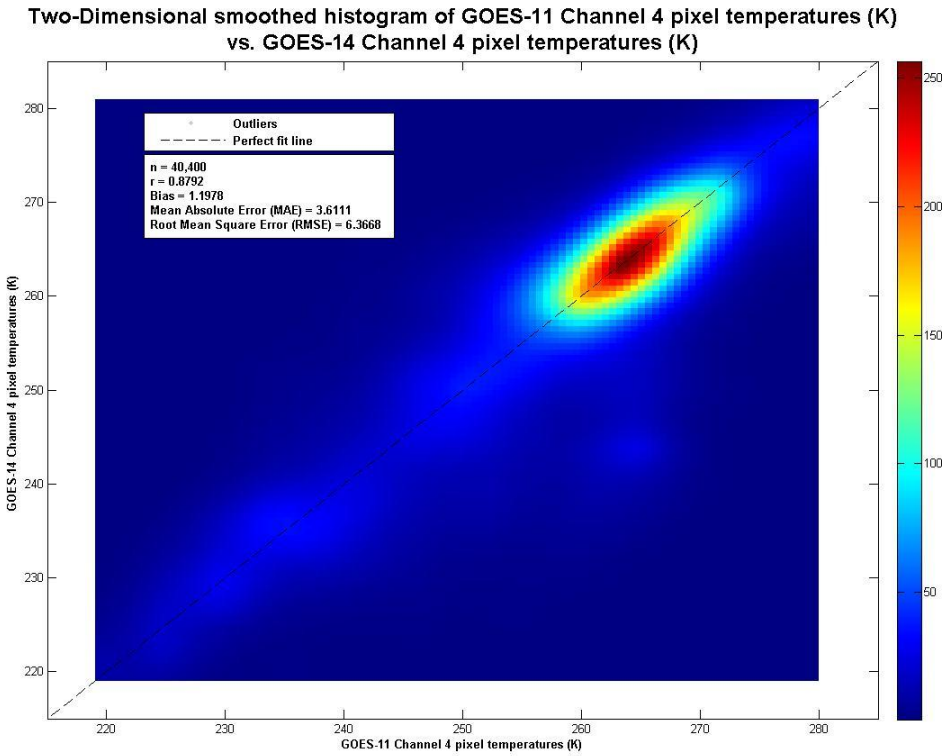

Figure 4.20: Two-dimensional smoothed histogram of GOES-11 band-4 pixel temperatures (K) vs. GOES-14 band-4 pixel temperatures (K).

4.6. Imager-to-Polar-Orbiter Comparisons

Data were collected during the checkout period near the GOES-14 sub-satellite point from the high spectral resolution IASI, polar-orbiting on EUMETSAT's MetOp-A satellite. GOES-14 Imager data were collected within 30 minutes of polar-orbiter overpass time. During the checkout period there were approximately 20 comparisons between GOES-14 and IASI. The methodology used, the CIMSS method, was nearly identical to that outlined in Gunshor et al. 2009, though applied to IASI data with no spectral gaps. The results are presented in Table 4.10. The mean brightness temperature difference for these comparisons show that GOES-14 is well calibrated based on the accuracy of IASI measurements and that it compares favorably with similar results to then-operational GOES-12 and GOES-11. Recall that the GOES-13 Imager initially had a very large bias in the 13.3 μm band. This is not the case with GOES-14. The large Imager band-6 bias on GOES-13 was subsequently reduced when the SRF was updated.

Table 4.10: Comparison of GOES-14 Imager to Infrared Atmospheric Sounding Interferometer (IASI) using the CIMSS-method. The bias is the mean of the absolute values of the differences.

Imager Band	Mean temperature differences (K)	Standard Deviations (K)	Number of cases
2	0.14	0.31	Shortwave Window band (9 night cases)
3	0.81	0.22	Water Vapor band (20 cases)
4	0.31	0.37	Longwave IR Window band (22 cases)
6	-0.53	0.33	CO_2 Absorption band (23 cases)

The GOES-14 Imager/Sounder IR radiometric calibration accuracy was evaluated with the Global Space-based Inter-Calibration System (GSICS) GEO-LEO baseline algorithm (Wu and Gunshor, 2009). During the GOES-14 PLT test, GOES-14 IR band data were inter-calibrated with two hyperspectral instruments in Low Earth Orbit (LEO): AIRS, which is polar-orbiting on NASA's Aqua satellite, and IASI. The broad-band GOES simulated radiance is spectrally convolved with the AIRS/IASI spectral radiances over the GOES spectral response function:

$$R_{LEO} = \frac{\int_{\nu} R_{\nu} \Phi_{\nu} d\nu}{\int_{\nu} \Phi_{\nu} d\nu}$$

where R_{LEO} is the simulated GOES measurement from AIRS/IASI radiances, R_{ν} is the AIRS/IASI radiance at wavenumber ν, and Φ_{ν} is GOES spectral response at wavenumber ν. As shown in Figure 4.21, AIRS has a problem with missing spectral gaps and unstable or dead detectors. The Japanese Meteorological Agency (JMA)'s gap-filling method is applied to compensate for the missing radiance (Tahara and Kato, 2009). The brightness temperature differences between the instruments were monitored over the homogeneous collocated GEO-LEO pixels during the test period and available at http://www.star.nesdis.noaa.gov/smcd/spb/fwu/homepage/GSICS_GOES14_AIRS_IASI.php.

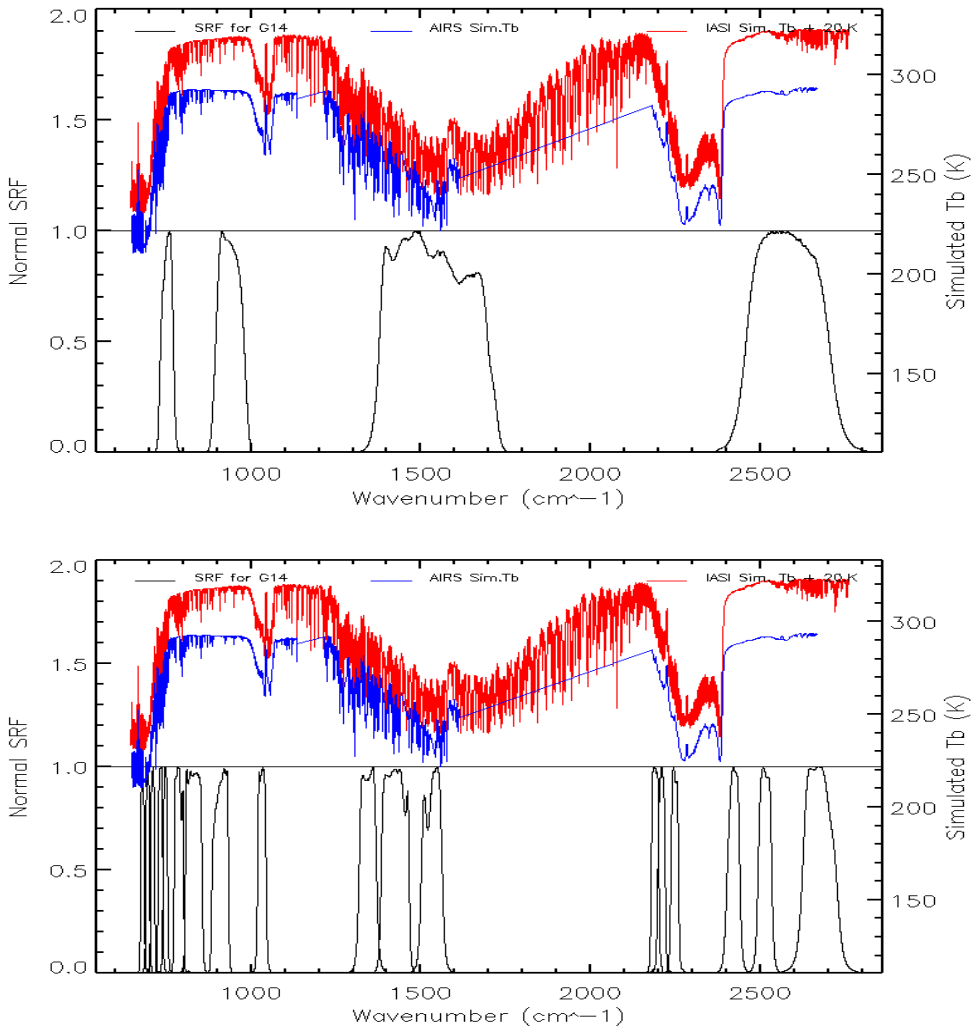

Figure 4.21: Spectral response function of GOES-14 Imager (top) and Sounder (bottom), together with the AIRS/IASI spectra.

Two sets of GEO-LEO inter-calibration data, based on the daytime and nighttime collocation pixels, are used to evaluate the Imager IR radiometric calibration accuracy. Both inter-calibrations with AIRS and IASI yielded very similar results in Table 4.11. Note that during the GOES-14 PLT, the Imager SRFs were updated on 24 November 2009 with Revision E and have been employed in the Satellite Operations Control Center (SOCC) data since. The mean brightness temperature (Tb) difference listed in Table 4.11 are calculated with the homogeneous collocation pixels after 24 November 2009. Unlike GOES-12 which has very small GEO-LEO Tb differences at the water vapor band (6.5 μm), both the GOES-AIRS and GOES-IASI inter-calibration results indicated large and consistent bias (~1K) for the GOES-14 water vapor band. Compared to the large Tb bias at the GOES-13 PLT test, GOES-14 has a smaller Tb difference (-0.5 K) for the 13.3 μm band (Gunshor et al. 2009; Wu et al. 2009). The shortwave band (3.9 μm) had a large Tb difference during the daytime. This was due to the bi-directional reflectance distribution function (BRDF) effect of solar reflectance. As shown in Figure 4.22 and 4.23, the Tb difference is consistent over the study period.

Table 4.11: Brightness temperature (Tb) biases between GOES-14 Imager and AIRS/IASI for the daytime collocated pixels and the double difference between AIRS and IASI through GOES-14 Imager daytime collocation data using the GSICS-method. The Tb biases between GOES-14 and IASI over the nighttime (9:30 pm) collocated pixels are also compared. The Tb biases were based on the collocated pixels acquired after 24 November 2009. Standard deviations are given in parentheses.

Band number	Central wavelength (µm)	daytime (K)			nighttime (K)
		GOES-AIRS	GOES-IASI	(GOES-AIRS) – (GOES-IASI)	GOES-IASI (9:30 pm)
2	3.9	-1.31 (±2.13)	-1.24 (±1.09)	-0.094 (±2.58)	-0.01 (±0.04)
3	6.5	0.99 (±0.12)	0.97 (±0.08)	-0.096 (±0.11)	0.77 (±0.11)
4	10.7	0.28 (±0.20)	0.02 (±0.18)	-0.31 (±0.34)	0.07 (±0.11)
6	13.3	-0.48 (±0.13)	-0.55 (±0.12)	-0.1 (±0.18)	-0.59 (±0.20)

These GSICS-method results are very consistent with the CIMSS-method results in Table 4.10.

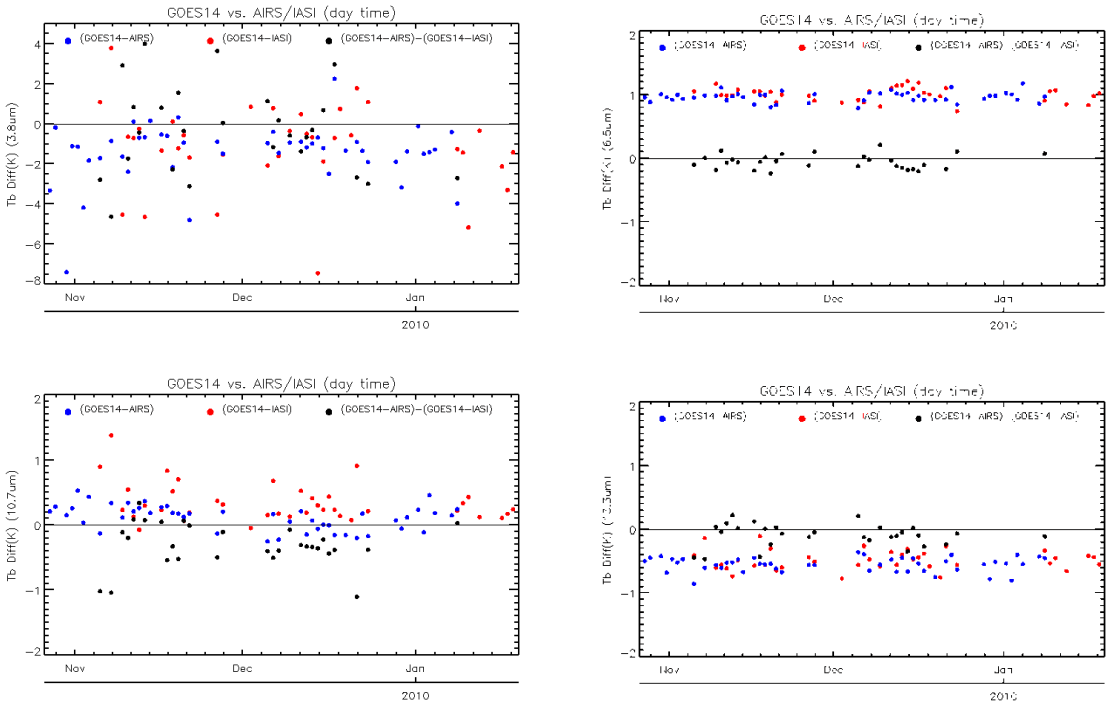

Figure 4.22: GOES-14 Imager and AIRS/IASI inter-calibration for the daytime.

One method for understanding the differences between the two sets of GOES-14 Imager SRF is to compare the results of the inter-calibration before versus after. The effect of the change in

SRF was evaluated with GOES-IASI inter-calibration at the night-time (9:30 pm – the local time of the MetOp-A ascending node) collocation pixels. As shown in Figure 4.23, the updated SRF changed the brightness temperatures (T_b) by -18 mK, -64 mK, +96 mK, and +130 mK, for the 3.9 µm, 6.5 µm, 10.7 µm, and 13.3 µm bands, respectively, as measured using the GSICS-method. The updated SRF changed the sign of the differences, but the magnitude was changed much less for the bias for the window bands, and slightly reduced the Tb bias overall.

Another method is to calculate the equivalent brightness temperatures from a given set of radiances for the two SRFs. These Planck conversions show differences on the order of approximately 0.3 K for band-3 (water vapor) and about 0.2 K for the longwave IR window band. Other bands show much smaller differences. Although the comparisons to IASI might give the impression that the SRFs did not change significantly, users need to be using the updated versions and especially the updated coefficients for converting between radiance and brightness temperatures since that did change significantly for some bands.

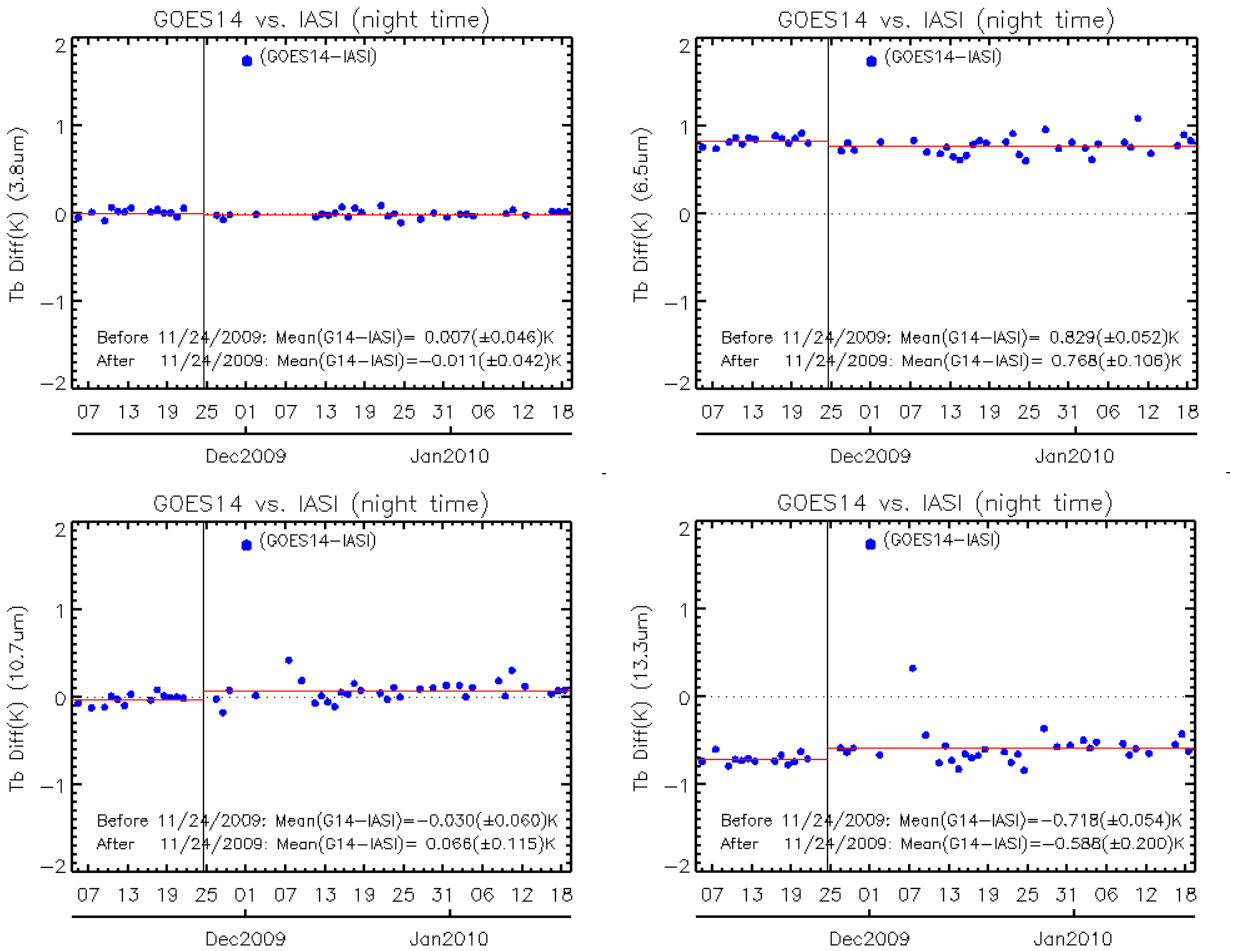

Figure 4.23: The Tb bias between GOES-14 and IASI Tb bias over the nighttime (9:30 pm) collocated pixels using the GSICS-method.

The GOES-14 Sounder radiometric calibration accuracy was also evaluated with the GSICS GEO-LEO baseline inter-calibration algorithm. Results presented in Table 4.12 and Figure 4.24

indicate that the GOES-14 Sounder is well calibrated, with biases less than 0.2 K for most bands (all less than 0.3 K) when compared with AIRS and IASI. This result is remarkable in view of the fact that GOES-11/12 Sounders have large biases, up to 8 K, for some of its shortwave bands (e.g., band-15). Also noted is that the standard deviation for band-1 is less than 0.2 K. This value is an indirect estimate of this band's noise, which has been 1-2 K for current and earlier GOES.

Table 4.12: GOES-14 Sounder IR vs. IASI brightness temperature difference at nighttime, compared to those of GOES-11/12 Sounder using the GSICS-method. The data in the parentheses are the standard deviation of the Tb difference at the collocation pixels.

Band number	Central wavelength (μm)	GOES-14 Mean (±stdv) (K)	GOES-12 Mean (±stdv) (K)	GOES-11 Mean (±stdv) (K)
1	14.71	0.274 (±0.195)	-0.006 (±0.233)	-0.023 (±0.230)
2	14.37	0.127 (±0.245)	0.078 (±0.197)	0.140 (±0.207)
3	14.06	0.103 (±0.610)	0.180 (±0.739)	0.318 (±0.966)
4	13.64	0.208 (±0.917)	-0.258 (±1.373)	0.151 (±1.148)
5	13.37	0.041 (±1.159)	0.313 (±1.837)	-1.765 (±1.399)
6	12.66	0.106 (±1.601)	-0.160 (±2.094)	-0.081 (±1.968)
7	12.02	-0.041 (±1.575)	-0.086 (±2.068)	0.178 (±2.200)
8	11.03	-0.067 (±1.363)	-0.109 (±1.906)	-0.034 (±1.576)
9	9.71	0.076 (±0.838)	-0.055 (±1.366)	0.009 (±1.551)
10	7.43	-0.040 (±0.747)	-0.328 (±1.088)	0.235 (±0.676)
11	7.02	-0.121 (±0.574)	-0.119 (±0.994)	0.178 (±0.510)
12	6.51	-0.178 (±0.438)	-0.236 (±0.680)	-0.056 (±0.535)
13	4.57	0.263 (±0.506)	-0.883 (±1.052)	-0.031 (±0.808)
14	4.52	-0.049 (±0.341)	-0.499 (±0.936)	0.232 (±1.124)
15	4.45	0.144 (±0.506)	-5.076 (±2.766)	-4.578 (±1.568)
16	4.13	0.076 (±0.517)	0.304 (±1.283)	0.258 (±0.874)
17	3.98	-0.116 (±0.648)	0.106 (±1.529)	0.153 (±0.842)

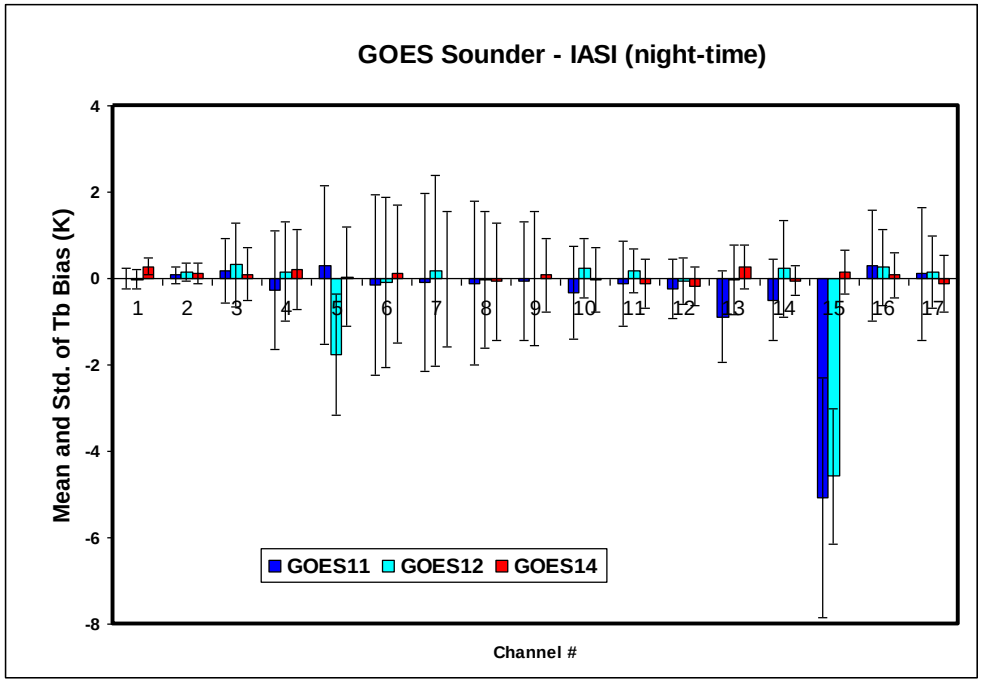

Figure 4.24: Mean and standard deviation of GOES-11/12/14 Sounder brightness temperature difference from nighttime IASI data in December 2009 using the GSICS-method.

4.7. Stray Light Analysis

By supplying data through the eclipse periods, the GOES-13/14/15 system addresses one of the major current limitations which are eclipse and related outages. This change is possible due to larger spacecraft batteries. Outages due to Keep Out Zones (KOZ) will be minimized. See Figure 4.25 for an image from 1 October 2009 comparing GOES-14 to GOES-12 through an eclipse time. Note the GOES-12 data outage. Outages due to Keep Out Zone (KOZ) will be replaced by Stray Light Zone outages and reduced by shifting frames away from the sun and possibly stray light correction via a SPS algorithm under development.

With the new capability of data during previous outages comes the risk of allowing images contaminated with the energy of the sun to be produced. An image with artificial brightness temperature excursions up to 75 K (e.g. band-2) may affect products. To determine how much good data can be acquired, at the same time minimizing the amount of bad data, many scans were conducted during the eclipse period in 2009.

While all Imager bands can be affected, the visible and shortwave (band-2) are affected the most. There are investigations into the possibility of correcting these stray-light affected images before distribution via GVAR.

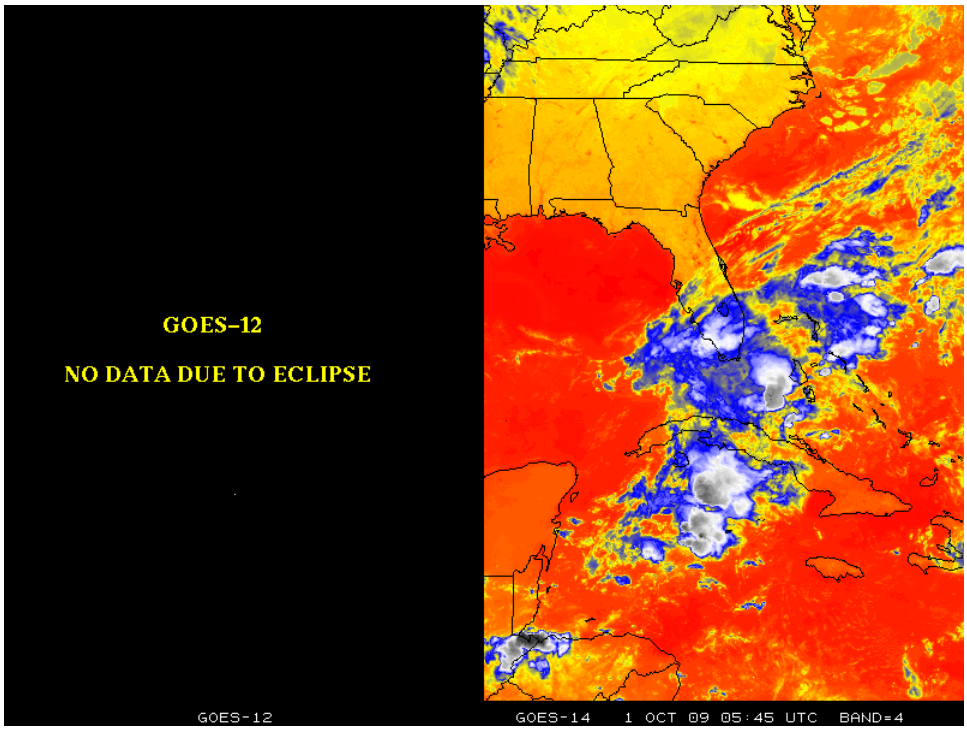

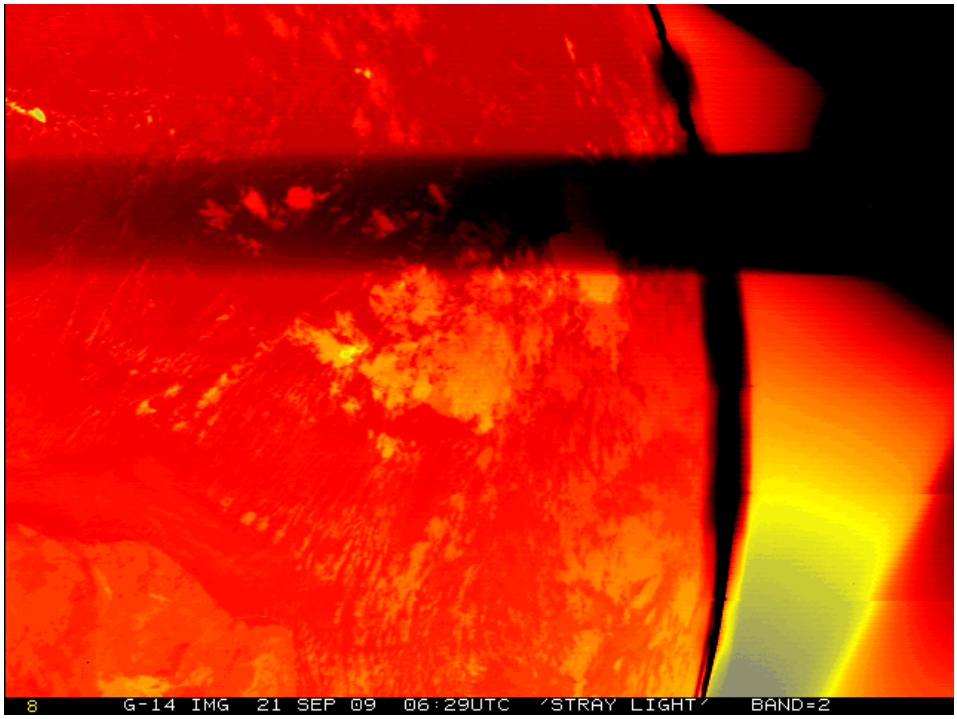

Figure 4.25: GOES-12 and GOES-14 Imager (top), and GOES-14 band-2 (bottom), from 21 September 2009. Note the large stray radiation from the sun.

In general, the GOES Sounder can be affected even more during the KOZ periods, due to the relatively slow Sounder scanning (not shown).

4.8. Instrument Performance Monitoring

During the GOES-14 post-launch test (PLT) period, a new version of the GOES IPM system was implemented to track the stability and noise of the sensor parameters that affect the instrument calibration. The GOES IPM system uses the near real-time GOES Variable Format (GVAR) Block 11 (B11) data routinely downloaded from the NOAA Comprehensive Large Array-data Stewardship System data source. Four types of calibrated related parameters are ingested from the GVAR B11 data, including the instrument telemetry data, infrared (IR) calibration coefficients, statistics of space-look and blackbody scan data. Instrument noise, such as NEdR and NEdT are also monitored for each detector. To detect any potential calibration anomaly, all these monitored parameters are displayed at various temporal scales for diurnal to long-term variations. Note that although the GOES PLT test period was schedule from 30 November 2009 through 4 January 2010, GOES-14 continued to transmit data until 19 January 2010; when it was placed into storage. The GOES-14 data analyzed in this study therefore ranges from the beginning of the PLT period to 19 January 2010. During this period, the monitoring results were updated daily at the GOES-14 IPM Web pages at

- http://www.star.nesdis.noaa.gov/smcd/spb/fwu/homepage/GOES14_Imager_IPM.php
- http://www.star.nesdis.noaa.gov/smcd/spb/fwu/homepage/GOES14_Sounder_IPM.php.

4.8.1. Telemetry Monitoring

About 14 Imager telemetry variables and 16 Sounder telemetry variables were monitored at the GOES-14 IPM system. Table 4.13 lists the name of the telemetry variables and the number of its detectors. Most of the telemetry detectors have apparent diurnal variations. However, no significant change with telemetry data was observed during the GOES-14 PLT test period. Figure 4.26 displays the 8 Platinum Resistance Thermometer (PRT) temperature data embedded at the GOES-14 Imager and Sounder blackbodies (BBs). The BB temperature, together with the other telemetry temperature data, clearly displays the heating of the instrument surface around the midnight when the Sun is above the equator (Johnson and Weinreb, 1996). However, due to the inhomogeneous heating attributes within the satellite, the detectors are not simultaneously warming up or cooling down. While the lowest BB temperature is relatively consistent every day, there are some variations with the daily peak temperature, which may result from sun-earth-satellite position changes. Similar patterns are also observed at the GOES-11/12/13 IPM system.

Table 4.13: Telemetry variables.

	Telemetry variables	Detector Number (Imager)	Detector Number (Sounder)
1	Electronics Temperature	2	2
2	Sensor Assembly Baseplate Temperature	6	6
3	BB Target Temperature	8	8
4	Scan Mirror Temperature	1	1
5	Telescope Primary Temperature	1	1
6	Telescope Secondary Temperature	2	2
7	Telescope Baffle Temperature	2	2
8	Aft Optics Temperature	1	1
9	Cooler Radiator Temperature	1	1
10	Wide Range IR Detector Temperature	1	1
11	Narrow Range IR Detector Temperature	1	1
12	Filter Wheel Housing Temperature	X	1
13	Filter Wheel Control Heater Voltage	X	1
14	Patch Control Voltage	1	1
15	Instrument Current	1	1
16	Cooler-Housing Temperature	1	1

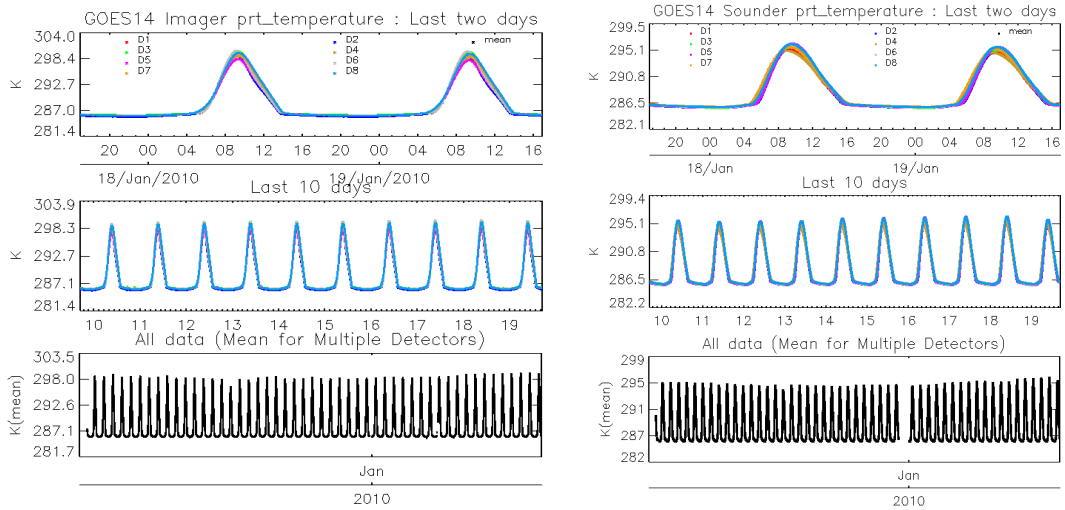

Figure 4.26: Monitoring of GOES-14 Imager and Sounder PRT temperature data. The top panels are 2 consecutive day observation data, the middle ones are for 10-day data, and the bottom panel shows the mean of the 8 detectors over the PLT period, from 30 November 2009 through 19 January 2010.

4.8.2. IR Calibration Coefficients Monitoring

The GOES IPM system monitors the calibration slope (first-order gain) and bias values at 30 ms and 20 ms time interval for the Imager and Sounder, respectively, according to its calibration procedure (Weinreb et al. 1997). The second-order parameters are not monitored because the fixed pre-launch second-order calibration coefficients are used for non-linear correction for all the IR bands. Similar to GOES-11/12, the calibration slopes and biases show diurnal variations with some difference in between the detectors at each IR band. This is due to the difference in the detector characteristics and the inhomogeneous instrument heating patterns (Figure 4.27). However, during the GOES-14 PLT period, discontinuity in both time-series of calibration slope and bias for the GOES-14 Sounder mid-wave and short-wave IR bands are observed around 1800 UTC, the telemetry house-keeping time everyday (Figure 4.27).

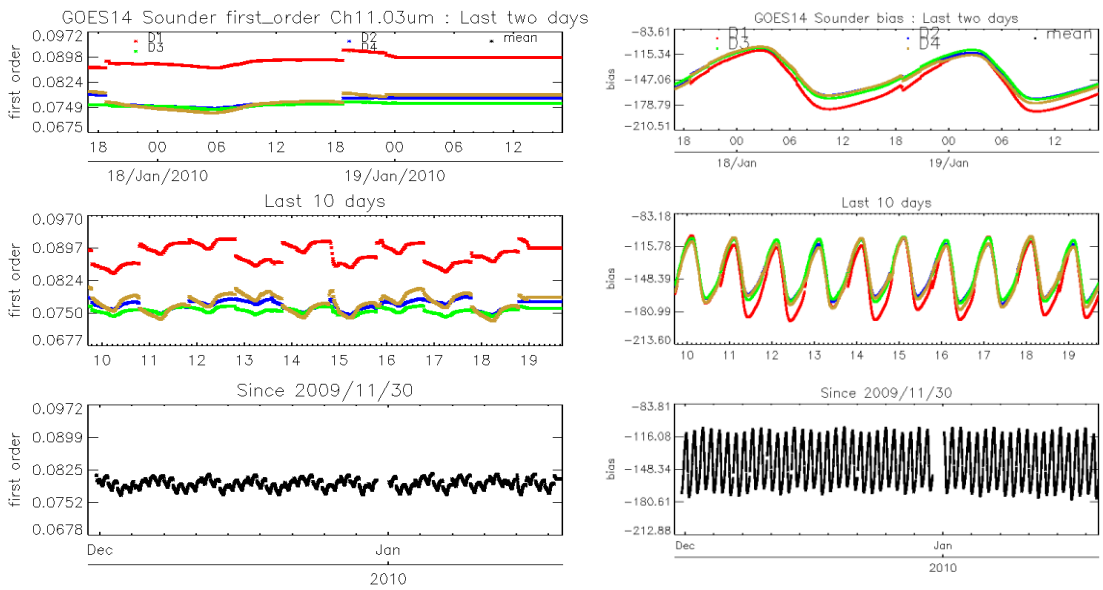

Figure 4.27: Monitoring of the first-order gain and the bias values for the GOES-14 Sounder band-8 (11.03 µm). A sudden disruption of the slope values can be observed around 1800 UTC in the two-day observation panel for the GOES-14 Sounder data.

4.8.3. Monitoring of Space-look (SPLK) Statistics

The Imager space-look monitoring includes the mean of the filtered space-look data and its variance at pre-clamp and post-clamp for each detector at each band. The Sounder space-look statistics include the mean filtered space-look and the variance.

The issue with GOES-14 Imager SPLK monitoring is the frequent zero data for the mean filtered pre-clamp space-look data at the GVAR B11 files (Figure 4.28). These zero GVAR data are not observed in the GOES-11/12 Imager SPLK data, but appear at GOES-13 Imager pre-clamp space-look data too. Communications with the scientist at NOAA SOCC determined that these zero mean filtered pre-clamp SPLK data are caused by the "idle" space-looks at 9.2-s intervals and do not affect the calibration accuracy (Weinreb and Mitchell, 2010).
Note with the GOES-14 Sounder SPLK data the sudden change around 1800 UTC, the telemetry house-keeping time for the short-wave and long-wave IR bands (Figure 4.29). The concurrence

with the sudden changes in the Sounder IR calibration coefficients are later found to relate with the GOES-14 Sounder loose-lens problem.

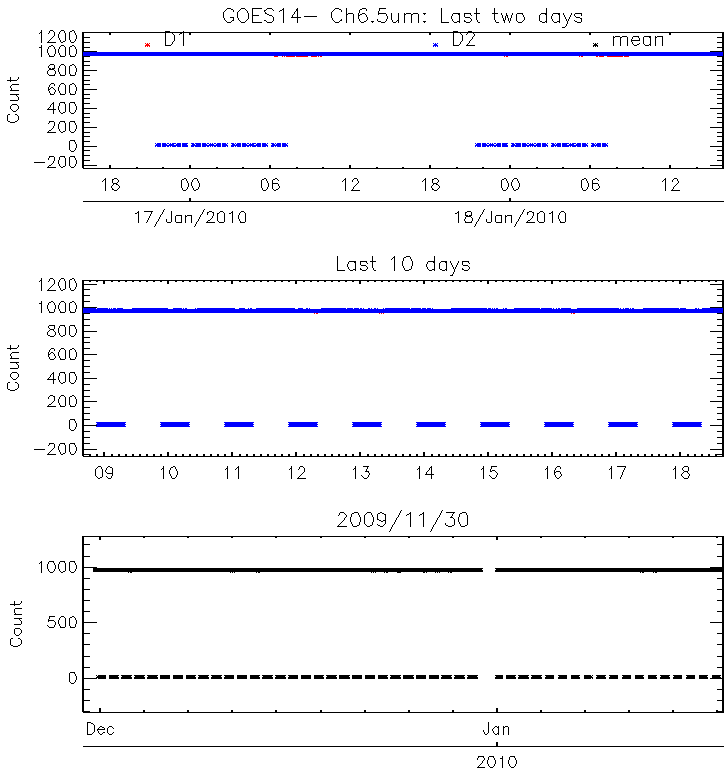

Figure 4.28: Monitoring of mean filtered pre-clamp space-look data for GOES-14 Imager band-3 (6.5 µm). The zero values happen periodically for the two detectors at the same time period every day.

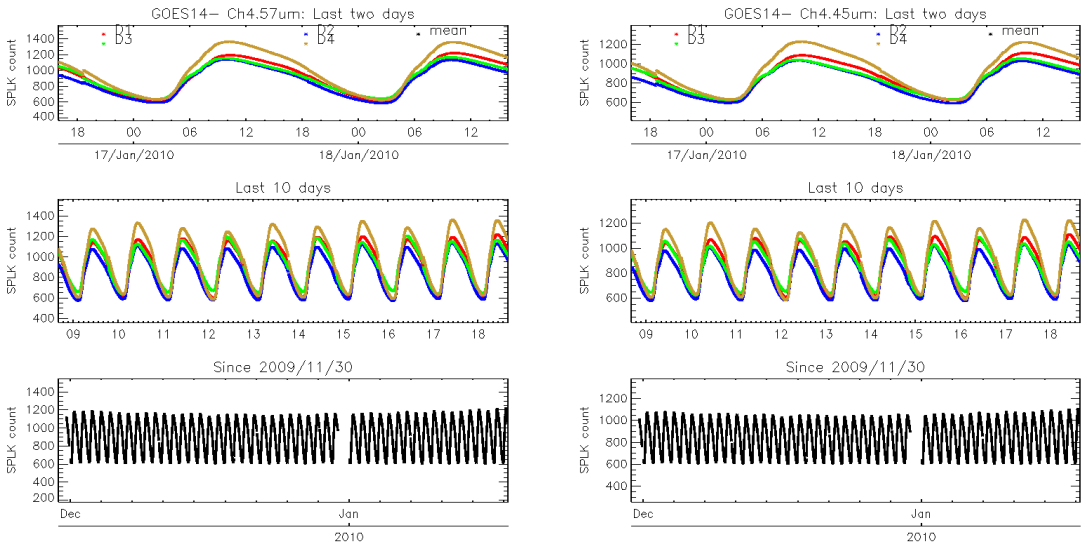

Figure 4.29: Monitoring of GOES-14 Sounder space-look data for band-14 (4.57 µm).

4.8.4. Monitoring Blackbody (BB) Scan Statistics

The Imager/Sounder blackbody data are monitored with the mean filtered blackbody values and the corresponding variance for each detector of each IR band. No significant trending of the blackbody data is found during the GOES-14 PLT test, as seen in Figure 4.30. The diurnal variations of the BB data are comparable with those of GOES-11/12/13. The GOES-11/12/13 IPM are available at the following Web pages:

- http://www.star.nesdis.noaa.gov/smcd/spb/fwu/homepage/GOES11_Imager_IPM.php
- http://www.star.nesdis.noaa.gov/smcd/spb/fwu/homepage/GOES12_Imager_IPM.php
- http://www.star.nesdis.noaa.gov/smcd/spb/fwu/homepage/GOES13_Imager_IPM.php
- http://www.star.nesdis.noaa.gov/smcd/spb/fwu/homepage/GOES11_Sounder_IPM.php
- http://www.star.nesdis.noaa.gov/smcd/spb/fwu/homepage/GOES12_Sounder_IPM.php
- http://www.star.nesdis.noaa.gov/smcd/spb/fwu/homepage/GOES13_Sounder_IPM.php

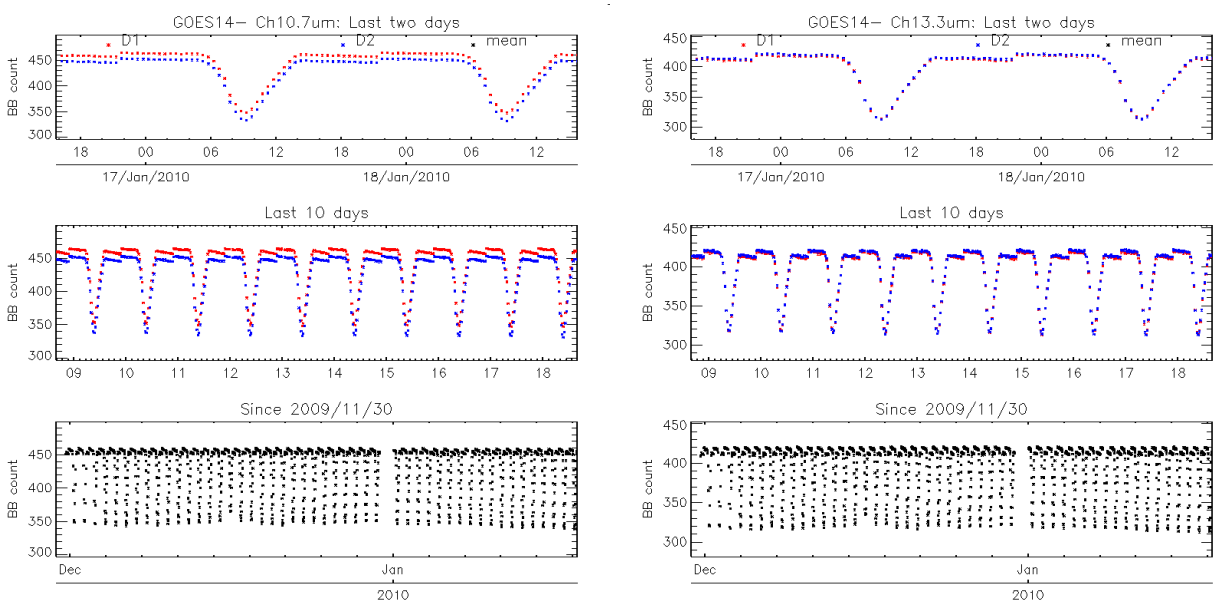

Figure 4.30: GOES-14 Sounder band-15 (4.45 µm) mean filtered BB data. The discontinuity in the BB data is also observed in the GOES-11/12 Imager BB data monitoring systems, which is related to scan angle effect of scan mirror emissivity at changes in the eastern/western clamp position.

4.8.5. Initial Post-launch Calibration for the Imager Visible Band

The visible bands of GOES-14 Imager experience continuous degradation once commissioned in orbit. A post-launch calibration method has been developed to correct for such degradation using the collocated cloud pixels of GOES-14 and Terra Moderate Resolution Imaging Spectroradiometer (MODIS) band-1 data (Wu and Sun, 2004).

$$R_{post} = R_{pre} * C_1$$

where R_{post} is the post-launch calibration reflectance/radiance for the GOES-14 Imager visible band; R_{pre} is the pre-launch calibration reflectance/radiance; and C_1 is the correction factor, C_1 = 1.0695. This result was derived based on the collocated GOES-14 and Terra MODIS pixels acquired on Y09D357.

4.9. Finer Spatial resolution GOES-14 Imager band-6

The improved (4 km field-of-view) spatial resolution of the 13.3 µm (band-6) required changes to the GVAR format. Several issues with implementing the new GVAR format were discovered, communicated, rectified, and verified. For example, the paired detectors on the higher-resolution 13.3 µm band were inadvertently swapped when the satellite was in an inverted mode. This situation was quickly resolved. The image in Figure 4.31 demonstrated the improved spatial resolution of this band on the GOES-14 imager, which is also the case with the GOES-15 Imager.

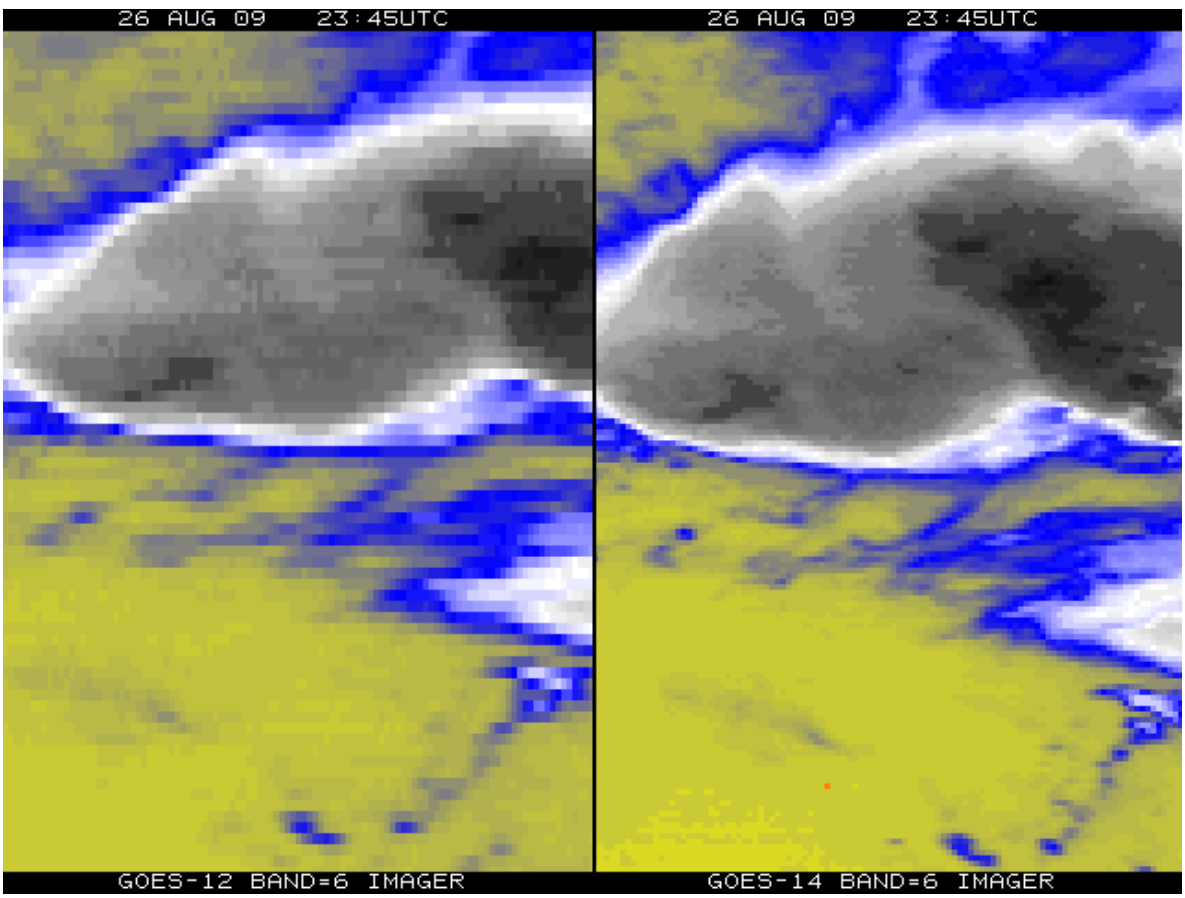

Figure 4.29: Improved Imager spatial resolution at 13.3 µm for GOES-14 (right) compared to GOES-12 (left) from 26 August 2009.

5. Product Validation

A number of products were generated with data from the GOES-14 instruments (Imager and Sounder) and then compared to the same products generated from other satellites or ground-based measurements. Products derived from the Sounder include: Total Precipitable Water (TPW), Lifted Index (LI), Clouds products, and Atmospheric Motion Vectors. The products derived from the Imager include: Clouds, Atmospheric Motion Vectors, Clear Sky Brightness Temperature (CSBT), Sea Surface Temperature (SST), and Fire Detection.

5.1. Total Precipitable Water (TPW) from the Sounder

5.1.1. Validation of Precipitable Water (PW) Retrievals from the GOES-14 Sounder

GOES-14 retrievals of precipitable water were validated against radiosonde observations of precipitable water for the period 30 November 2009 to 4 January 2010. GOES-14 retrievals were collocated in space (within 11 km) and time (within 30 minutes) to daily radiosonde observations at 0000 UTC and 1200 UTC. At the same time, these GOES-14 retrievals were collocated in space (within 11 km) and time (within 60 minutes) to GOES-12 retrievals. The relative performance of the GOES-14 PW retrievals, GOES-12 PW retrievals, and first guess PW supplied to the retrieval algorithm could then be compared since all of these PW values were collocated to the same radiosonde observation. Table 5.1 provides a summary of these statistics for Total Precipitable Water (TPW) and the PW at three layers (surface-900 hPa; 900-700 hPa, and 700-300 hPa). The statistics indicate that the quality of the GOES-14 Sounder PW retrievals compare very well to the quality of the operational GOES-12 PW retrievals. It should be remembered that the GOES-14 retrievals used a GOES-12 dataset for the radiance bias adjustment for initial processing.

Table 5.1: Verification statistics for GOES-12 and GOES-14 retrieved precipitable water, first guess (GFS) precipitable water, and radiosonde observations of precipitable water for the period 30 November 2009 to 4 January 2010.

Statistic	GOES-12/RAOB	GOES-14/RAOB	GUESS/RAOB	RAOB
Total Precipitable Water				
RMS (mm)	2.31	2.46	2.64	
Bias (mm)	-0.18	-0.10	-0.06	
Correlation	0.98	0.97	0.97	
Mean (mm)	11.24	11.32	11.36	11.42
Sample	3677	3677	3677	3677
Layer Precipitable Water (surface to 900 hPa)				
RMS (mm)	1.04	1.01	1.03	
Bias (mm)	-0.45	-0.42	-0.43	
Correlation	0.98	0.98	0.98	
Mean (mm)	4.03	4.07	4.06	4.49
Layer Precipitable Water (900 hPa to 700 hPa)				
RMS (mm)	1.27	1.37	1.39	
Bias (mm)	-0.12	-0.06	-0.02	
Correlation	0.96	0.96	0.96	
Mean (mm)	4.85	4.91	4.95	4.97
Layer Precipitable Water (700 hPa to 300 hPa)				
RMS (mm)	1.27	1.26	1.36	
Bias (mm)	0.37	0.35	0.36	
Correlation	0.83	0.82	0.81	
Mean (mm)	2.30	2.28	2.28	1.93

Figures 5.1 through 5.4 present time series of various comparison statistics (GOES retrieved TPW vs. radiosonde observed TPW) for GOES-14 (in green with open circles) and GOES-12 (in red with filled circles) for the same time period (30 November 2009 to 4 January 2010) as in Table 5.1. Each tick mark represents a data point (2 points per day) with the calendar day label centered at 0000 UTC of that day. A majority of the GOES-14 data points are very close to, if not on top of, the GOES-12 data points.

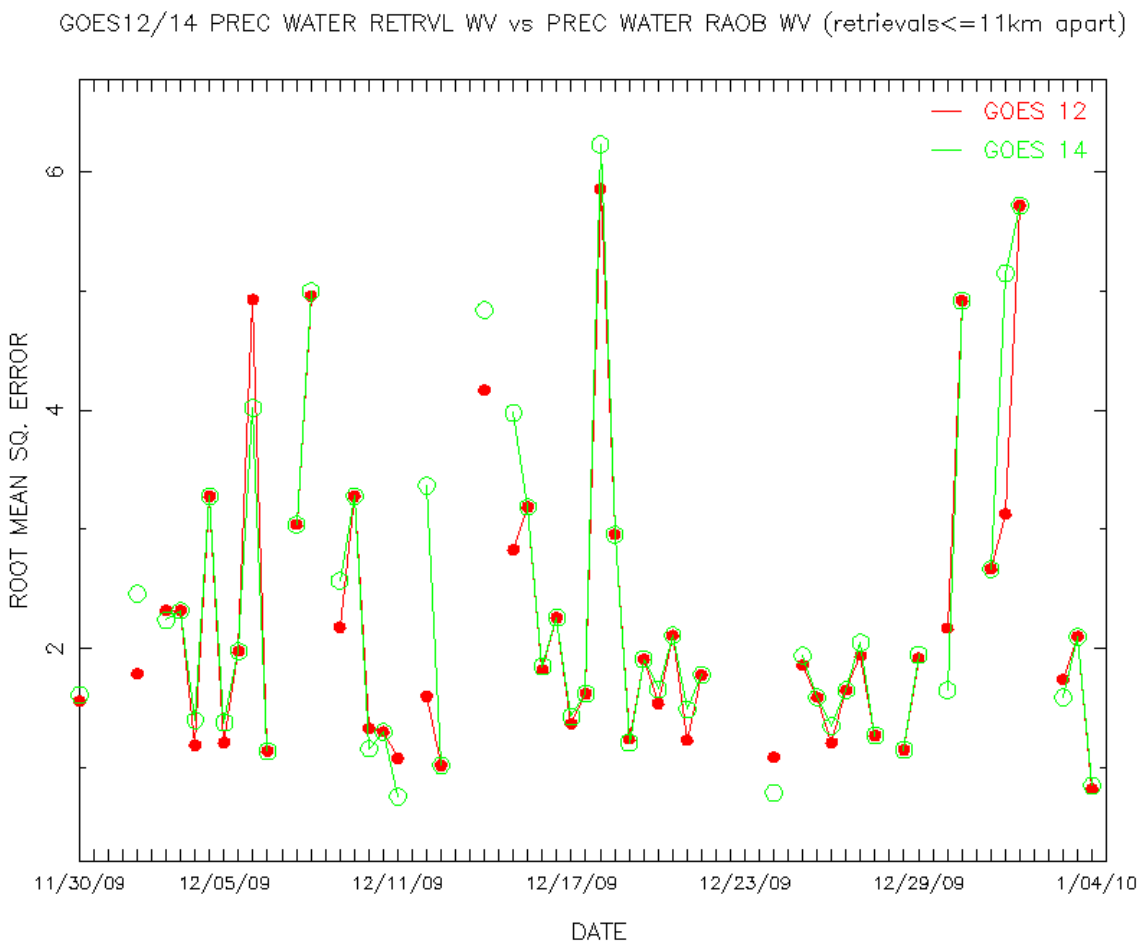

Figure 5.1: Time series of Root Mean Square Error (RMSE) between GOES-12 and GOES-14 retrieved precipitable water and radiosonde observation of precipitable water over the period 30 November 2006 to 4 January 2010.

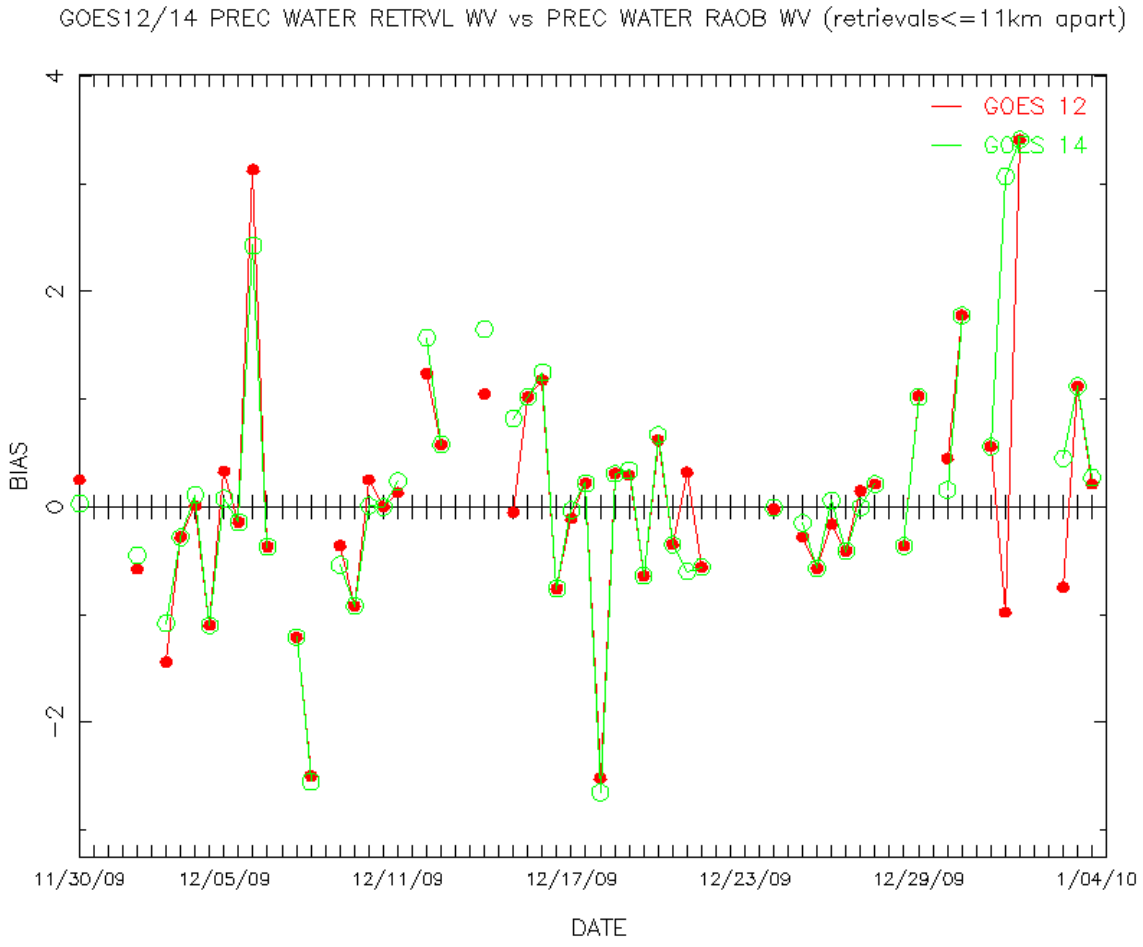

Figure 5.2: Time series of bias (GOES-radiosonde) between GOES-12 and GOES-14 retrieved precipitable water and radiosonde observation of precipitable water over the period 30 November 2009 to 4 January 2010.

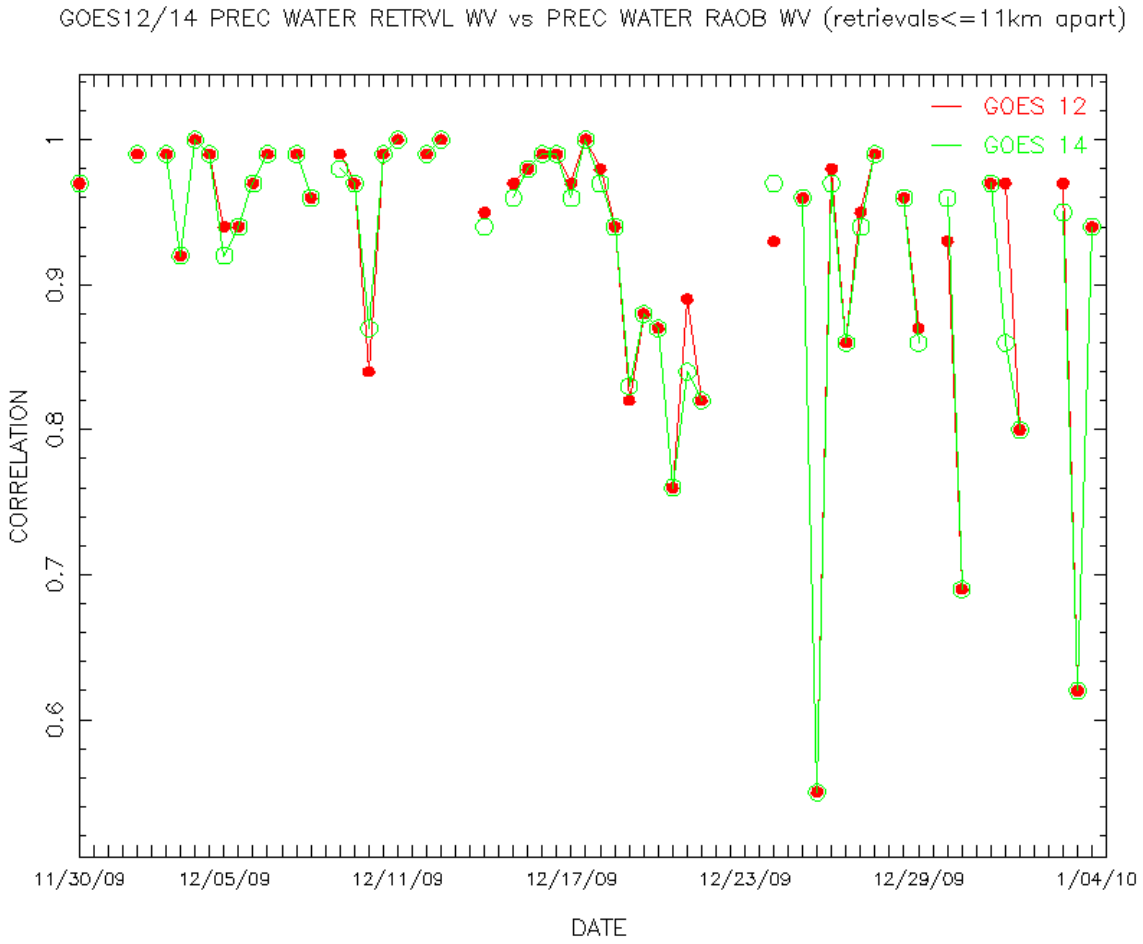

Figure 5.3: Time series of correlation between GOES-12 and GOES-14 retrieved precipitable water and radiosonde observation of precipitable water over the period 30 November 2009 to 4 January 2010.

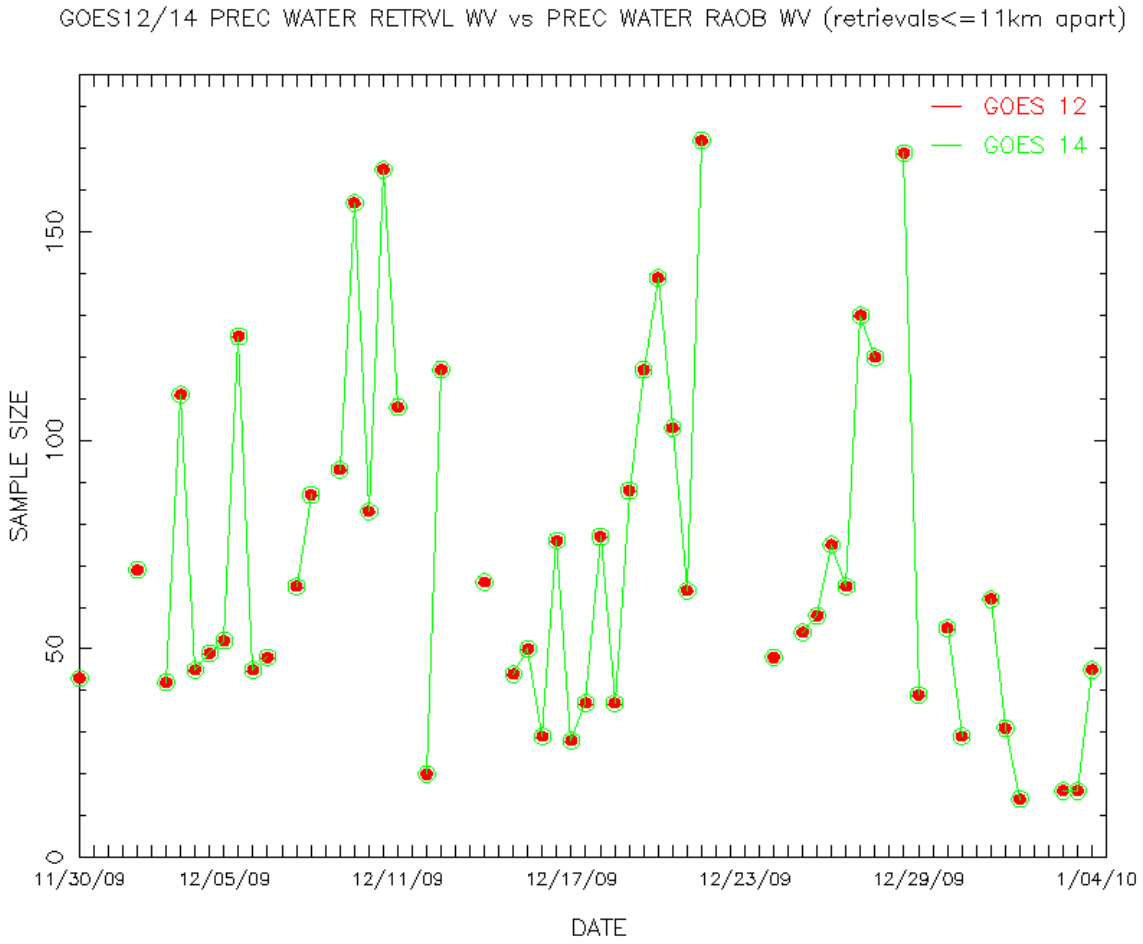

Figure 5.4: Time series of the number of collocations between GOES-12 and GOES-14 retrieved precipitable water and radiosonde observation of precipitable water over the period 30 November 2009 to 4 January 2010.

Total precipitable water retrievals (displayed in the form of an image) for GOES-12 and GOES-14 are presented in Figure 5.5 over the same area at approximately the same time (4 December 2009). These retrievals are generated for each clear radiance Field-Of-View (FOV). Radiosonde measurements of TPW are plotted on top of the images. Qualitatively, there is good agreement between the GOES-12 and GOES-14 TPW retrievals that, in turn, compare reasonably well with the reported radiosonde measurements of TPW. When comparing measurements from two satellites, one must consider the different satellite orbital locations; even precisely co-located fields-of-view are seen through different atmospheric paths.

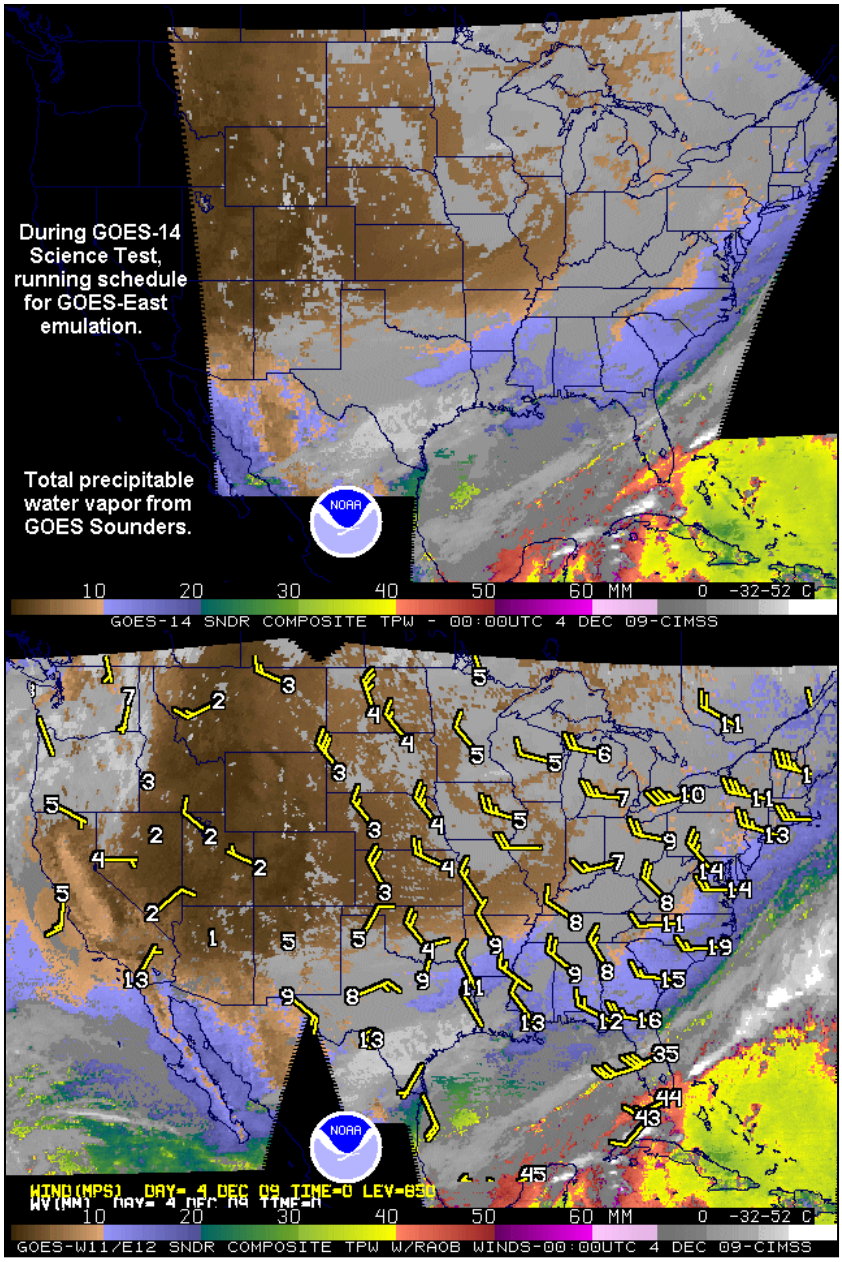

Figure 5.5: GOES-14 (top) and GOES-11/12 (bottom) retrieved TPW (mm) from the Sounder displayed as an image. The data are from 0000 UTC on 4 December 2009. Measurements from radiosondes are overlaid as white text; cloudy FOVs are denoted as shades of gray.

Figure 5.6 shows one time period with two retrieval methods, note that the GPS/Met data are over-plotted on each image.

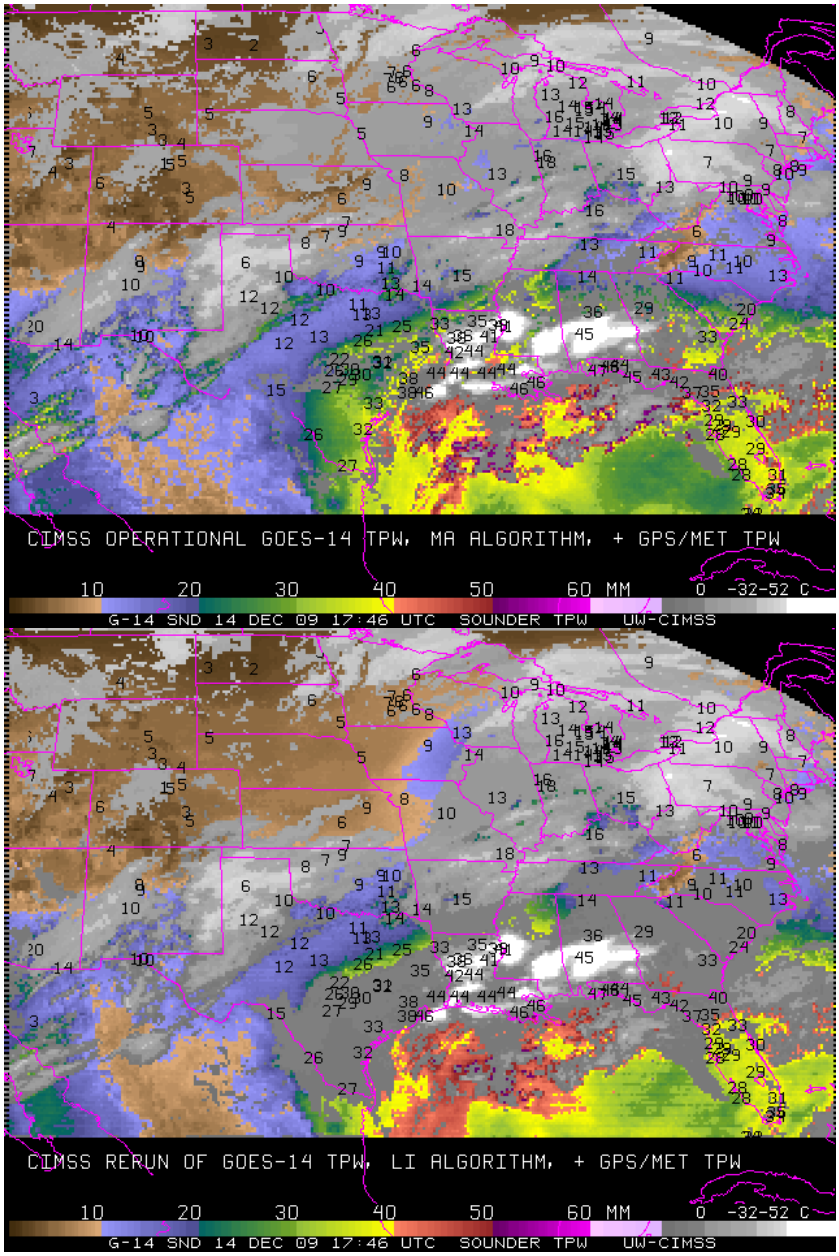

Figure 5.6: GOES-14 Sounder TPW from two retrieval algorithms (i.e., Ma (upper-panel) and Li (lower-panel). Both images are from 14 December 2009.

5.2. Lifted Index (LI) from the Sounder

The lifted index (LI) product is generated from the retrieved temperature and water vapor profiles (Ma et al. 1999) that are generated from clear radiances for each FOV. Figure 5.7 shows lifted index retrievals (displayed in the form of an image) for GOES-12 and GOES-14 over the same area at approximately the same time, showing no discernable bias in the LI values. Both images are shown in the GOES-12 projection. Of course the overall large (stable) LI values also illustrates that ideally satellite post-launch check-outs should be conducted in seasons with more atmospheric moisture/instability.

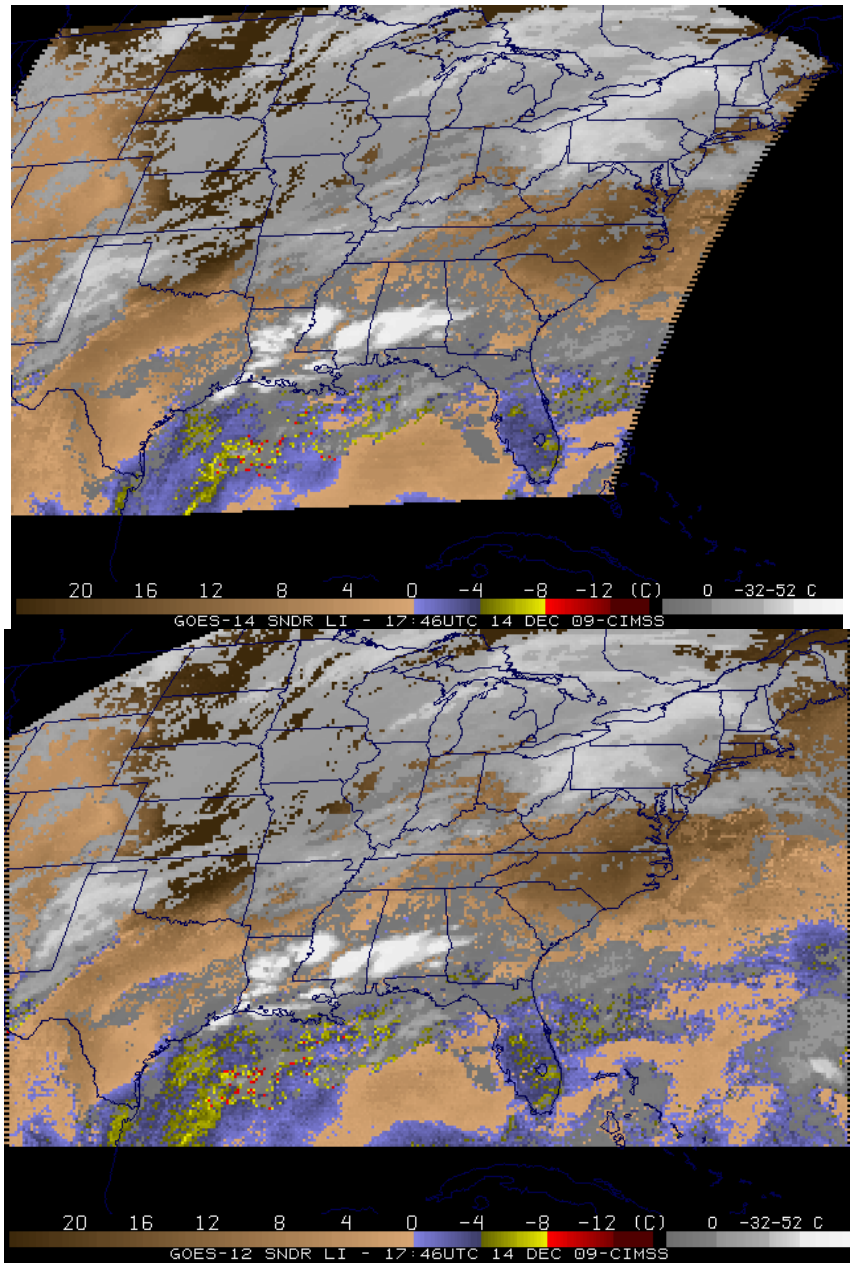

Figure 5.7: GOES-14 (top) and GOES-12 (lower) retrieved Lifted Index (LI) from the Sounder displayed as an image. The data are from 1746 UTC on 14 December 2009.

5.3. Cloud Parameters from the Sounder and Imager

The presence of the 13.3 µm band on the GOES-14 Imager, similar to the GOES-12 Imager, makes near full-disk cloud products possible. This product complements that from the GOES Sounders.

Figures 5.8 and 5.9 shows a comparison of GOES-14 Imager (and Sounder) cloud-top pressure derived product images from late 2009. Note the improved coverage of the Imager-based

product. Another comparison between GOES-14 and GOES-12 Sounders showed generally good correlations, as seen in Figures 5.10 through 5.12.

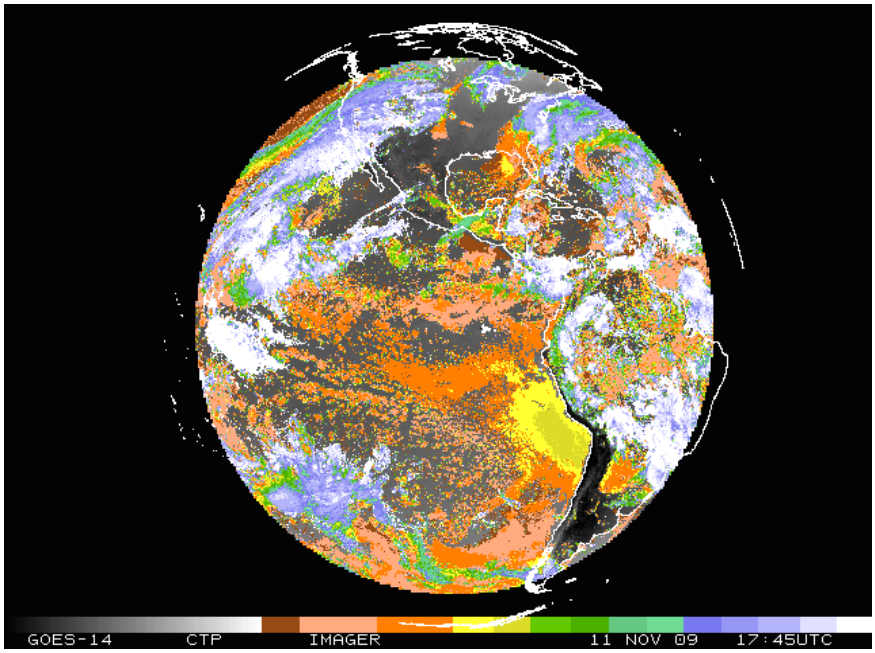

Figure 5.8: GOES-14 Imager cloud-top pressure from 11 November 2009 starting at 1745 UTC.

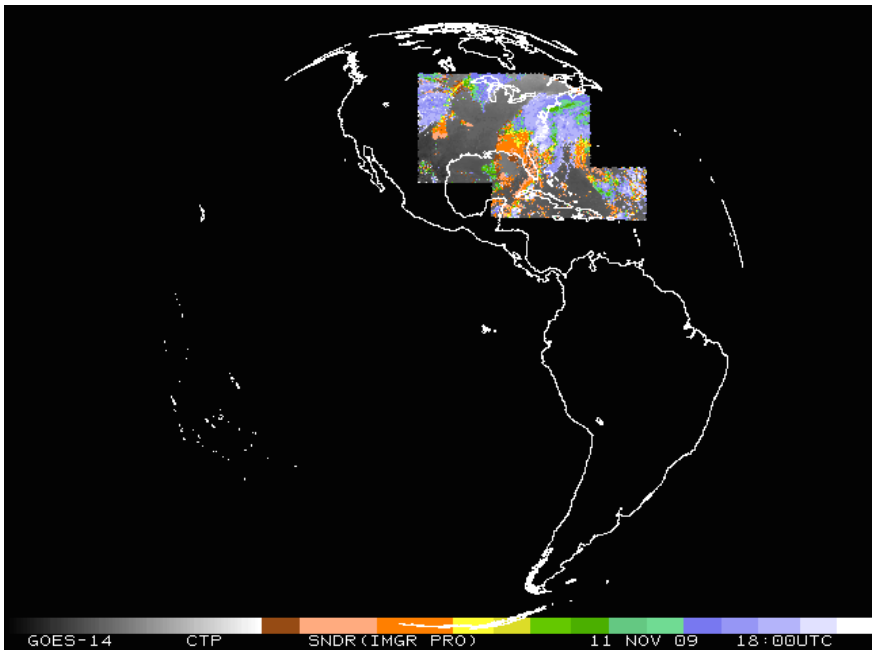

Figure 5.9: GOES-14 Sounder cloud-top pressure from 11 November 2009 starting at 1745 UTC. The Sounder data have been remapped into the GOES-14 Imager projection.

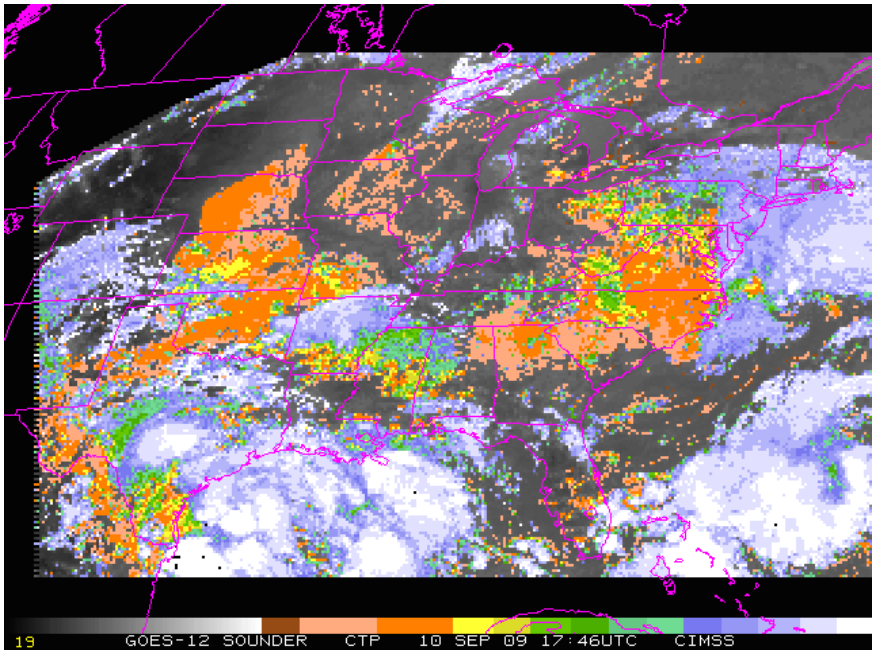

Figure 5.10: GOES-12 cloud-top pressure from the Sounder from 1746 UTC on 10 September 2009.

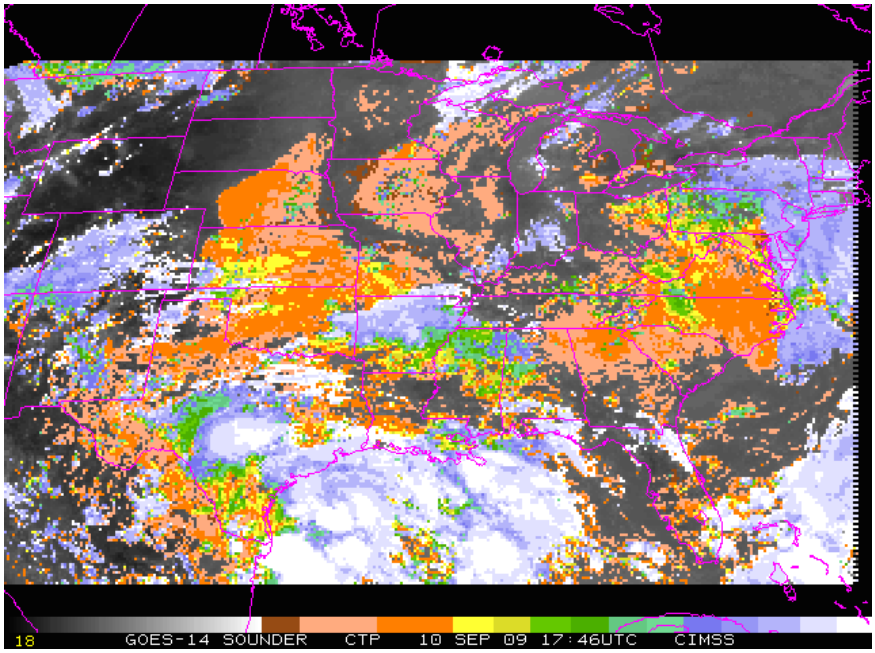

Figure 5.11: GOES-14 cloud-top pressure from the Sounder from the nominal 1746 UTC on 10 September 2009.

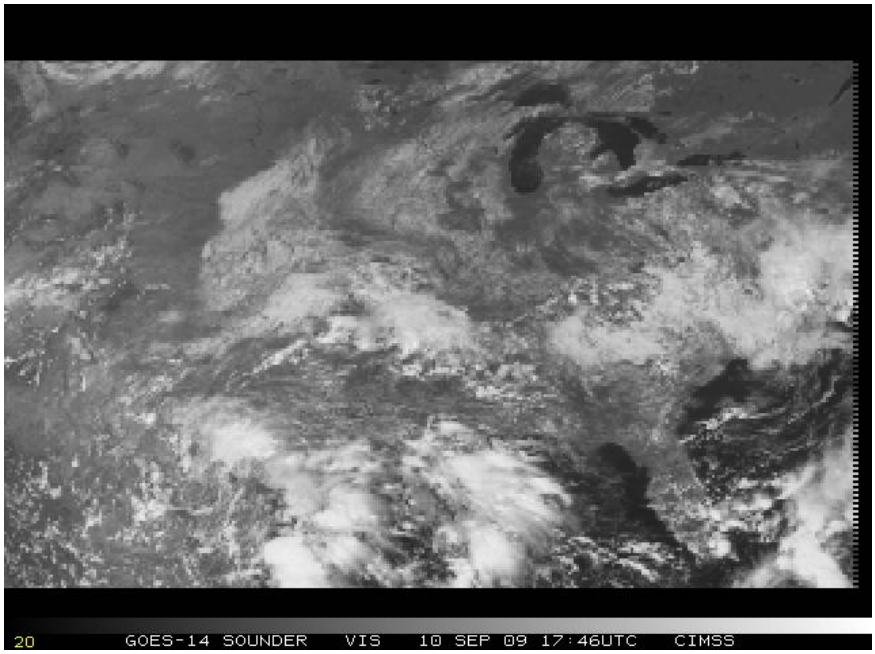

Figure 5.12: GOES-14 Sounder visible image from the nominal 1746 UTC on 10 September 2009.

5.4. Atmospheric Motion Vectors (AMVs) from the Imager

Atmospheric Motion Vectors (AMVs) from GOES are derived using a sequence of three images. Features targeted in the middle image (cirrus cloud edges, gradients in water vapor, small cumulus clouds, etc.) are tracked from the middle image back to the first image, and forward to the third image, thereby yielding two displacement vectors. These vectors are averaged to give the final wind vector, or AMV. This report summarizes the quality of AMVs from GOES-14 as part of the Post Launch Science Test (PLST) in late 2009.

The varied imaging schedules activated during the GOES-14 Science Test provided an opportunity to run AMV assessments for what are currently considered operational as well as special case scenarios. Thinned (for display clarity) samples of AMVs from GOES-14 on 7 January 2010 at 1045 UTC are shown for Cloud-Drift (Figure 5.13) and Water Vapor (Figure 5.14) AMVs.

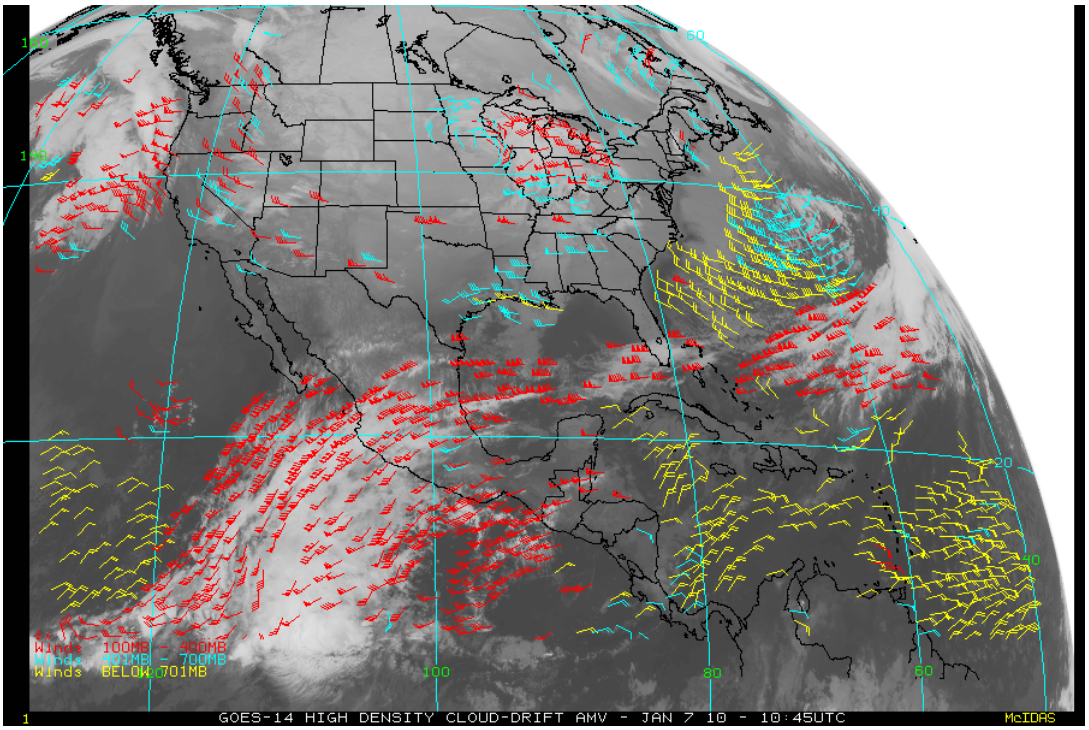

Figure 5.13: GOES-14 NHEM cloud drift AMV on 7 January 2010 at 1045 UTC.

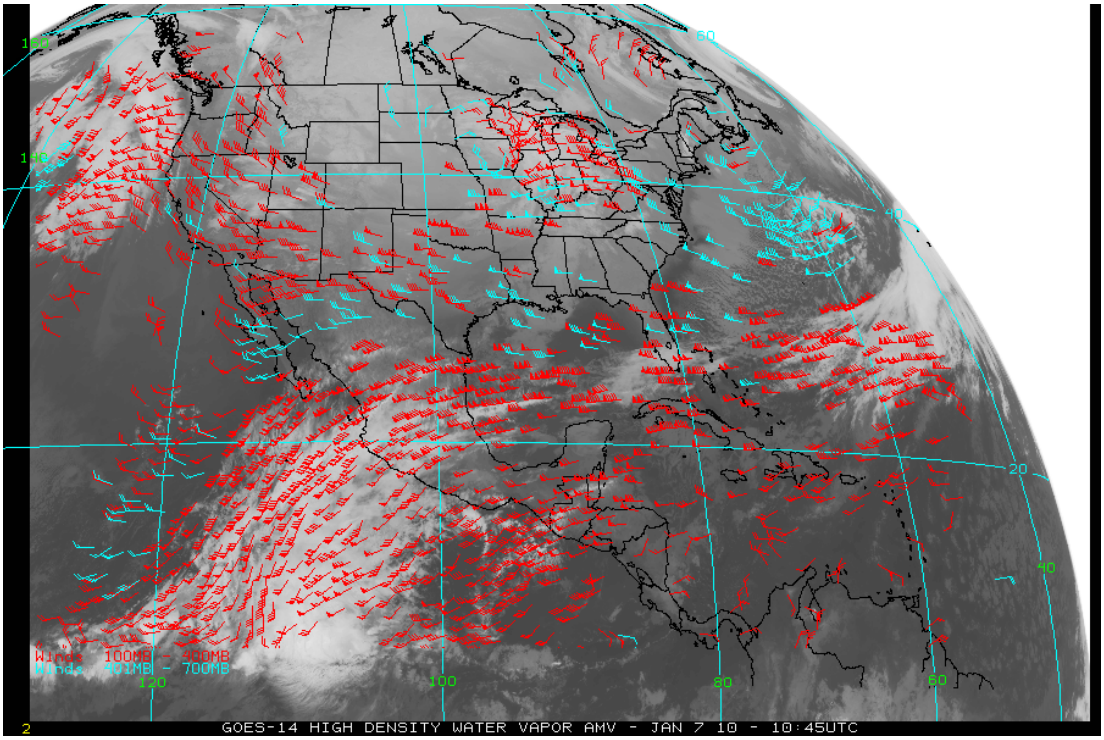

Figure 5.14: GOES-14 NHEM water vapor AMV on 7 January 2010 at 1045 UTC.

During the PLST, objective statistical comparisons were made using collocated radiosonde (RAOB) data matched to the various GOES-14 AMVs. Table 5.2 shows the results of these GOES vs. RAOB match statistics.

Table 5.2: Verification statistics for GOES-14 vs. RAOB Match Verification Statistics NHEM winds (m/s): 30 November 2009 – 16 January 2010

NHEM	RMS	MVD	Std Dev	Speed Bias	Mean Speed (Sat)	Mean Speed (RAOB)	Sample Size
Cloud-Drift	6.61	5.27	3.98	-0.92	23.06	23.99	6897
Water Vapor	7.19	5.89	4.12	-0.37	27.11	27.48	14203
Short Wave IR	4.71	3.98	2.52	-1.32	8.77	10.10	4338
Visible	6.29	5.52	3.01	1.75	10.23	8.48	214*

*Note: Visible AMV sample sizes were limited due to limited daylight hours at RAOB valid times

Comparison statistics were also generated for collocated GOES-12 and GOES-14 AMV datasets with RAOB observations. To be considered in the statistical evaluation, the respective GOES AMVs had to be within 1/10 degree horizontal and 25 hPa vertical. The small differences confirm that the AMV products from GOES-14 are at least comparable in quality with the existing GOES-12 operational AMVs.

Table 5.3: Verification statistics for GOES-12 and GOES-14, collocated (0.1 deg, 25 hPa) RAOB Match Verification Statistics for NHEM winds (m/s): 30 November 2009 – 16 January 2010

NHEM	RMS	MVD	Std Dev	Speed Bias	Mean Speed (Sat)	Mean Speed (RAOB)	Sample Size
GOES-12 Cloud-Drift	5.53	4.45	3.29	-0.85	19.92	20.75	337
GOES-14 Cloud- Drift	5.69	4.48	3.51	-1.03	19.77	20.82	337
GOES-12 Water Vapor	6.57	5.51	3.59	-0.21	29.21	29.41	791
GOES-14 Water Vapor	6.60	5.47	3.68	-0.50	28.93	29.42	791
GOES-12 Short Wave IR	3.98	3.55	1.81	1.07	8.26	7.17	40
GOES-14 Short Wave IR	4.13	3.64	1.95	1.14	8.43	7.26	40
GOES-12 Visible	6.61	5.52	3.64	0.85	10.19	9.36	24*
GOES-14 Visible	5.95	5.11	3.05	0.98	10.32	9.35	24*

*Note: Visible AMV sample sizes were limited due to limited daylight hours at RAOB valid times

In addition, normally an image navigation correction is attempted before the wind generation. In this process the second and third images are corrected to the first image. As a test, this was needed for GOES-12 in 12 of the 36 cases, yet it was not needed in any of the GOES-14 cases, indicating that GOES-14 image registration is improved.

5.5. Clear Sky Brightness Temperature (CSBT) from the Imager

The GOES-14 Imager Clear Sky Brightness Temperatures (CSBT) product spatially averages the clear fields of view for use in global numerical weather prediction (NWP) applications. In particular, the CSBT can be used to initialize global numerical models. In general, there is fair agreement between the GOES-11, GOES-12 and GOES-14.

A sample GOES-12 Imager Clear Sky Brightness Temperature cloud mask image was generated and is shown in Figure 5.15.

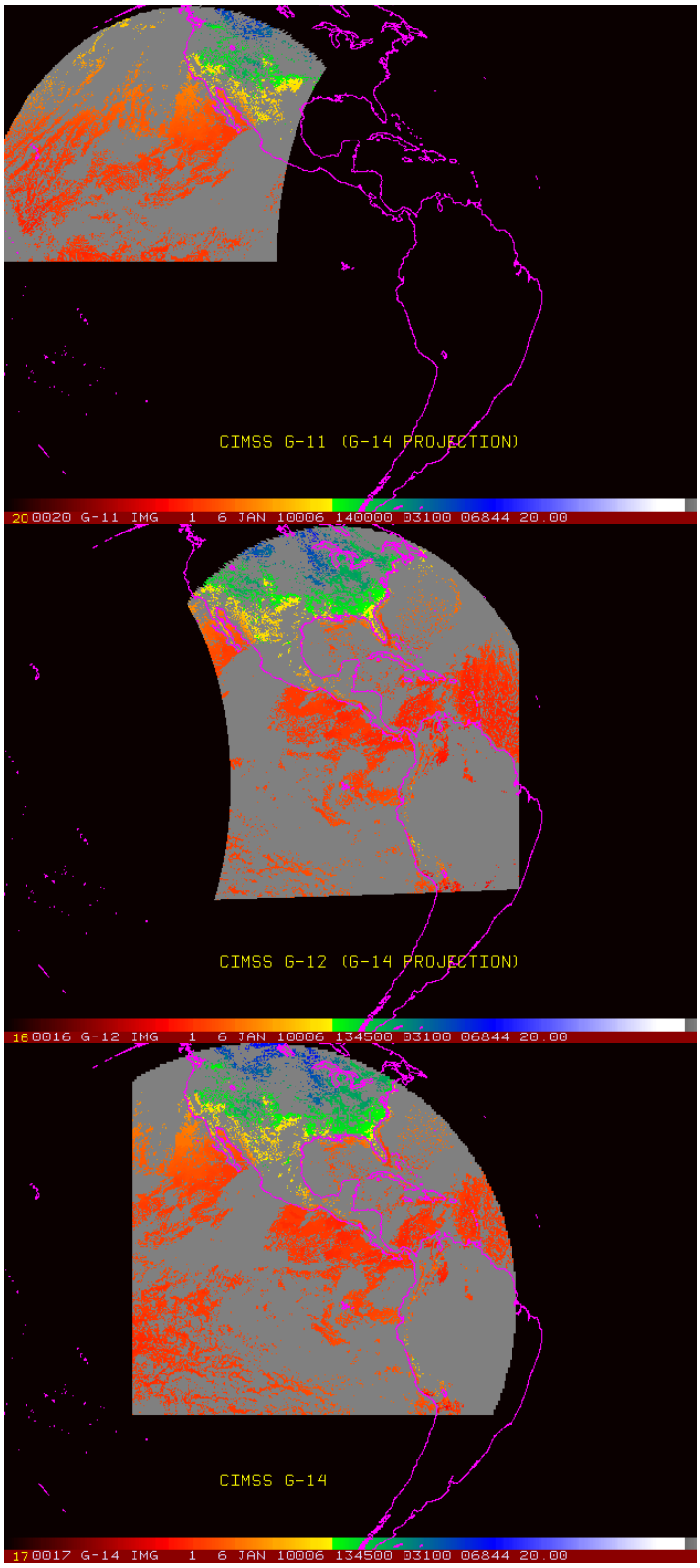

Figure 5.15: GOES-11 (top), GOES-12 (middle) and GOES-14 (bottom) Imager Clear-Sky Brightness Temperature cloud mask from 1400 UTC on 6 January 2010. Each image is shown in the GOES-14 satellite projection.

5.6. Sea Surface Temperature (SST) from the Imager

GOES-14 Imager data were collected for both the north and south hemispheric sectors every half hour from 30 November 2009 to 4 January 2010 for use as input for Sea Surface Temperature (SST) retrievals. The north hemispheric sector is centered at latitude 14°19′53″ N, longitude 71°38′51″ W; the south hemispheric sector is centered at latitude 31°55′10″ S, longitude 71°04′53″ W. Pre-processed visible and IR imagery data were used to create multi-spectral imagery files as input of SST retrieval. Examples of the radiance imagery are shown in Figure 5.16.

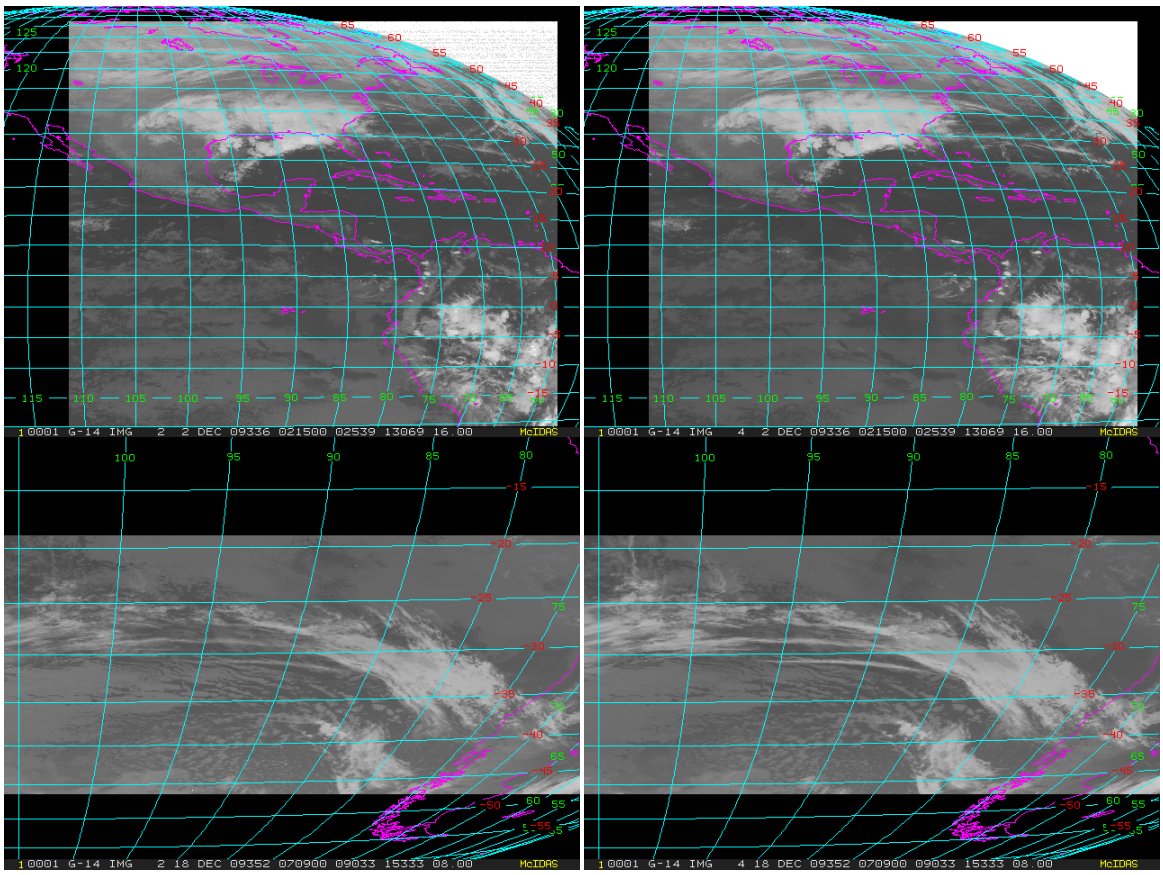

Figure 5.16: GOES-14 north sector band-2 (upper-left); GOES-14 north sector band-4 (upper-right); GOES-14 south sector band-2 (lower-left); GOES-14 south sector band-4 (lower-right).

5.6.1. SST Generation

The SSTs were generated using Radiative Transfer Model (RTM) regression coefficients which are derived from simulated data using a representative set of atmospheric profile data and a range of satellite zenith angles consistent with the satellite sub point of 105°W. The exact form of the current GOES operational SST equation used is

$$SST = a_0 + a_0 S + \sum_i (a_i + a_i\ S)\ T_i$$

where *i* is GOES-Imager band number (2, 4), S = satellite zenith angle – 1, and T_i is the band brightness temperature (K). Due to a lack of a 12 µm band on GOES-14, a single dual window form was used for both day and night with a correction for scattered solar radiation in the 3.9 µm band being applied for the daytime case (for details see Merchant et al. 2009). To determine clear sky pixels, a cloud mask was then derived using Bayes' theorem which estimates the probability of a particular pixel being clear of cloud given the satellite-observed brightness temperatures, a measure of local texture and band brightness temperatures calculated for the given location and view angle using NCEP GFS surface and upper air data and the JCSDA Community Radiative Transfer Model (CRTM) fast model. The method is described in detail in Merchant et al. (2005).

Hourly SST were created by compositing three half hour SST McIDAS Area files with an applied threshold of ≥98% clear sky probability. Satellite retrieval SST was matched with buoy data to create a match-up dataset for validation. Examples of the GOES-14 SST images are shown in Figure 5.17.

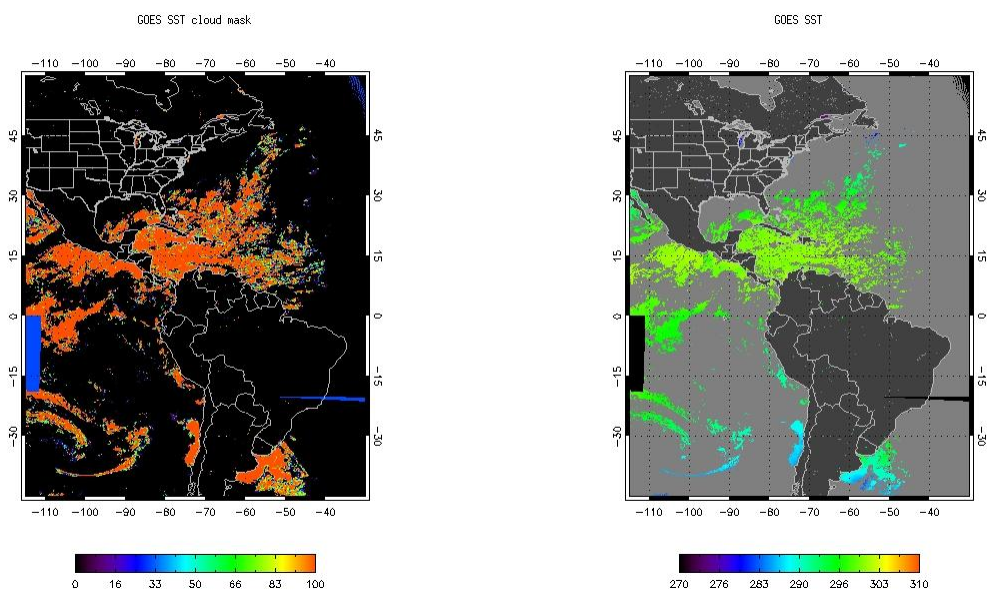

Figure 5.17: GOES-14 SST imagery (Hourly SST composite with applied 98% clear sky probability (left) and hourly composite clear sky probability).

5.6.2. SST Validation

GOES-14 SST retrievals were compared to those from GOES-12. Figure 5.18 shows the GOES-12 SST against buoy SST validation for daytime and nighttime and Figure 5.19 shows the GOES-14 SST against buoys. To maintain consistency between the GOES-12 and GOES-14

validation, the simple bias correction normally used to correct for the expected difference between the SST derived from the RTM simulated coefficients and the observations has not been applied. The lack of a bias correction explains the large biases seen for both satellites. The standard deviation (RMS) for GOES-14 is also worse than the RME values for GOES-12 but this result is almost certainly due to the large difference between the longitude of the GOES-14 radiance imagery (at 71°W) and the satellite sub point (at 105°W) which does not exist for the GOES-12 data. Consequently, the GOES-14 data used in this test were obtained at much higher satellite zenith angles than for GOES-12 which has the effect of increasing the uncertainty in the retrieved SST. Such a large difference is not expected in normal operations.

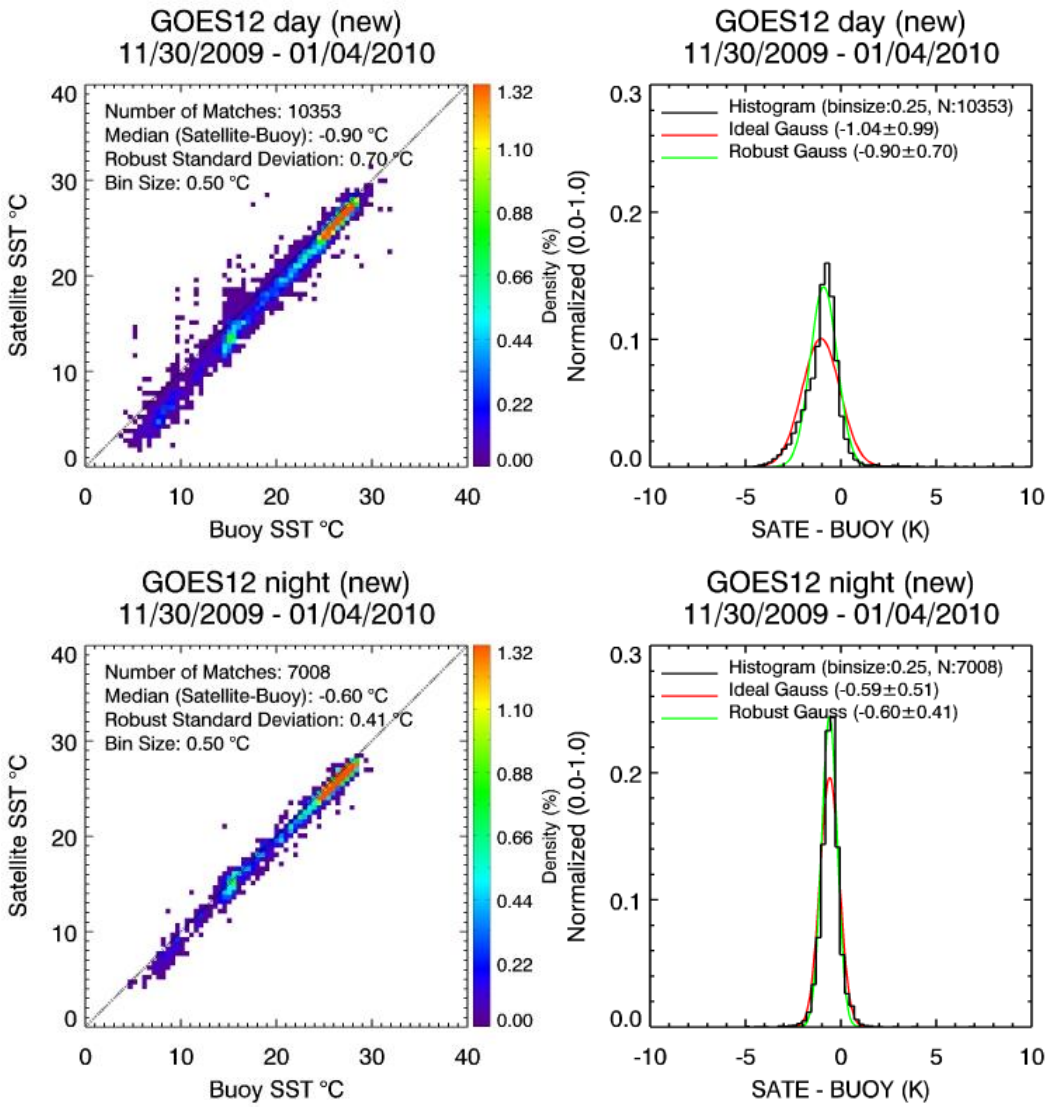

Figure 5.18: GOES-12 SST daytime and nighttime retrievals vs. buoys.

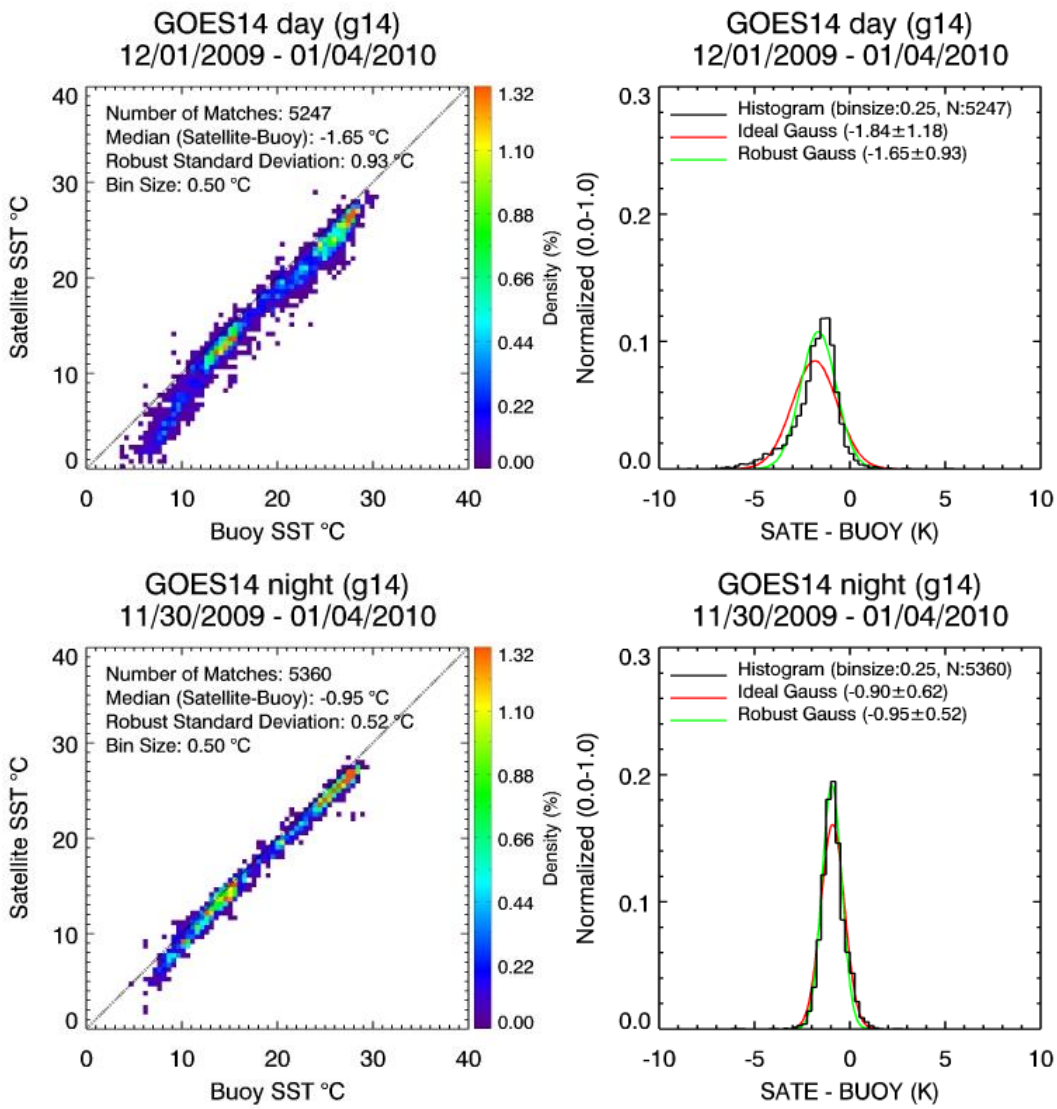

Figure 5.19: GOES-14 SST daytime and nighttime retrievals vs. buoys.

5.7. Fire Detection

Basic fire detection relies primarily on shortwave window (3.9 µm, band-2) data from the GOES Imager. This band, along with the IR window (11 µm, band-4), provides the basis for locating the fire and other information aids in estimating the sub-pixel fire size and temperature. The number of fires that can be successfully detected and characterized is related to the saturation temperature, or upper limit of the observed brightness temperatures, in the 3.9 µm band. A higher saturation temperature is preferable as it affords a greater opportunity to identify and estimate sub-pixel fire size and temperature. That said, the maximum saturation temperature should still be low enough to be transmitted via the GVAR data stream. Low saturation temperatures can result in the inability to distinguish fires from a hot background in places where the observed brightness temperature meets or exceeds the saturation temperature.

A comparison of GOES-11 (GOES West), GOES-14, and GOES-12 (GOES East) 3.9 µm shortwave IR images in Figure 5.20 indicated that there were a number of fires burning across parts of southern British Columbia, Canada on 1 December 2009, as confirmed by the NOAA Hazard Mapping System. The 3 sets of images are displayed in the native projection of their respective satellites. The fire "hotspots" showed up as warmer (darker black enhancement) pixels.

The plot in Figure 5.21 shows that the warmest 3.9 µm IR brightness temperature on the GOES-14 imagery was 325.8 K at 2215 UTC, compared to 317.7 K on GOES-11 at 2015 UTC and 304.9 K on GOES-12 at 1945 UTC. This difference in maximum fire pixel brightness temperature and time was due to such factors as different satellite viewing angles (compounded by the steep slopes of the mountainous terrain) and possible brief obscuration by clouds and/or smoke. More information on this case can be found at http://cimss.ssec.wisc.edu/goes/blog/archives/4053.

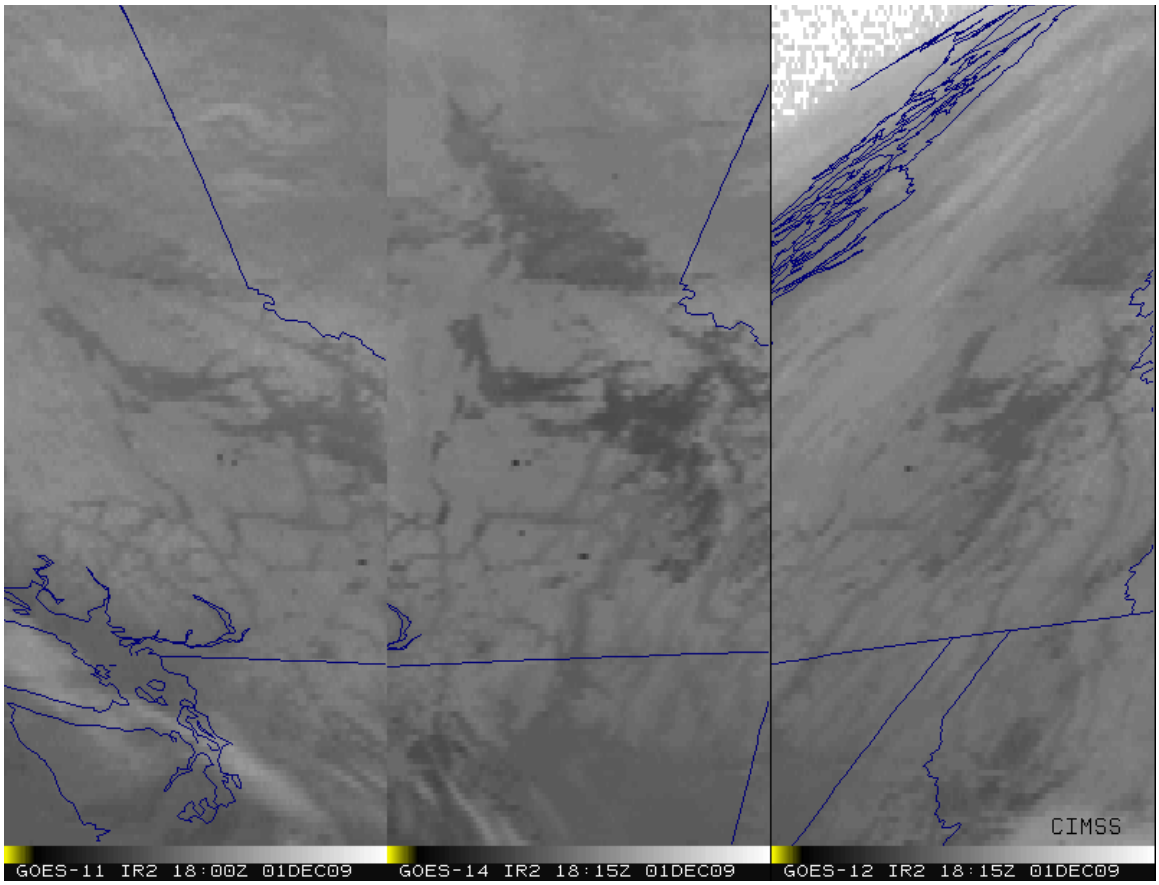

Figure 5.20: GOES Imager 3.9 µm images from GOES-11 (left), GOES-14 (center) and GOES-12 (right). Each satellite is shown in its native perspective.

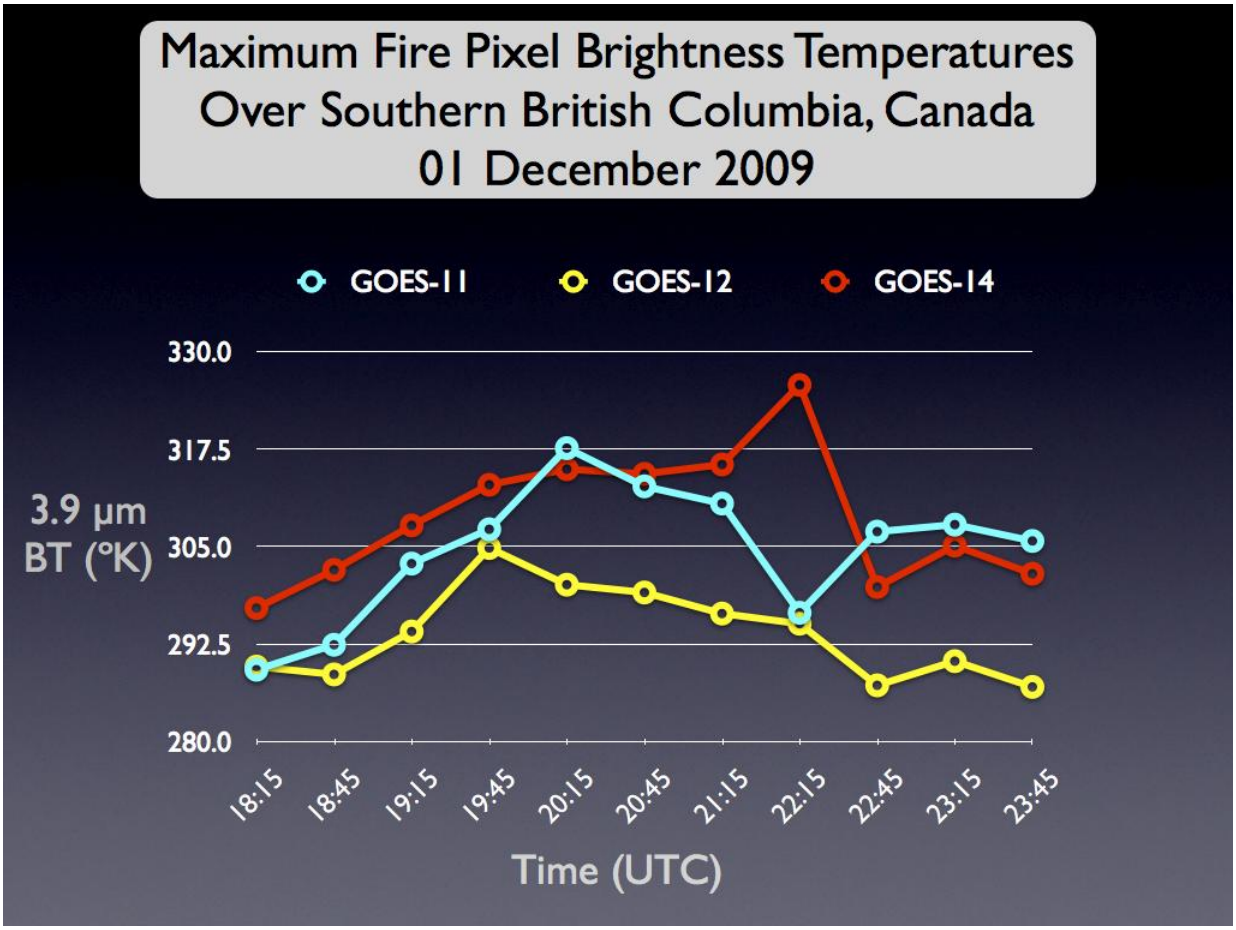

Figure 5.21: GOES Imager 3.9 µm time series from GOES-11, GOES-12 and GOES-14.

The GOES-14 Imager 3.9 µm band has a saturation temperature of approximately 338.1 K. For reference, the GOES-12 Imager 3.9 µm band has a saturation temperature of approximately 336 K, although this value has changed over time, peaking at approximately 342K.

Preliminary indications are that GOES-14 is performing comparably to GOES-11 and GOES-12.

The Biomass Burning team at CIMSS currently produces fire products for GOES-11/12 covering North and South America. These data can be viewed at the Wildfire Automated Biomass Burning Algorithm, which can be found at http://cimss.ssec.wisc.edu/goes/burn/wfabba.html.

5.8. Volcanic Ash Detection

Volcanic ash was detected by both GOES-12 and GOES-14 several times during the test period. On both 15 and 30 December the ash signature in visible and multispectral imagery showed up better in GOES-14 imagery than in GOES-12 imagery. For the multispectral imagery, there seems to be a better alignment between the bands used to produce the imagery using GOES-14 than when using GOES-12. With GOES-12, there was a distinct "venetian blind" or striping effect to the imagery making it harder to detect the ash. In GOES-14 multispectral imagery there was much less striping resulting in an improvement for ash detection.

On 3 January 2010 the Galeras volcano in Colombia (located in the Andes Mountains near Colombia's border with Ecuador) experienced an explosive eruption around 0043 UTC. Figure 5.22 shows a comparison of GOES-11/12 and GOES-14 imagery of the eruption.

Volcanic ash detection from GOES-14 should be comparable or slightly improved (due to the improved Signal-to-Noise Ratio (SNR)) compared to GOES-12. With operations through the eclipse periods, additional events may be captured.

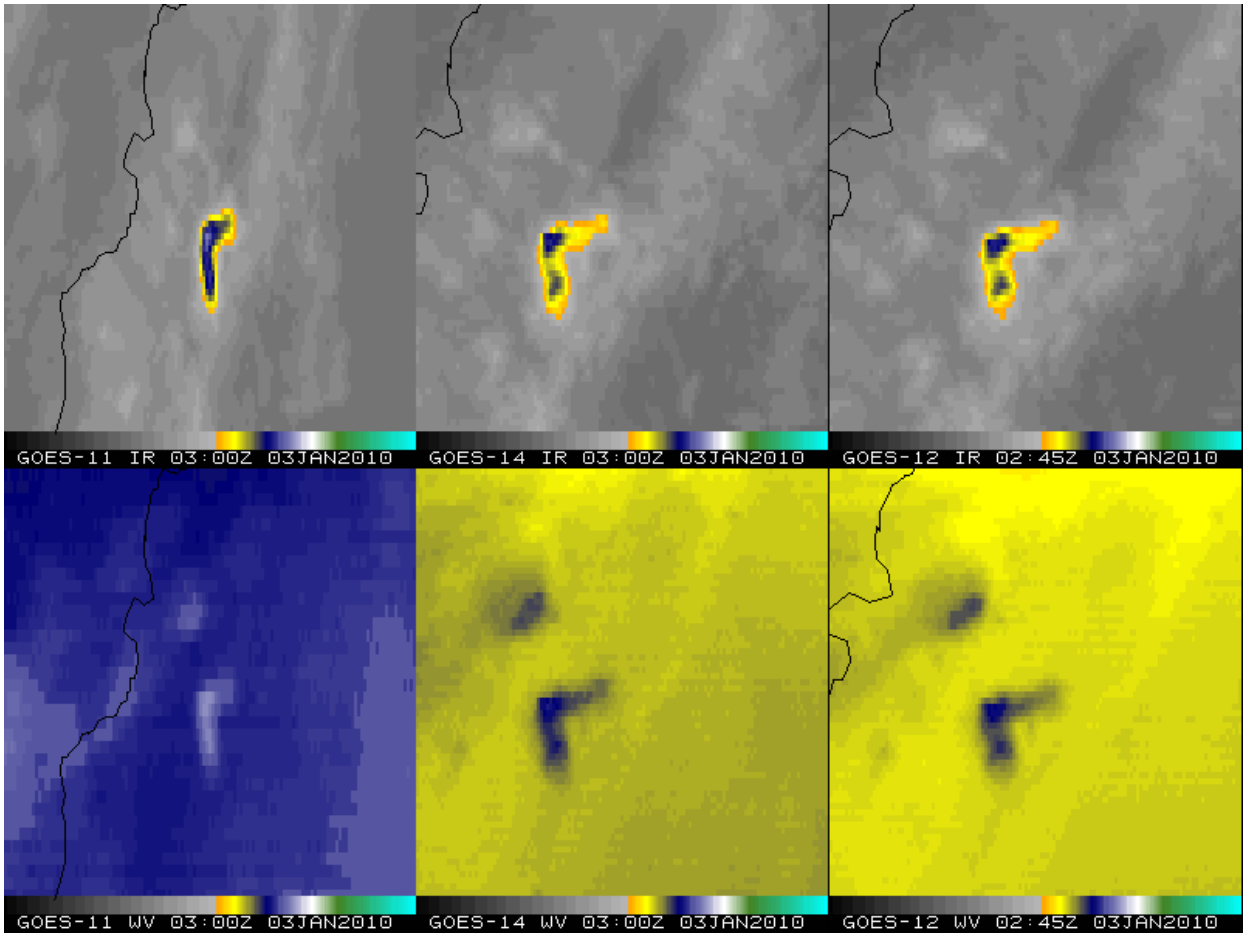

Figure 5.22: GOES-11, GOES-14, and GOES-12 10.7 µm IR and 6.7/6.5 µm water vapor images.

5.9. Total Column Ozone

Total Column Ozone (TCO) is an experimental product from the GOES Sounder. The GOES-14 Sounder TCO is expected to be of similar, or higher, quality as derived from earlier GOES Sounders. Note the similar overall patterns between GOES-12 and GOES-14 shown in Figure 5.23 and 5.24. The larger amount of noise from the GOES-12 is also clearly seen.

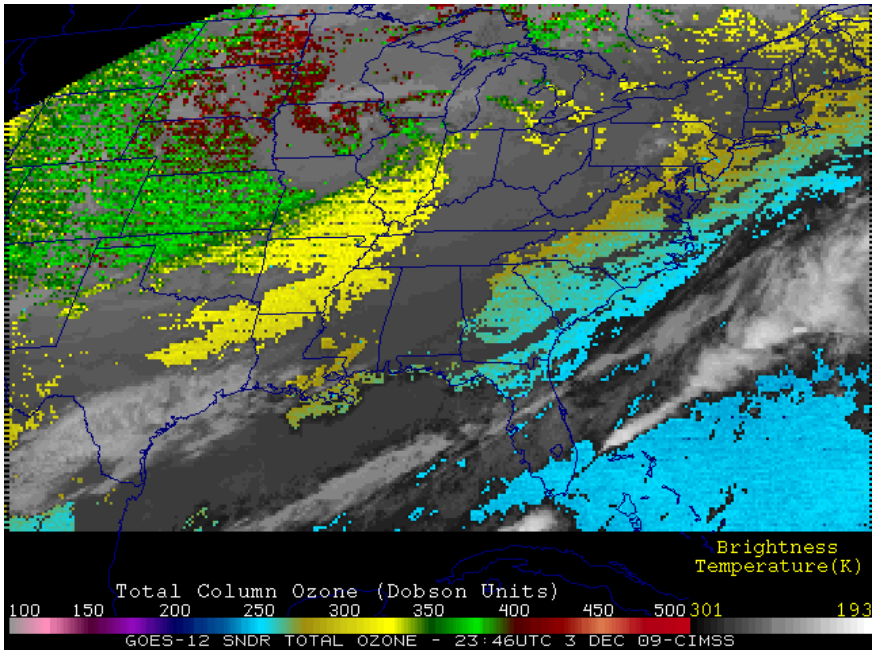

Figure 5.23: Example of GOES-12 Imager Total Column Ozone on 14 January 2010 at 1200 UTC.

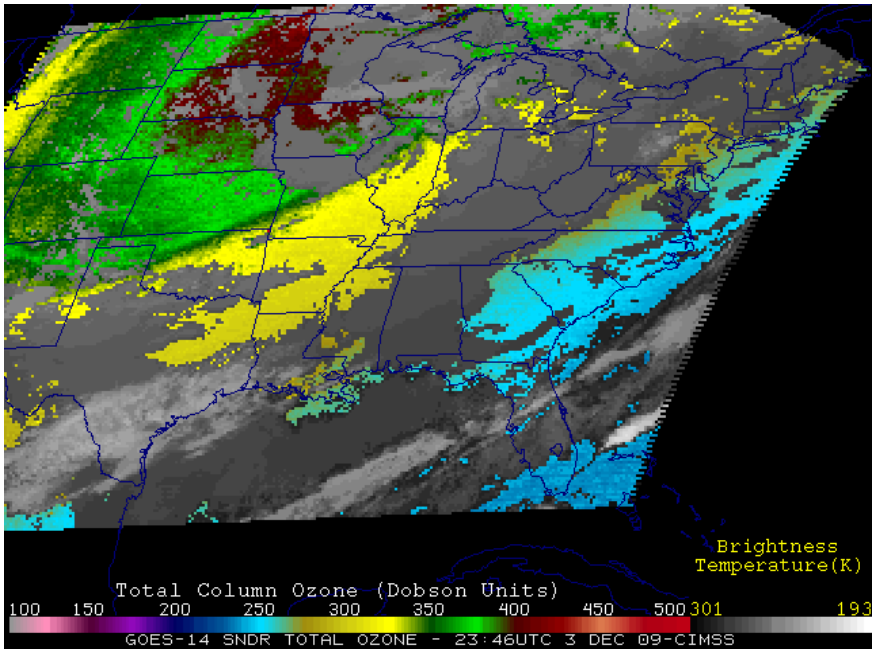

Figure 5.24: Example of GOES-14 Imager Total Column Ozone on 14 January 2010 at 1200 UTC. The image is displayed in the GOES-12 perspective.

5.10. GOES Surface and Insolation Product (GSIP)

The GOES Surface and Insolation Products (GSIP) system is producing operationally a suite of products relating primarily to upward and downward solar radiative fluxes at the surface and top of the atmosphere. As shown in Figures 5.25 and 5.26, the similarity of surface insolation as derived from GOES-12 and GOES-14 data, as well as the other products, which are not shown, illustrates that GSIP is well on the way to generating datasets from the GOES-14 Imager.

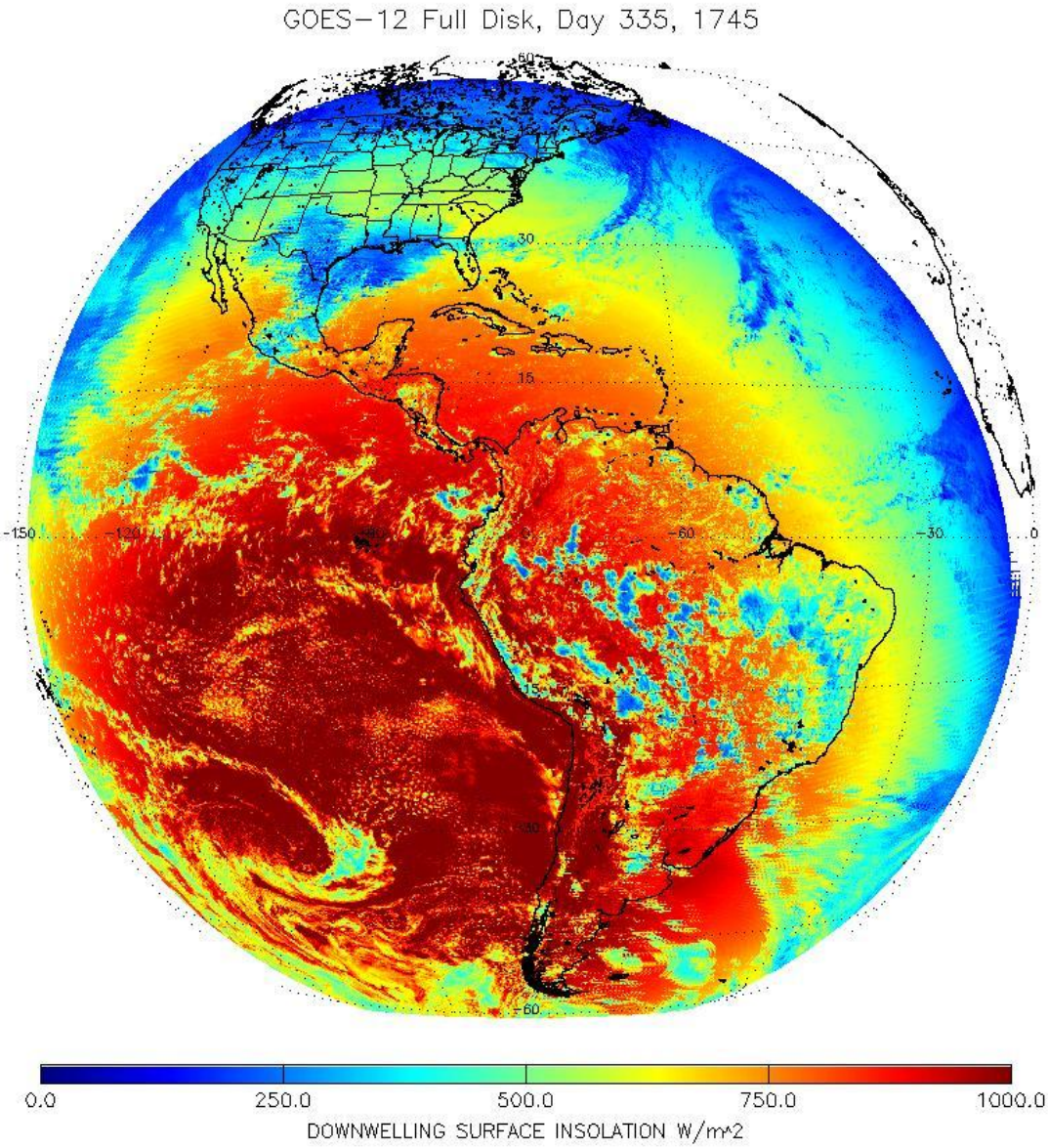

Figure 5.25: GOES-12 Imager downwelling surface insolation on 1 December 2009 beginning at 1745 UTC.

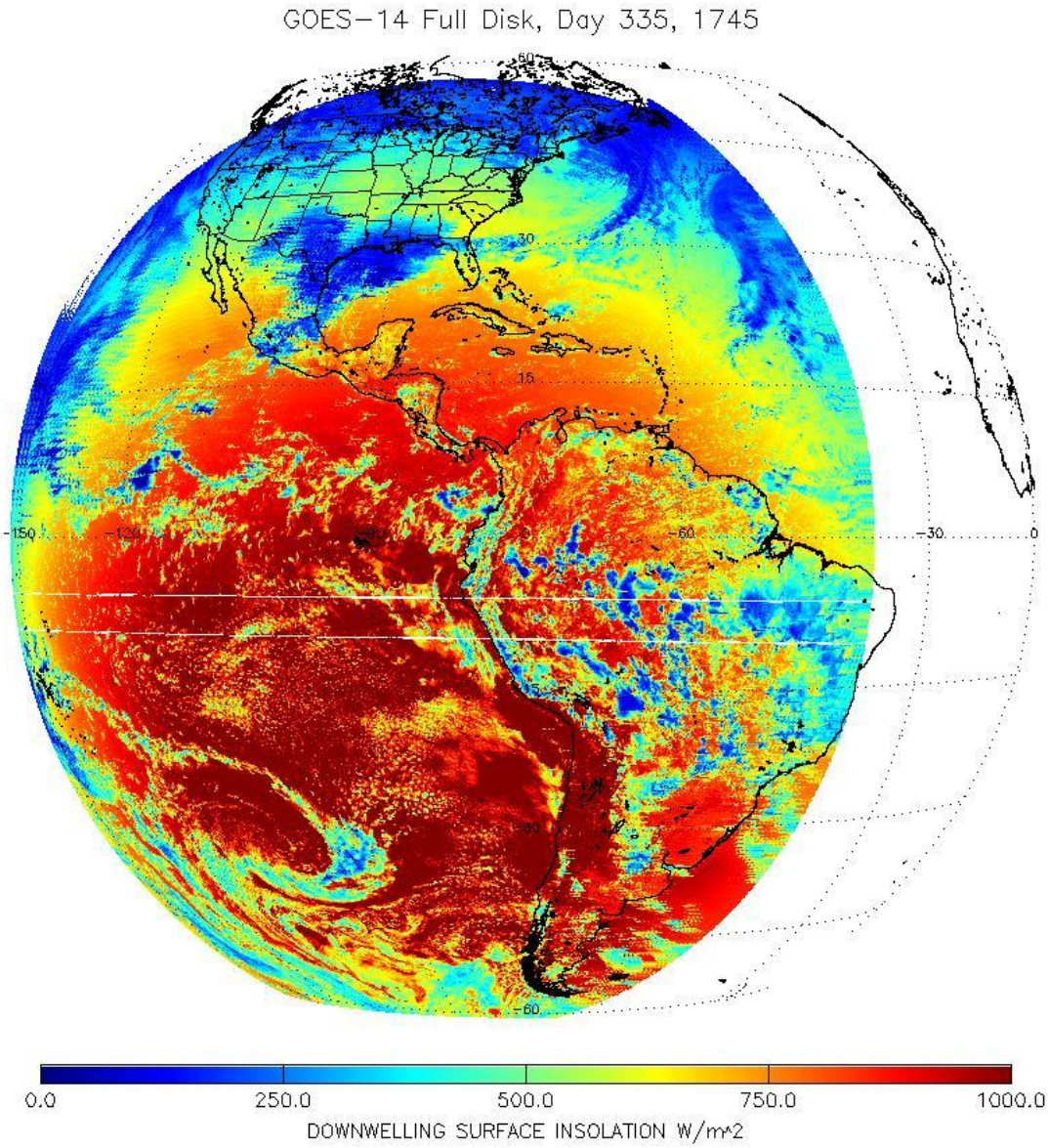

Figure 5.26: GOES-14 Imager downwelling surface insolation on 1 December 2009 beginning at 1745 UTC.

6. Other Accomplishments with GOES-14

6.1. GOES-14 Imager Visible (band-1) Spectral Response

A comparison of enhanced visible band images from GOES-12 and GOES-14 at 1315 UTC on 1 September 2009 is shown in Figures 6.1 and 6.2. Images from both satellites have been remapped to a Mercator projection over the state of Wisconsin. The obvious "meteorological" phenomenon is the early morning fog in the Mississippi, Wisconsin, and Kickapoo River basins, in addition to numerous other valleys and river basins feeding into the Mississippi River.

There are a couple of significant differences to note between the two visible images. First of all, the fog is a bit brighter and a little more extensive in the GOES-14 image compared to the GOES-12 image. This difference is primarily due to the relative age of the visible sensors (which noticeably degrades with time). The second major difference is the relative contrast of lakes, rivers, vegetation, and land usage. GOES-12 has slightly more contrast between land and lakes (and/or other bodies of water) than GOES-14. This is most likely due to the differing SRF.

On the other hand, GOES-14 is able to discern urban centers more readily than GOES-12, as well as variations in vegetation type. Examples of this are around the large metropolitan region of southeastern Wisconsin and northeastern Illinois (i.e. Milwaukee to Chicago). Also, both the Baraboo Range (located just to the northwest of Madison) and the "Military Ridge" (which runs east to west from Madison to Prairie du Chien) stand out more boldly in the GOES-14 image compared to the GOES-12 image. This difference is primarily due to the slight variation in the spectral width of the two visible bands on the GOES-12 and GOES-14 Imagers. A comparison of the visible band spectral response function for GOES-12 and GOES-14 shows that the sharper cutoff for wavelengths beyond 0.7 µm on the GOES-14 visible band makes it less sensitive to the signal from the mature corn crops, allowing greater contrast between the thick vegetation of the agricultural fields and the more sparsely vegetated cities, towns, and highway corridors.

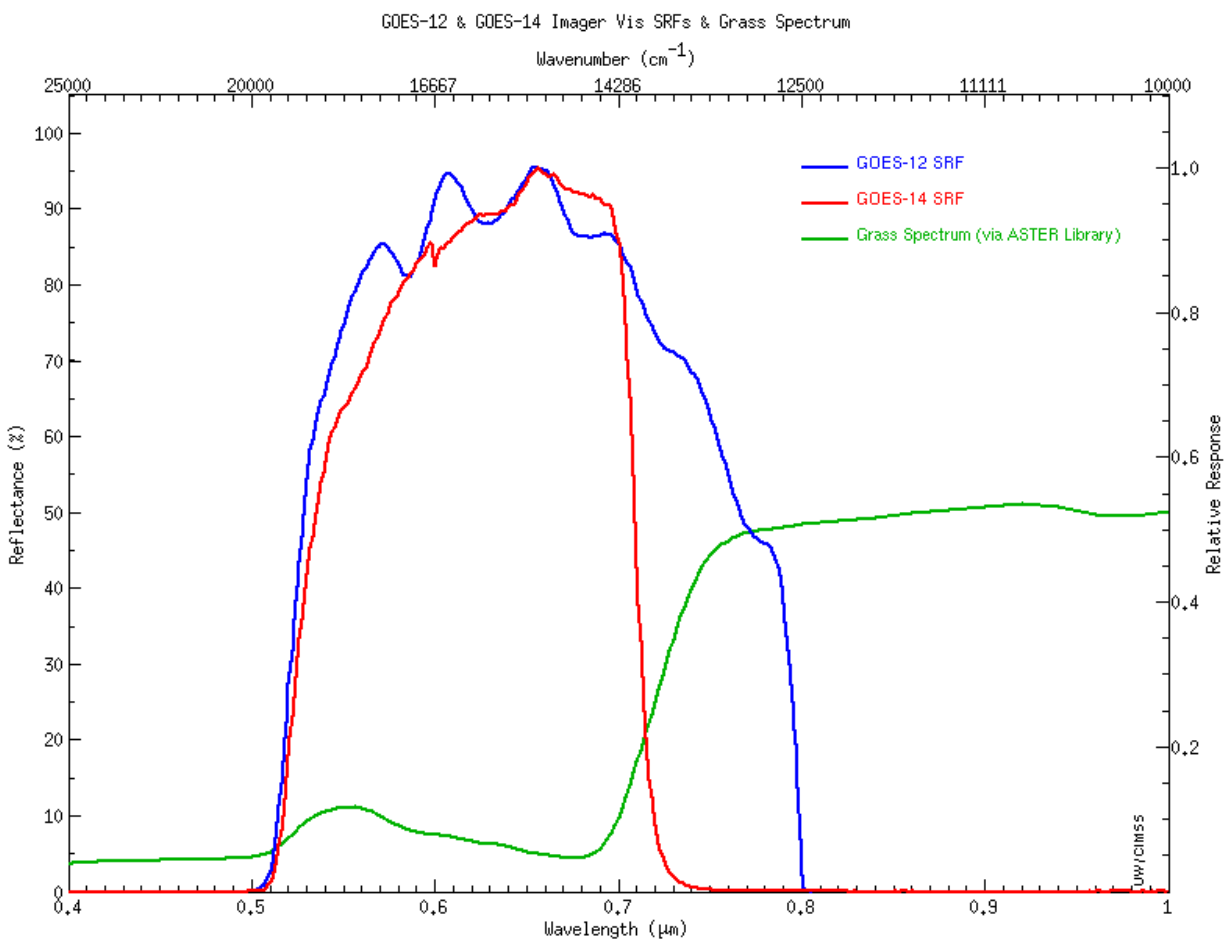

Figure 6.1: GOES-12 (blue) and GOES-14 (red) Imager visible (approximately 0.65 or 0.63 µm) band SRFs, with a representative spectrum for grass over-plotted (green).

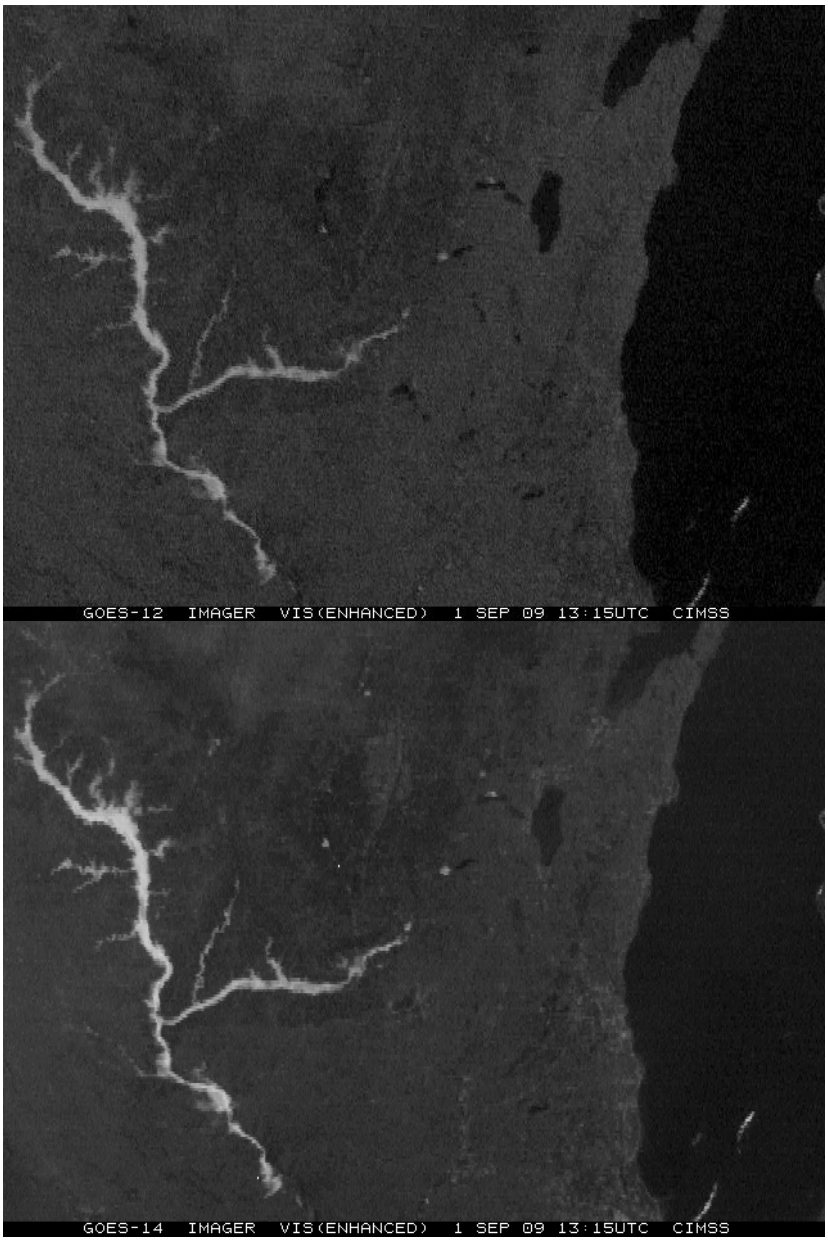

Figure 6.2: Comparison of the visible (0.65 µm) imagery from GOES-12 and GOES-14 (0.63 µm) on 1 September 2009 demonstrates how certain features, such as surface vegetation, are more evident with the GOES-14 visible data.

More information on this case can be found at http://cimss.ssec.wisc.edu/goes/blog/archives/3355.

6.2. Lunar calibration

Several GOES-14 Imager datasets were acquired during the PLT. The main objective of these tests was to observe the lunar images as soon as possible in order to establish a baseline for future study of instrument degradation. While not intended, lunar images may allow an attempt on absolute calibration, although this theory has not been fully researched.

Figure 6.3: GOES-14 Imager visible (0.65 µm) band image of the moon from 9 August 2009 for a scan that started at 2053 UTC.

6.3. Improved Image Navigation and Registration (INR) with GOES-14

McIDAS images of GOES-12 and GOES-14 visible band data showed that large chunks of ice (known as "ice fields") were drifting north-northeastward across the western portion of Lake Erie on 14 January 2010**.** The improved INR is clearly evident with GOES-14. Southerly to southwesterly winds were beginning to increase on that day, helping to move the ice features across the surface of the lake. The animation can be found at http://cimss.ssec.wisc.edu/goes/blog/archives/category/goes-14.

NOAA also has analyzed the INR data and determined that the 15-minute star windows required 4 hours around an eclipse are not necessary. Going back to a 30-minute star window will allow NOAA to run the regular schedule during that 4-hour period around satellite midnight instead of frames limited to only 5-minutes. As a result, more earth-scene data can be scanned during that part of the night, and still meet the INR requirements.

6.4. Special 1-minute Scans

On 19 December 2009, a comparison of 15-minute interval GOES-12 and 1-minute interval GOES-14 visible images centered off the east coast of the Delmarva Peninsula offers a compelling demonstration of the value of more frequent imaging for monitoring the development and evolution of cloud features. During this 1815 – 1904 UTC time period, only 3 images were available from GOES-12, compared to 44 images using GOES-14. This animation can be found at http://cimss.ssec.wisc.edu/goes/blog/wp-content/uploads/2009/12/ecb_g12g14_vis_anim.gif.

6.5. Spatial Line-shifted Over-sampling Test

One of the Science Tests (C8) was intended to simulate GOES-R ABI-like (2 km) spatial resolution data. Data for this test were gathered from four different sectors at different times during the day. For each sector three successive images were taken in rapid succession, in order to minimize any changes between the images, but with the scan lines offset by a half of the normal (4 km) distance between image lines. It was then hoped that this line-shifted over-sampled data could be de-convolved to produce imagery at 2 km resolution similar to that which will be available from ABI.

Unfortunately, the data for this test failed to be collected as rapidly as needed to avoid cloud motions. The results with this less than optimal data are presented in Appendix C. A similar test undertaken during the GOES-13 checkout failed, so this test was at least successful in its intent. Hopefully this test will be repeated during the Science Test for GOES-15.

7. Coordination with University of Alabama/Huntsville

As part of NOAA's GOES-14 Science Test, SRSO (1-minute data) were requested by the NASA MSFC Earth Science Office to support research in algorithm development related to applications of future space based geostationary lightning mapping systems (i.e., GOES-R GLM) in high-impact weather events. Accordingly, ground based assets including the UAH ARMOR dual-polarization radar, KOUN dual-polarization radar, WSR-88D radar, and VHF lightning mapping arrays in N. Alabama (NALMA), Washington D.C. (DCLMA), Oklahoma (OKLMA) and Cape Canaveral, Florida (KSC), combined with the GOES-14 SRSO, comprise the set of tools to be used for the investigation. Collectively, the satellite data combined with the aforementioned datasets provide a robust means of examining cell evolution, including relationships of cloud kinematic trends with lightning and microphysical properties.

The specific objectives of the SRSO requests at MSFC can be summarized as follows: 1) Capture lightning-producing convection (hopefully severe) within view of the GOES-14 and ground-based assets; 2) For suitable lightning-producing cases identify precipitation and/or kinematic structure and behavior as observed from ground and space-based assets and compare to null cases (i.e., no lightning, but convective) in coincident SRSO domains; and 3) Capture winter storm cases to test hypotheses about thermodynamic and kinematic environments responsible for electrification, and the altitude and extent of charge regions. Of particular interest is the interaction of the warm conveyor belt with wrap-around precipitation in the deformation zone. The GOES super-rapid-scan data makes it easy to track individual

cumuliform convective elements with time and to correlate these features with radar observations and ground strike data from commercial networks in later post-analysis. These features will be compared with the studies of Market et al. (2006, 2009), who also looked at lightning in synoptic-scale snowstorms.

Table 7.1: Summary of significant case study dates for MSFC GOES-14 SRSO

Date	Location	Case	Data
2009-12-2/3	Northern Alabama	Weak lightning-producing convection; tornado warning.	SRSO, ARMOR dual-polarization, NALMA, regional WSR-88D
2009-12-8/9	Northern Alabama	Deep convection, copious lightning, severe wind event	SRSO, ARMOR dual-polarization, NALMA, regional WSR-88D
2009-12-18/19	Washington D.C.	Winter storm case (possible lightning)	SRSO, DCLMA, WSR-88D
2009-12-24	Eastern Oklahoma	Winter storm with thundersnow	SRSO, OKLMA, KOUN dual-polarization, WSR-88D

Table 7.1 presents a summary listing of the significant case dates (i.e., those designated as "primary" research cases) selected from the SRSO attempts. It must be noted that relative to objectives 1-3, this data collection was highly successful. Of course, several other SRSOs were conducted (e.g., focused Cape Canaveral area), but these SRSOs did not result in overly positive results.

7.1. Deep Convection: Example Case Studies

7.1.1. Marginal Lightning and Severe Weather: 2 December 2009

A thin line of precipitation pushed through N. Alabama on the afternoon of 2 December 2009. A tornado warning was issued by the National Weather Service in Huntsville, at 2105 UTC on a small storm in eastern Jackson County AL (Figure 7.1, red arrow). Figure 7.2 shows a dual Doppler analysis of this storm in eastern Jackson County at 2103 UTC. Rotation is not well defined in this storm, and it produced no detectable lightning; however, ARMOR reflectivity data indicated a small hook-like appendage on the southwestern flank of the warned cell. Note that the KHTX 88D had a much closer view of the system. Storms just to the south of this cell eventually did produce lightning at about 2130 UTC (Figure 7.3).

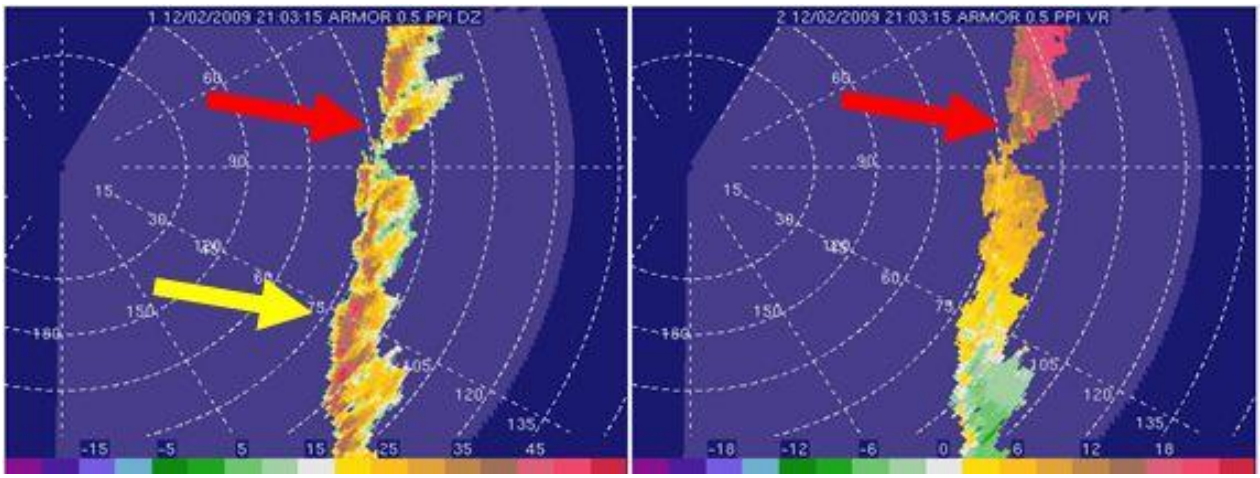

Figure 7.1: PPI from ARMOR at 2103 UTC on 2 December 2009 at 0.7° elevation. Reflectivity (upper-left), radial velocity (upper-right), differential reflectivity (lower-left) and specific differential phase (lower-right) are all shown. The cell that prompted the tornado warning is highlighted by the red arrow. Cells just to the south of the tornado-warned storm briefly produced lightning about 2130 UTC (yellow arrows).

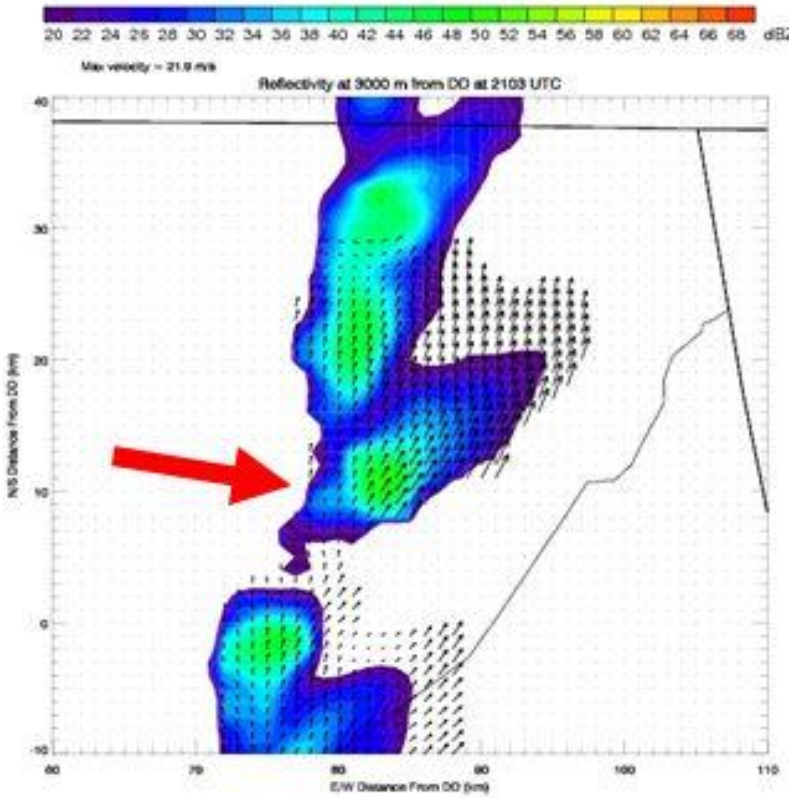

Figure 7.2: Dual Doppler Analysis using the WSR 88D radar at Hytop AL (KHTX) and UA Huntsville's ARMOR radar (2103 UTC). Shown are reflectivity (shaded) and ground-relative wind vectors. The cell that prompted the tornado warning is highlighted by the red arrow. Cells just to the south of the tornado-warned storm are producing lightning. Only very slight rotation is evident in the hook region of the dual-Doppler analysis.

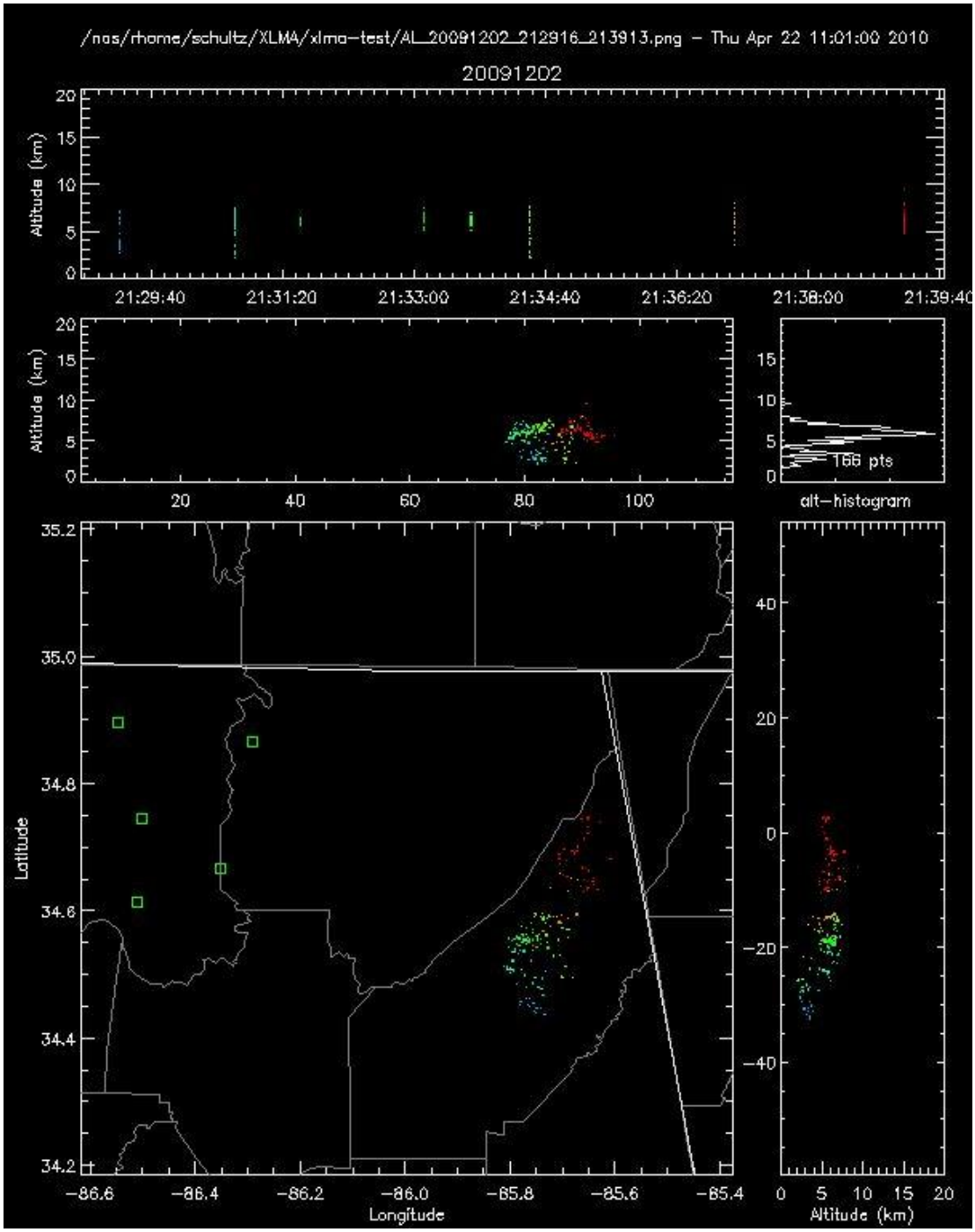

Figure 7.3: Total lightning measurements using the North Alabama Lightning Mapping Array for 2 December 2009 at 2130-2140 UTC. Vertical lines in the top panel represent lightning flashes, while the lower three panels represent the distribution of VHF sources in the XY (lower-right), XZ (middle) and YZ (lower-right) directions. Cooler colors represent flashes that occur earlier, while warmer colors show flashes that occur later in the period. Not unexpectedly, the source heights in this storm are relatively low in altitude.

Note: No satellite data have been analyzed for this case yet.

7.1.2. Severe Convection: 8-9 December 2009

This event (Figure 7.4) was long-lived (perhaps the best of the SRSO convective data collections), and characterized by 4-6 inches of heavy precipitation, local flooding, and severe wind damage to trees and power lines.

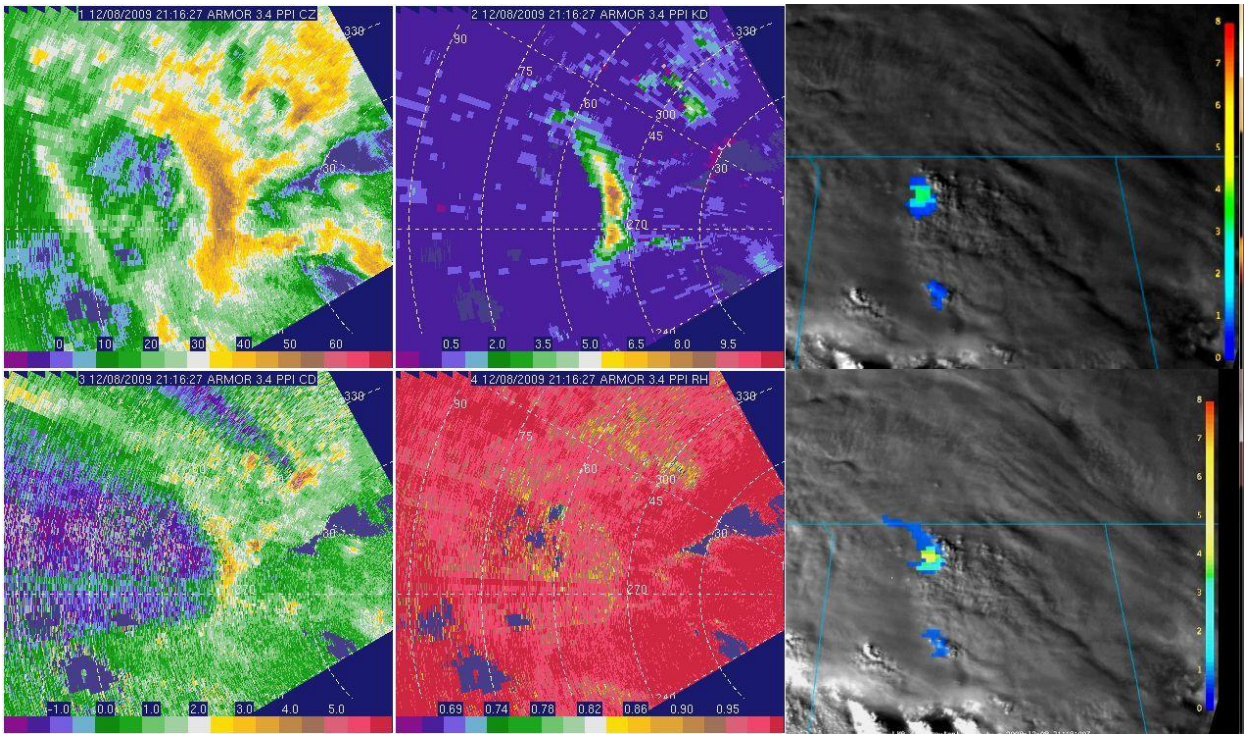

Figure 7.4: ARMOR image 2116 UTC at 3.4° elevation. Displayed are: reflectivity (CZ, upper-left), specific differential phase (KD, upper-middle), visible GOES-14 with lightning Flash Extent Density (FED, upper-right) at 2116 UTC, differential reflectivity (CD, lower-left), correlation coefficient (RH, lower-middle), and visible GOES-14 with FED at 2118 UTC (lower-right). A large drop core is identified in the dual-polarization data 50 km east of the radar along the apex of the bowed reflectivity feature.

The first round of thunderstorms for this event occurred on the afternoon of 8 December as a warm front lifted northward through north Alabama, and the event was extensively sampled by the NALMA and the ARMOR radar in volume scanning mode. Several percolating thunderstorm tops were observed in the SRSO visible imagery and an accompanying imagery loop which can be found at http://cics.umd.edu/~ebruning/GOES14sciencetest.html. Near most of the growing tops in the GOES-14 satellite data associated with this storm, lightning was observed (not parallax corrected), further identifying/confirming the location of thunderstorm updrafts.

The most prolific lightning producing thunderstorm within this first wave of precipitation moved through N. Alabama between 2000 and 2300 UTC. Peak total flash rates with this thunderstorm cell were observed to be ~6-7 flashes per minute. In Figures 7.4 through 7.5 these flash rates

peak near the apex of a slight bow in the system where the heaviest rainfall (indicated by KDP) is located. The cell underwent growth between 2115 and 2120 UTC, a period where the largest 1 minute flash rates were observed. Several more clusters of low flashing thunderstorms were observed through 0000 UTC and thereafter as a cold front progressed eastward. These storms continued to produce severe weather, heavy rain and flooding (hence numerous events exist for this SRSO).

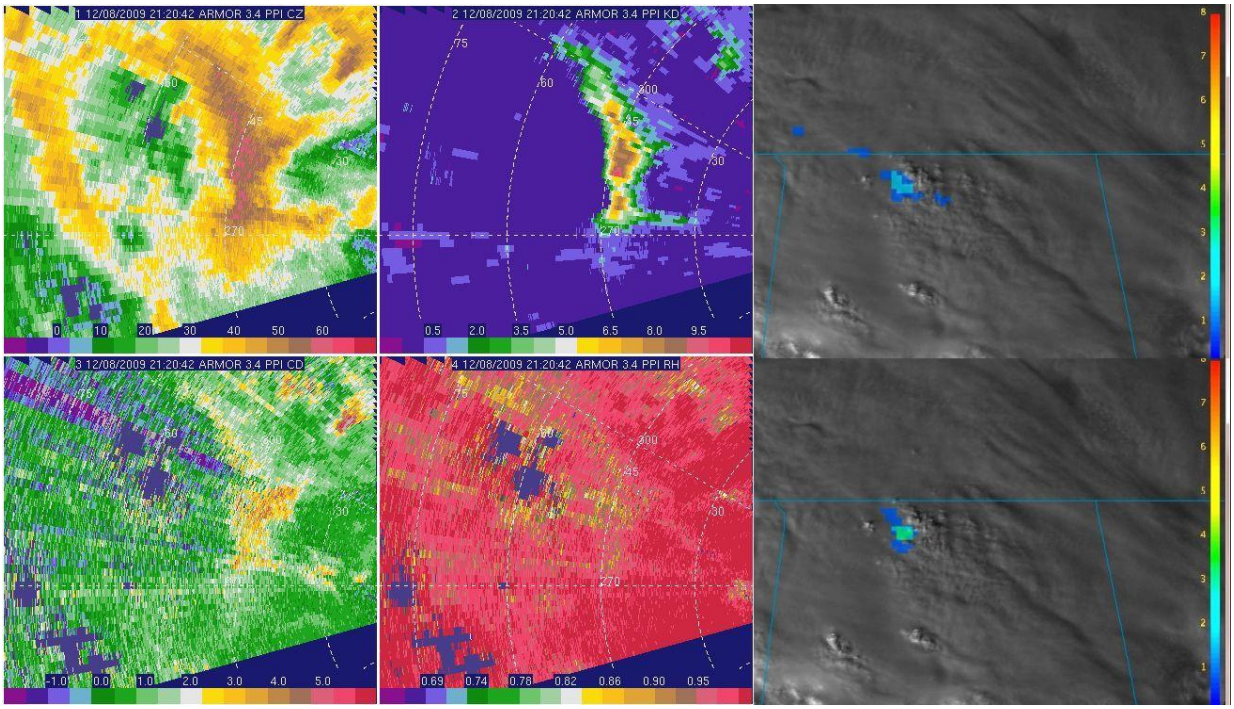

Figure 7.5: As in previous figure, but 2121 UTC for ARMOR image, 2120 UTC for specific differential phase, and 2121 UTC for lightning FED.

7.2. Winter Storm Events

7.2.1. Washington DC, 19 December 2009

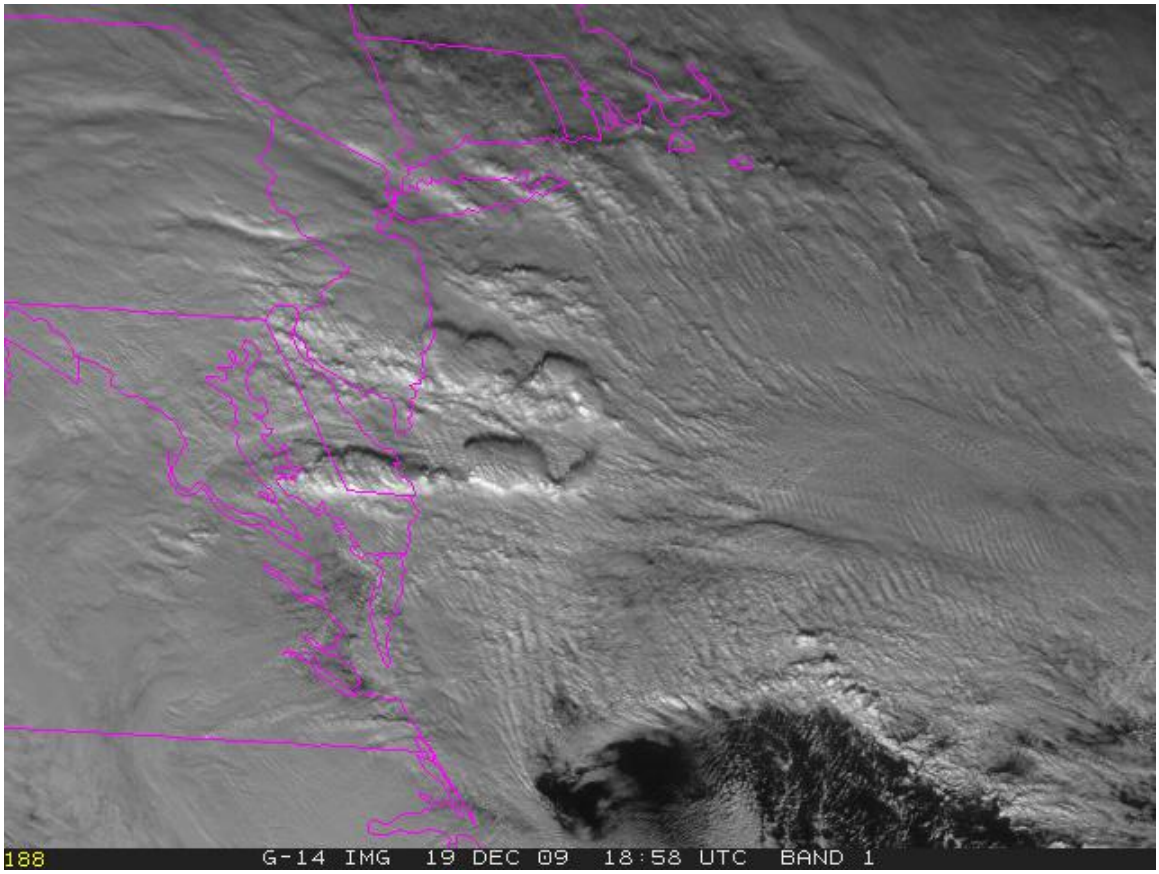

Figure 7.6: GOES-14 super-rapid-scan imagery from 1858 UTC on 19 December 2009 showing deep convective cells over the Delmarva Peninsula and southern New Jersey. Heavy snow was ongoing over adjacent parts of Maryland, Virginia, and Pennsylvania.

A coastal low-pressure system was responsible for a major snowfall on 19 December 2009 over Virginia and Maryland, including the DC metro area, which received between 16-20 inches storm total snow accumulation. There were a number of public and media reports of thunder in the Arlington VA area, though the Washington DC Lightning Mapping Array did not detect any flashes. During 1800-1900 UTC, two northward-moving, east-west oriented bands (Figure 7.6) of deep convection were observed on visible imagery over lower southern Maryland, Delaware and southern New Jersey (for reference, the imagery loop can be viewed at http://rammb.cira.colostate.edu/projects/svr_vis/eastcoast_snowstorm/ch1loop.asp.

The 1-minute scans that were captured in real-time were provided via Website and distributed to the Storm Prediction Center (SPC) operations and were used whenever available.

The absence of detected lightning in such deep convection is scientifically interesting as a null case. The GOES super-rapid-scan data make it easy to track individual cumuliform convective

elements with time and to correlate these features with radar observations and ground strike data from commercial networks in later post-analysis. In fact, some of these commercial networks reported ground strikes nearer to Philadelphia.

While lightning was also observed during the historical February 2010 snow storm in the DC area (http://cics.umd.edu/~ebruning/snow/Feb6-DCLMA.html), super-rapid-scan science test data were not available for this case.

7.2.2. Oklahoma, 24 December 2009

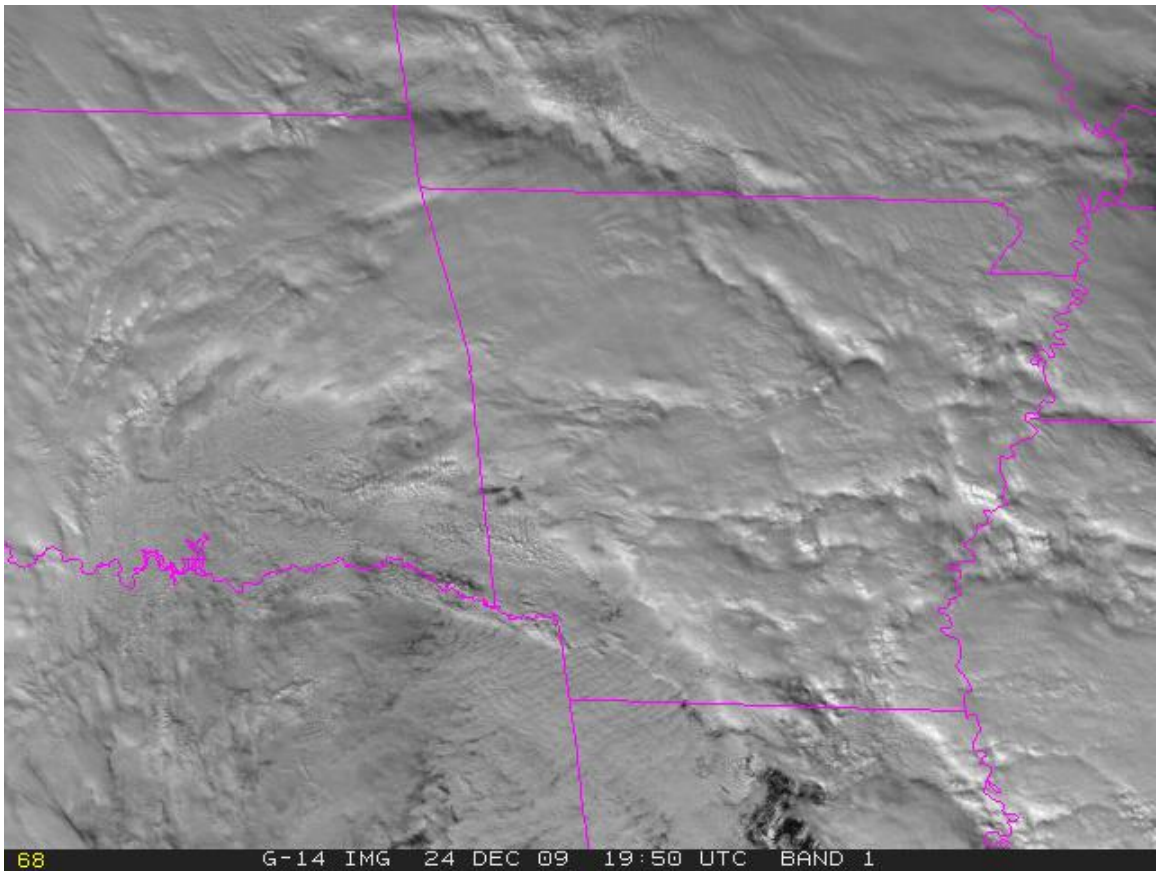

Figure 7.7: GOES-14 super-rapid-scan imagery from 1950 UTC on 24 December 2009. The convective activity over eastern Oklahoma was moving to the west-northwest, while the snow-bearing clouds along the western edge of the image were moving more south-southwesterly.

The satellite presentation in this case (Figure 7.7) was similar to that of the 19 December Washington DC case, with heavy snow under a dense, relatively homogeneous overcast in the wrap-around precipitation west and northwest of the low center, and evidence of deeper convection to the east and southeast of the low, where cirrus was relatively absent. Loops of some of the super rapid scan data from this case can be found at http://rammb.cira.colostate.edu/projects/svr_vis/24dec09/ch1loop_okc.asp.

In addition, a satellite animation comparing these 1-min observations to the routine 15 or 30-min observations can be found at http://cimss.ssec.wisc.edu/goes/blog/archives/4163, specifically http://cimss.ssec.wisc.edu/goes/blog/wp-content/uploads/2009/12/ecb_g12g14_vis_anim.gif.

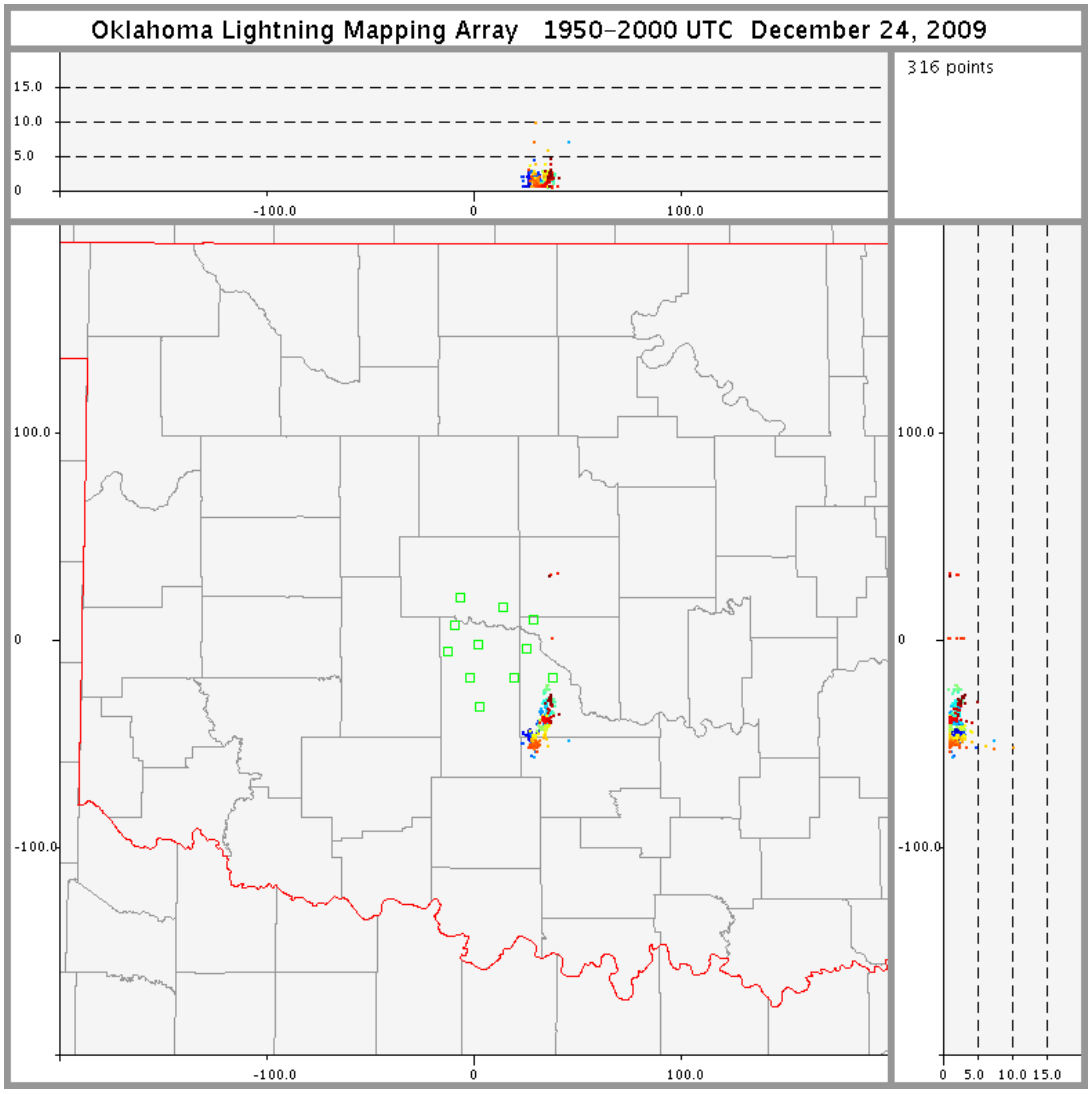

Figure 7.8: Lightning observed by the Oklahoma Lightning Mapping Array in McClain County between 1950 and 2000 UTC on 24 December 2009. (Image courtesy of Don MacGorman, NOAA/OAR/NSSL.)

The Oklahoma Lightning Mapping Array (Figure 7.8) detected a few lightning flashes in the wrap-around precipitation at 1200, 1500, and 1900-2000 UTC. Detections were generally at low altitude, so radio towers or other tall objects might have played a role in flash initiation.

7.3. SRSO for Lightning Summary

Several excellent and varied cases were collected via GOES-14 SRSO activities supporting lightning algorithm research and physics at NASA MSFC. Future research will use the SRSO

information (both visible and IR) to examine use of the satellite data in future GOES-R applications that will integrate ABI imagery with Geostationary Lightning Mapper data.

8. Coordination with Snow Study for Canadian Olympics

During the Science Test, GOES-14 data were collected in support of a snow study related to the 2010 Winter Olympic and Paralympic Games in Vancouver and Whistler, British Columbia, Canada. Although the Science Test took place in December, long before the February Olympics, there was an opportunity to provide data for the spin-up period for this study. The emphasis was on forecasting weather conditions up to 6 hours in advance. The GOES data were to be used in conjunction with high resolution (e.g., 1 km or less) numerical weather prediction models, utilizing data at frequent observational intervals.

The weather research and development project was called the Science and Nowcasting of Olympic Weather for Vancouver 2010 or simply SNOW-V10. It was conducted by an international team of scientists from nine countries assembled by the World Meteorological Organization and Environment Canada, Canada's National Meteorological and Hydrological Service. SNOW-V10 is part of the World Meteorological Organization's (WMO) World Weather Research Programme (WWRP) and is the first WWRP project conducted during the Winter Games. For more information see http://www.wmo.int/pages/mediacentre/infonotes/infonote_61_en.html.

Special 1-minute GOES-14 Rapid Scan data were collected on 20 December 2009 in support of SNOW-V10. Principal recipients of the data were George Isaac and Paul Joe of Environment Canada. However, operational use of GOES-14 was not made until after GOES-14 was put into storage mode. Therefore, no specific results from this data collection are available.

9. Overall Recommendations Regarding this and Future GOES Science Tests

The following conclusions and recommendations were drawn during the GOES-14 Science Test:

- The updated (Rev F or any subsequent version) Imager and Sounder SRF should be used for any subsequent product generation. In the future, the latest system SRF should be made available well before the start of the science test.

- Science Tests should continue as a vital aspect of the checkout of each GOES satellite, as studying real-time data is an effective way to detect problems both in the data stream and in ground systems.

- Science Test duration should be at least 5 weeks for 'mature' systems (and ideally should be during times with active convection over the continental U.S.). Much longer test periods will be needed for brand new systems such as GOES-R. It is expected on the order of a year will be needed for the many steps of engineering, science, products, validation and user readiness.

- A Science Test could be preceded by several weeks of GOES-East and/or GOES-West schedule emulations. This schedule would allow for more routine testing in operations, and then more flexibility during the science test itself.

- An additional aspect to the Science Test could involve yearly checkout of GOES data when individual spacecraft are taken out of storage and turned on for other purposes.

- While the GOES-14 GVAR data are captured and saved by a number of research groups, these unique and important pre-operational data should be part of the official GOES archive and be made available.

Acknowledgments

A large number of people played important roles in the success of the GOES-14 Science Test. The contributors listed on the front cover of this report provided analysis of GOES-14 radiance data and Imager and Sounder products. Dan Lindsey and John Knaff (StAR/RAMMB), Gary Wade (StAR/ASPB), and Scott Bachmeier (UW/CIMSS) are specially thanked for their participation in the daily coordination where decisions were made to determine which test schedules should be implemented in order to either capture interesting weather events, or to meet the requirements for the various data tests and generation of products. In addition, thanks to Kevin Ludlum (GOES Scheduling Lead) and the rest of the GOES-14 Team at NOAA/NESDIS Office of Satellite Operations (OSO), for coordinating and establishing the numerous schedules and sectors used during the Science Test. Tom Renkevens and Brian Hughes of the Satellite Services Division User Services are also thanked. Hyre Bysal, Chris Wheeler, Ken Mitchell and Mike Weinreb are thanked for their GOES engineering and calibration expertise.

The following are also acknowledged for their detailed reviews of the final document: Katherine Maclay, Leanne Avila, and Thomas Wrublewski.

This project was funded by the NOAA/NESDIS Office of Systems Development (OSD).

The views, opinions, and findings contained in this article are those of the authors/contributors and should not be construed as an official National Oceanic and Atmospheric Administration or U.S. Government position, policy, or decision.

References/Bibliography

Daniels, J.M., T.J. Schmit, and D.W. Hillger, 2001: Imager and Sounder Radiance and Product Validations for the GOES-11 Science Test, *NOAA Technical Report NESDIS 103*, (August), 49 pp.

Eilers, P.H.C., and Goeman, J.J., 2004: Enhancing scatter plots with smoothed densities, Bioinformatics 20(5):623-628.

Gunshor, M., T. Schmit, W. Menzel and D. Tobin, 2009: Inter-calibration of broadband Geostationary Imagers using AIRS, *J. Atmos. Oceanic Tech.*, **26**, 746-758.

Johnson, R., and M. Weinreb, 1996: GOES-8 Imager mid-night effects and slope correction. *Proc. SPIE*, Vol. 2812, 596, dio:10.1117/12.254104.

Jolliffe, I.T., and D.B. Stephenson, 2003: Forecast Verification. A Practitioner's Guide in Atmospheric Science, Wiley and Sons Ltd, 240 pp.

Hillger, D.W., and T.J. Schmit, 2007: Imager and Sounder Radiance and Product Validation for the GOES-13 Science Test. *NOAA Technical Report, NESDIS 125*, (September), 75 pp.

Hillger, D.W., and T.J. Schmit, 2009: The GOES-13 Science Test: A Synopsis. *Bull. Amer. Meteor. Soc.*, **90**, 6-11.

Hillger, D.W., T.J. Schmit, and J.M. Daniels, 2003: Imager and Sounder Radiance and Product Validation for the GOES-12 Science Test. *NOAA Technical Report, NESDIS 115*, (September), 70 pp.

Hillger, D.W., and T.H. Vonder Haar, 1988: Estimating Noise Levels of Remotely Sensed Measurements from Satellites Using Spatial Structure Analysis. *J. Atmos. Oceanic Technol.*, **5**, 206-214.

Ma, X. L., T. Schmit, and W.L. Smith, 1999: A non-linear physical retrieval algorithm - its application to the GOES-8/9 Sounder. *J. Appl. Meteor.*, **38**, 501-513.

Menzel, W.P., F.C. Holt, T.J. Schmit, R.M. Aune, G.S. Wade, D.G. Gray, and A.J. Schreiner, 1998: Application of GOES-8/9 Soundings to weather forecasting and nowcasting. *Bull. Amer. Meteor. Soc.*, **79**, 2059-2078.

Merchant, C.J., A.R. Harris, E. Maturi, and S. MacCallum, 2005: Probabilistic physically-based cloud-screening of satellite infrared imagery for operational sea surface temperature retrieval. *Quart. J. Roy. Meteorol. Soc.*, **131**(611), 2735-2755.

Merchant, C.J., A.R. Harris, E. Maturi, O. Embury, S.N. MacCallum, J. Mittaz, and C.P. Old, 2009: Sea Surface Temperature Estimation from the Geostationary Operational Environmental Satellite 12 (GOES-12), *J. Atmos. Oceanic Technol.*, **26**, 570-581.

Schmit, T.J., E.M. Prins, A.J. Schreiner, and J.J. Gurka, 2002a: Introducing the GOES-M Imager. *Nat. Wea. Assoc. Digest*, **25**, 2-10.

Schmit, T.J., W.F. Feltz, W.P. Menzel, J. Jung, A.P. Noel, J.N. Heil, J.P. Nelson III, G.S. Wade, 2002b: Validation and Use of GOES Sounder Moisture Information. *Wea. Forecasting*, **17**, 139-154.

Tahara, Y. and K. Kato, 2009: New spectral compensation method for inter-calibration using high spectral resolution sounder, *Met. Sat. Center Technical Note*, No. 52, 1-37.

Wu, X. and S. Sun, 2004: Post-launch calibration of GOES Imager visible band using MODIS, *Proc. SPIE*, Vol. 5882, doi:10.1117/12.615401.

Wu, X., T. Schmit, and M. Gunshor, 2009: Correction for GOES-13 Imager 13.3 μm Channel Spectral Response Function. NOAA/NESDIS/STAR Calibration Product Oversight Panel (CalPOP) Technical Memorandum, 13 March, 9 pp.

Weinreb, M.P., M. Jamison, N. Fulton, Y. Chen, J.X. Johnson, J. Bremer, C. Smith, and J. Baucom, 1997: Operational calibration of Geostationary Operational Environmental Satellite-8 and -9 Imagers and Sounders. *Appl. Opt.*, **36**, 6895-6904.

Weinreb, M. and K. Mitchell, 2010: Personal communication on the issues with GOES-14 Imager space-look count.

Appendix A: Results from the Line-shifted Over-sampling Test

A1. Scientific Objectives/Goals

This test aimed to emulate ABI-like high spatial resolution infrared imagery for GOES-R Risk Reduction activities.

An over-sampling technique combines three images to make one spatial enhanced image that emulates ABI-like 2 km resolution infrared imagery.

The scientific objectives and goals are:

- Acquire time-continuous over-sampled images.
- Provide the over-sampled images and movies with a user-friendly format and easy access. These images and movies will be a part of the emulated ABI dataset that assists the pre-launch developmental work of GOES-R products generation.
- Estimate image motion both from over-sampled images and original images to demonstrate how the ABI-like 2 km resolution infrared imagery will improve cloud and atmospheric motion estimation. The only over-sampling technique provides both ABI-like high spatial resolution and high temporal resolution at the same time with a limited geographical coverage (but not ABI-like high spectral resolution).

A2. History

The over-sampling technique was originally proposed for the Japanese Multi-functional Transport Satellite (MTSat) that was lost in 1999 due to launch vehicle failure. A preliminary demonstration of the over-sampled imagery collection concept was conducted using the GOES-10 Imager during the spacecraft post-launch test period in October 1997 with the cooperation of NASA/GSFC/GOES Project. The test included three imaging sequences acquired at different geographical locations in order to provide a variety of image content. The GOES-10 data were used to develop and demonstrate the image analysis techniques.

The second test was undertaken with GOES-12, but some of the data were lost by data handling failure. The third attempt was conducted with the GOES-13 Post-Launch Test / NOAA Science Test, but the data collector failed to generate a half-pixel shift between successive images. The data collector that ingests downlinked Imager data was not originally designed to operate a half-pixel shift frame, and as a result, complex operations were required for the test. These complexities are likely the reason for the data collection failure.

A3. Concept

The GOES Imager produces 4km pixel Field-Of-View imagery sampled in the east-west direction at 2.3 km sampling intervals, which means the imagery is over-sampled in the east-west direction. No over-sampling in the north-south direction is generated in normal routine operations. Over-sampling in the north-south direction is accomplished by collecting a series of three images that together produce a composite image with 2 km north-south sampling. As shown in Figure A1, the geographical coverage of the first and third images is a 1150 km (east-

west) by 250 km (north-south) area at nadir, and the second is a 1150 km by 500 km area offset from the first image by 2 km (one-half infrared pixel) in the north-south direction.

Together the first and third images produce a 1150 km by 500 km image that is offset from the second image by a half pixel. The composite image that has a 2.3 km (east-west) by 2 km (north-south) lattice is generated by these three images on a line-by-line interweavement basis as shown in Figure A2, this image is then enhanced using the spatial domain digital filters generated by the Imager's Modulation Transfer Function (MTF).

A4. Testing Activities

A4.1. Data Acquisition

A preliminary verification was conducted on 4 December 2009 at 1616-1622 UTC during the NOAA Science Test. The verification was successful and a half-pixel shift was properly generated. Table A1 shows the frame definitions of the verification. Figure A3 shows a comparison of over-sampled images to normal routine images.

Organized data acquisition was not undertaken because of operational and scheduling difficulties in the testing.

A4.2. Data Distribution

Since generating an over-sampled image needs specific data handling such as line composition and filtering, code to generated the over-sampled image with the McIDAS AREA format was developed. This code allows handling the enhanced image in the same environment as used for nominal GOES data.

Web-friendly movies of the over-sampled images were not generated because of lack of scenes.

A4.3. Image Motion Estimation

The over-sampling technique can emulate both ABI-like high spatial resolution and high temporal resolution at the same time, which is an ideal approach for the evaluation of cloud and atmospheric motion vectors.

Here, likening the land features that are stable with time to clouds, the motion vectors were calculated, and their standard deviation was evaluated. The land features that were likened to the clouds were the areas of Glen Canyon National Recreation Area shown in Figure A4.

The histogram of motion speed indicates that the motion speed is distributed with a non-zero center. The reason the mean speed is not zero may be the effects of satellite position and/or attitude changes. The distribution of the motion speed is caused by the error of pattern matching at the sub-pixel level. The standard deviation of the motion speed in the over-sampled images decreases to 37% of normal routine images. As a result, the improvement of the motion vectors can be expected for GOES-R product generation. Because the accuracy of the motion vectors is affected by INR and cloud deformation, it is desired that the scenes having various cloud patterns will be acquired at constant time intervals for more accurate evaluation of the motion vectors.

A5. Summary and Proposals for GOES-15

The over-sampling testing was conducted on 4 December 2009 as a part of the GOES-14 NOAA Science Test. Following the successful data acquisition, GOES-R ABI-like high resolution infrared imagery was generated. A new tool was developed to provide user-friendly access to the over-sampled images. The image motion of the over-sampled images was analyzed to estimate its improvement. The analysis showed that the pattern matching error will be reduced with GOES-R.

In analyzing the test data, NOAA-17 flew 15 minutes later over the area GOES-14 observed in the testing, as shown in Figure A5. As a result, the earth may be viewed in a stereographical manner to investigate how the ABI-like high resolution infrared imagery would benefit the GOES-R products.

In the GOES-R era, a high resolution stereograph will be obtained at intervals of 5 or 15 minutes by a combination of GOES-East and GOES-West, which will provide accurate cloud-top height estimation which will benefit most of the GOES-R products. To demonstrate the stereograph of the ABI-like high resolution imagery, the over-sampling testing with the flyover of polar orbiters in GOES-15 post launch testing, is proposed.

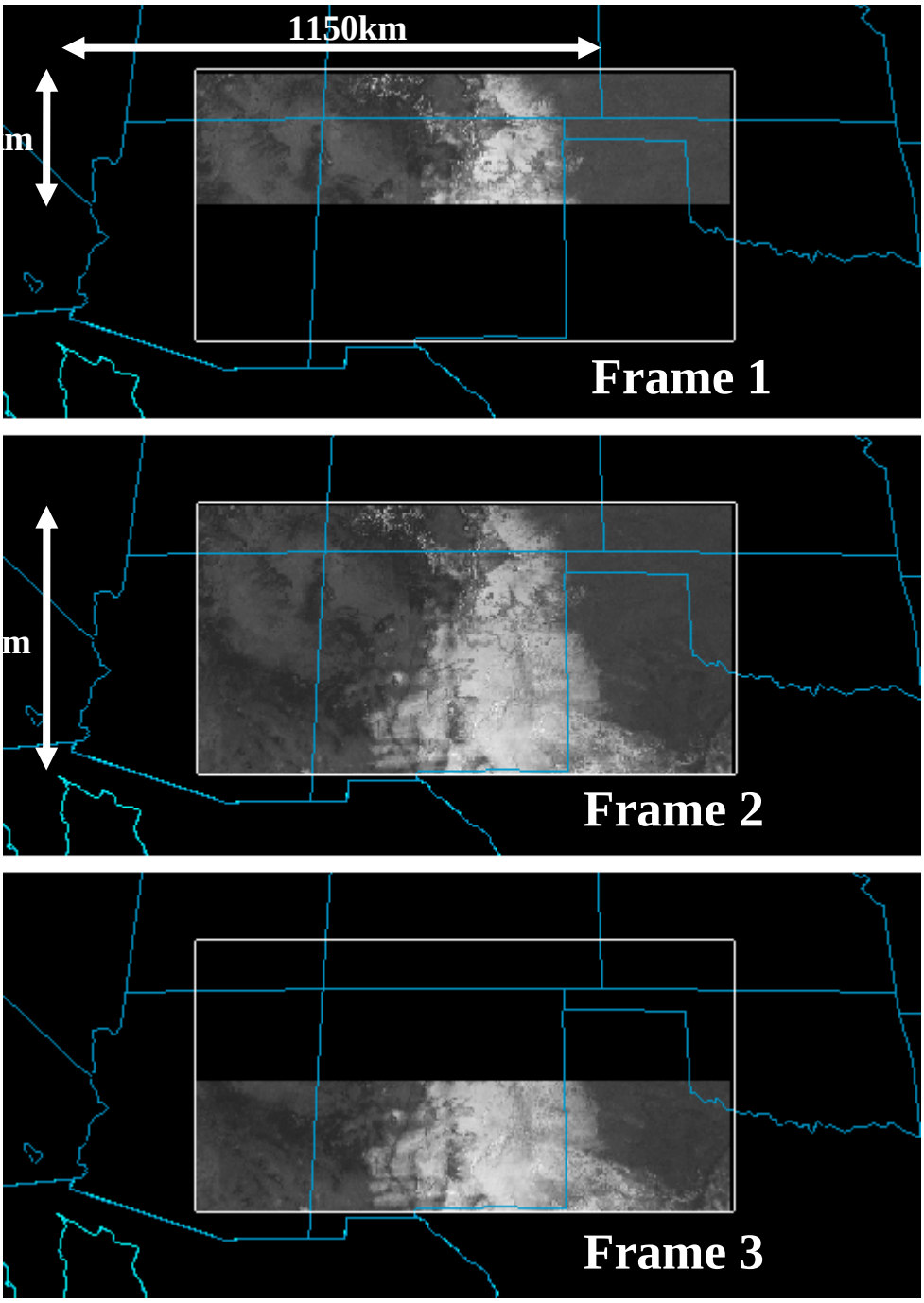

Figure A1: Frame Coverage of Over-sampling Testing. The first frame is 1150 km (east-west) by 250 km (north-south). The second frame is 1150 km by 500 km, offset from the first frame by 2 km (one-half pixel) in the north-south direction. The third frame is 1150 km by 250 km, with its north-south start address equal to the stop address of the first frame.

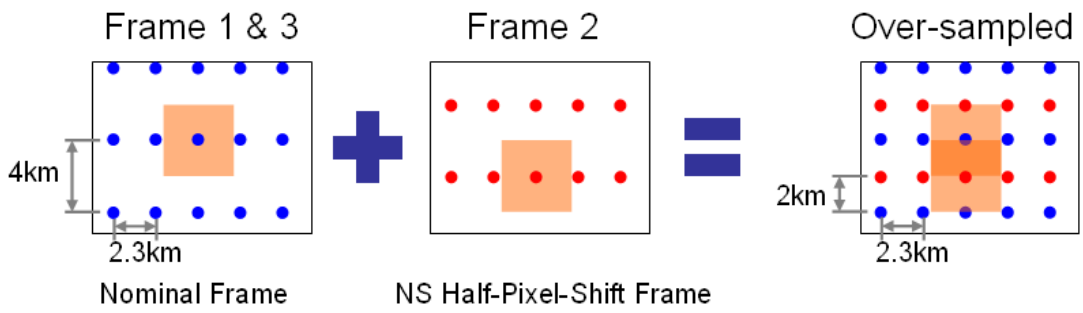

Figure A2: Composite image generation on over-sampling testing. Blue and red dots indicate the center of the pixel Field-Of-View that is shown by rose-colored squares. The second frame is offset from the first and third frame by 2 km (one-half pixel) in the north-south direction.

Table A1: GOES-14 Over-sampling Test Frame Definitions. Note that frame time intervals between two sequences are *not constant.*

Sequence Number	Frame Number	2009-12-04 Time of Frame Start (UTC)	Time Difference (sec)		Frame Size (IR pixels)	
			Within Sequence	Between Sequence	EW	NS
1	1	161623	---	---	504	64
	2	161723	60		504	128
	3	161911	168		504	64
2	1	162003	---	220	504	64
	2	162053	50	210	504	128
	3	162143	100	152	504	64

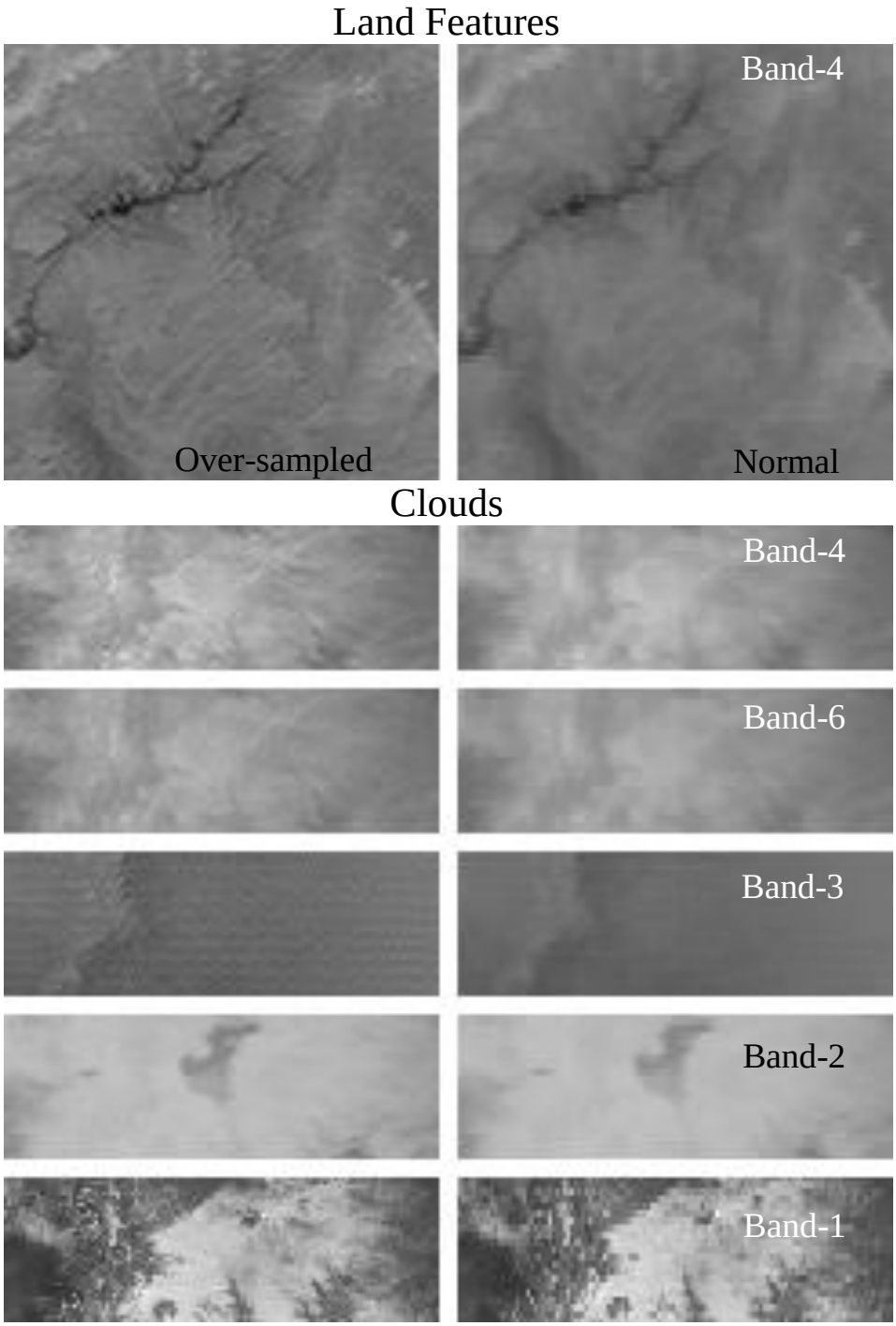

Figure A3: Comparison of Over-sampled Images to Normal Images. Top: The rivers and bays located in Glen Canyon National Recreation Area, Utah and Arizona can be seen clearly in the over-sampled image. Clouds: The over-sampled images also show clear cloud features in all IR bands. Remarkable noise appears in the over-sampled image of band-3 since the striping of this band is enhanced by the filters. An additional filter can reduce the striping noise. Band-1 (visible band) is the only reference that shows cloud contents in the scene.

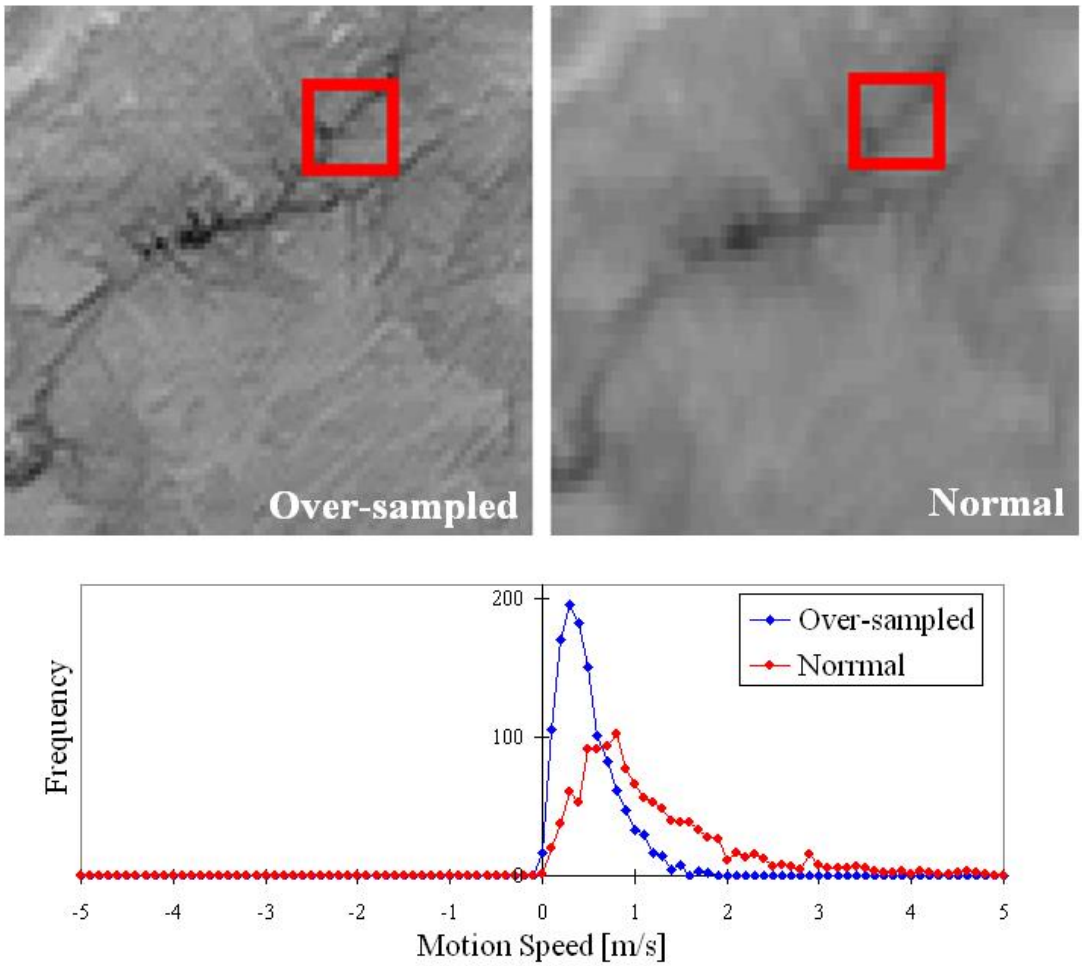

Figure A4: Image Motion Evaluation of Land Features. The land features of the rivers and bays around Glen Canyon National Recreation Area were used to evaluate image motion errors. The top images show the area used for the evaluation. The red squares of the top images indicate the size of pattern matching (i.e., 17 by 17 pixels on the over-sampled image.) The algorithm that is used for the pattern matching is the cross-correlation method with elliptical fitting of a matching surface. The bottom chart illustrates the histogram of the motion speed. The motion speed of the over-sampled image (blue line) is distributed with an average of 0.5 m/s and a standard deviation of 0.31 m/s, while the motion speed of the normal image (red line) shows an average of 1.2 m/s and a standard deviation of 0.84 m/s.

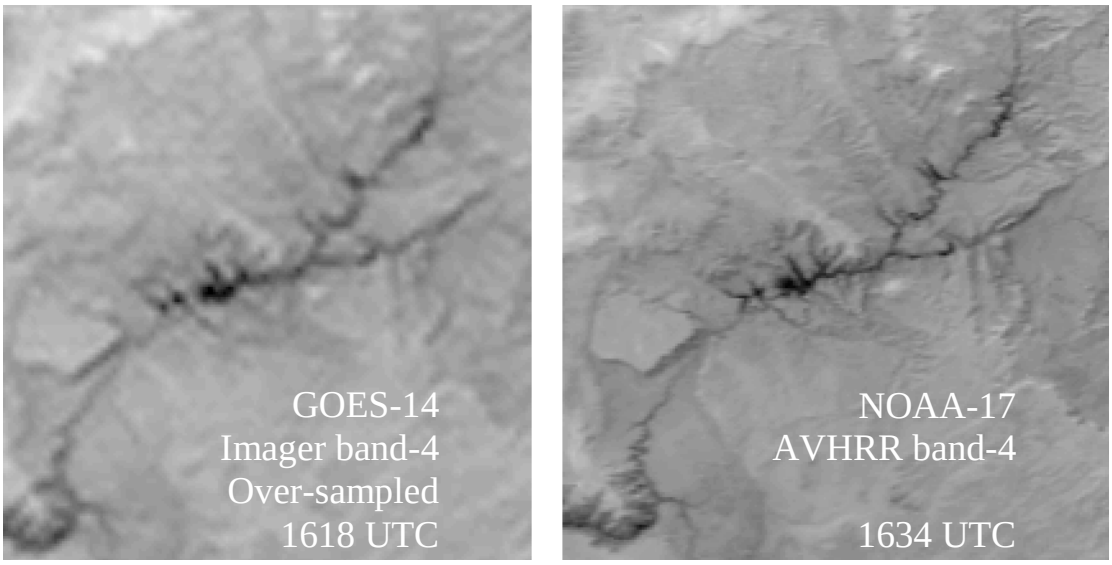

Figure A5: NOAA-17 and GOES-14 Images. NOAA-17 flew over the area GOES-14 observed in the over-sampling testing, 15 minutes later.

Appendix B: Web Sites Related to the GOES-14 Science Test

GOES-14 NOAA/Science Post Launch Test: http://rammb.cira.colostate.edu/projects/goes-o

GOES-14 RAMSDIS Online: http://rammb.cira.colostate.edu/ramsdis/online/goes-14.asp
(contained real-time GOES-14 imagery and product during the Science Test)

CIMSS Satellite Blog: Archive for the 'GOES-14' Category:
http://cimss.ssec.wisc.edu/goes/blog/archives/category/goes-14

NESDIS/StAR: GOES-14 News: http://www.star.nesdis.noaa.gov/star/GOES-14FirstImage.php

NOAA: GOES-14: http://www.noaa.gov/features/monitoring/goes-14/

CIMSS GOES Calibration:
http://cimss.ssec.wisc.edu/goes/calibration

NOAA: GOES Imager SRF:
http://www.oso.noaa.gov/goes/goes-calibration/goes-imager-srfs.htm

NOAA: GOES Sounder SRF:
http://www.oso.noaa.gov/goes/goes-calibration/goes-sounder-srfs.htm

STAR Calibration:
http://www.star.nesdis.noaa.gov/smcd/spb/fwu/homepage/GOES_Imager.php

NOAA, Office of Systems Development: The GOES-O Spacecraft:
http://www.osd.noaa.gov/GOES/goes_o.htm (including GOES-O Data Book)

United Launch Alliance: GOES-O: http://rammb.cira.colostate.edu/projects/goes-o/GOES-O_msnBk_j.pdf

NASA GSFC: GOES-O Mission Overview video:
http://svs.gsfc.nasa.gov/vis/a010000/a010400/a010422/

NASA GSFC: GOES-O Project: GOES-O Spacecraft:
http://goespoes.gsfc.nasa.gov/goes/spacecraft/goes_o_spacecraft.html

NASA-HQ: GOES-O Mission: http://www.nasa.gov/mission_pages/GOES-O/main/index.html

Boeing: GOES-N/P: http://www.boeing.com/defense-space/space/bss/factsheets/601/goes_nopq/goes_nopq.html

CLASS: http://www.class.ngdc.noaa.gov/saa/ products/welcome

Appendix C: Acronyms Used in this Report

ABI	Advanced Baseline Imager (GOES-R)
AIRS	Atmospheric InfraRed Sounder
AMV	Atmospheric Motion Vector
ARMOR	Advanced Radar for Meteorological and Operational Research
ASPB	Advanced Satellite Products Branch
BB	Black Body
BRDF	Bi-directional Reflectance Distribution Function
CICS	Cooperative Institute for Climate Studies
CIMSS	Cooperative Institute for Meteorological Satellite Studies
CIRA	Cooperative Institute for Research in the Atmosphere
CONUS	Continental United States
CRTM	Community Radiative Transfer Model
CSBT	Clear Sky Brightness Temperature
CSU	Colorado State University
DPI	Derived Product Image
EUMETSAT	European Organization for the Exploitation of Meteorological Satellites
FED	Flash Extent Density (lightning)
FOV	Field Of View
GEO	Geostationary Earth Orbit
GOES	Geostationary Operational Environmental Satellite
GOES-R	Next generation GOES, starting with GOES-R
GPS	Global Positioning System
GSICS	Global Space-based Inter-Calibration System
GSIP	GOES Surface and Insolation Product
GVAR	GOES Variable (data format)
HK	Housekeeping
hPa	Hectopascals (equivalent to *millibars* in non-SI terminology)
IASI	Infrared Atmospheric Sounding Interferometer
IPM	Instrument Performance Monitoring
INR	Image Navigation and Registration
IR	InfraRed

JMA	Japanese Meteorological Agency
KOZ	Keep Out Zone
LEO	Low Earth Orbit
LI	Lifted Index
LMA	Lightning Mapping Array
LW	Longwave
LWIR	LongWave InfraRed
MAE	Mean Absolute Error
McIDAS	Man-Computer Interactive Data Access System
MetOp	Meteorological Operational (satellite)
MSFC	Marshall Space Flight Center
MTF	Modulation Transfer Function
MTSat	Multi-functional Transport Satellite
NASA	National Aeronautics and Space Administration
NEdR	Noise Equivalent delta Radiance (Sometimes given as NEdN)
NEdT	Noise Equivalent delta Temperature
NESDIS	National Environnemental Satellite, Data, and Information Service
NSSTC	National Space Science and Technology Center
NOAA	National Oceanic and Atmospheric Administration
OSD	Office of Systems Development
OPDB	Operational Products Development Branch
ORA	Office of Research and Applications (now StAR)
OSDPD	Office of Satellite Data Processing and Distribution
OSO	Office of Satellite Operations
PLST	Post Launch Science Test
PLT	Post Launch Test
PPI	Plan Position Indicator
PRT	Platinum Resistance Thermometer
PW	Precipitable Water
RAMMB	Regional and Mesoscale Meteorology Branch
RAMSDIS	RAMM Advanced Meteorological Satellite Demonstration and Interpretation System

RAOB	Radiosonde Observation
RMS	Root Mean Square
RMSE	Root Mean Square Error
RSO	Rapid Scan Operations
RT	Real Time
RTM	Radiative Transfer Model
SAB	Satellite Analysis Branch
SNR	Signal to Noise Ratio
SOCC	Satellite Operations Control Center
SPB	Sensor Physics Branch
SPC	Storm Prediction Center
SPEC	Specifications
SPLK	Space Look
SPoRT	Short-term Predication Research and Transition center
SPS	Sensor Processing System
SRF	Spectral Response Function
SRSO	Super Rapid Scan Operations
SSEC	Space Science and Engineering Center
SST	Sea Surface Temperature
StAR	SaTellite Applications and Research (formerly ORA)
SW	Shortwave
SWIR	Split-Window InfraRed
Tb	Brightness temperature
TCO	Total Column Ozone
THOR	Tornado and Hazardous weather Observations Research center
TPW	Total Precipitable Water
UAH	University of Alabama, Huntsville
UTC	Coordinated Universal Time
μm	Micrometers (*micron* was officially declared obsolete in 1968)
UW	University of Wisconsin (Madison)
WMO	World Meteorological Organization
WV	Water Vapor

WWRP	World Weather Research Program
XRS	X-Ray Sensor

NESDIS 109 **Description of the System to Nowcast Salinity, Temperature and Sea nettle (*Chrysaora quinquecirrha*) Presence in Chesapeake Bay Using the Curvilinear Hydrodynamics in3-Dimensions (CH3D) Model. Zhen Li, Thomas F. Gross, and Christopher W. Brown, December 2002.**

NESDIS 110 **An Algorithm for Correction of Navigation Errors in AMSU-A Data. Seiichiro Kigawa and Michael P. Weinreb, December 2002.**

NESDIS 111 **An Algorithm for Correction of Lunar Contamination in AMSU-A Data. Seiichiro Kigawa and Tsan Mo, December 2002.**

NESDIS 112 **Sampling Errors of the Global Mean Sea Level Derived from Topex/Poseidon Altimetry. Chang-Kou Tai and Carl Wagner, December 2002.**

NESDIS 113 **Proceedings of the International GODAR Review Meeting: Abstracts. Sponsors: Intergovernmental Oceanographic Commission, U.S. National Oceanic and Atmospheric Administration, and the European Community, May 2003.**

NESDIS 114 **Satellite Rainfall Estimation Over South America: Evaluation of Two Major Events. Daniel A. Vila, Roderick A. Scofield, Robert J. Kuligowski, and J. Clay Davenport, May 2003.**

NESDIS 115 **Imager and Sounder Radiance and Product Validations for the GOES-12 Science Test. Donald W. Hillger, Timothy J. Schmit, and Jamie M. Daniels, September 2003.**

NESDIS 116 **Microwave Humidity Sounder Calibration Algorithm. Tsan Mo and Kenneth Jarva, October 2004.**

NESDIS 117 **Building Profile Plankton Databases for Climate and EcoSystem Research. Sydney Levitus, Satoshi Sato, Catherine Maillard, Nick Mikhailov, Pat Cadwell, Harry Dooley, June 2005.**

NESDIS 118 **Simultaneous Nadir Overpasses for NOAA-6 to NOAA-17 Satellites from 1980 and 2003 for the Intersatellite Calibration of Radiometers. Changyong Cao, Pubu Ciren, August 2005.**

NESDIS 119 **Calibration and Validation of NOAA 18 Instruments. Fuzhong Weng and Tsan Mo, December 2005.**

NESDIS 120 **The NOAA/NESDIS/ORA Windsat Calibration/Validation Collocation Database. Laurence Connor, February 2006.**

NESDIS 121 **Calibration of the Advanced Microwave Sounding Unit-A Radiometer for METOP-A. Tsan Mo, August 2006.**

NESDIS 122 **JCSDA Community Radiative Transfer Model (CRTM). Yong Han, Paul van Delst, Quanhua Liu, Fuzhong Weng, Banghua Yan, Russ Treadon, and John Derber, December 2005.**

NESDIS 123 **Comparing Two Sets of Noisy Measurements. Lawrence E. Flynn, April 2007.**

NESDIS 124 **Calibration of the Advanced Microwave Sounding Unit-A for NOAA-N'. Tsan Mo, September 2007.**

NESDIS 125 **The GOES-13 Science Test: Imager and Sounder Radiance and Product Validations. Donald W. Hillger, Timothy J. Schmit, September 2007**

NESDIS 126 **A QA/QC Manual of the Cooperative Summary of the Day Processing System. William E. Angel, January 2008.**

NESDIS 127 **The Easter Freeze of April 2007: A Climatological Perspective and Assessment of Impacts and Services. Ray Wolf, Jay Lawrimore, April 2008.**

NESDIS 128 **Influence of the ozone and water vapor on the GOES Aerosol and Smoke Product (GASP) retrieval. Hai Zhang, Raymond Hoff, Kevin McCann, Pubu Ciren, Shobha Kondragunta, and Ana Prados, May 2008.**

NESDIS 129 **Calibration and Validation of NOAA-19 Instruments. Tsan Mo and Fuzhong Weng, editors, July 2009.**

NESDIS 130 **Calibration of the Advanced Microwave Sounding Unit-A Radiometer for METOP-B. Tsan Mo, August 2010**

NOAA SCIENTIFIC AND TECHNICAL PUBLICATIONS

The National Oceanic and Atmospheric Administration **was established as part of the Department of Commerce on October 3, 1970. The mission responsibilities of NOAA are to assess the socioeconomic impact of natural and technological changes in the environment and to monitor and predict the state of the solid Earth, the oceans and their living resources, the atmosphere, and the space environment of the Earth.**

The major components of NOAA regularly produce various types of scientific and technical information in the following types of publications

PROFESSIONAL PAPERS – Important definitive research results, major techniques, and special investigations.

CONTRACT AND GRANT REPORTS – Reports prepared by contractors or grantees under NOAA sponsorship.

ATLAS – Presentation of analyzed data generally in the form of maps showing distribution of rainfall, chemical and physical conditions of oceans and atmosphere, distribution of fishes and marine mammals, ionospheric conditions, etc.

TECHNICAL SERVICE PUBLICATIONS – Reports containing data, observations, instructions, etc. A partial listing includes data serials; prediction and outlook periodicals; technical manuals, training papers, planning reports, and information serials; and miscellaneous technical publications.

TECHNICAL REPORTS – Journal quality with extensive details, mathematical developments, or data listings.

TECHNICAL MEMORANDUMS – Reports of preliminary, partial, or negative research or technology results, interim instructions, and the like.

U.S. DEPARTMENT OF COMMERCE
National Oceanic and Atmospheric Administration
National Environmental Satellite, Data, and Information Service
Washington, D.C. 20233

Corrigendum

Correction of daytime brightness temperature differences compared to AIRS and IASI measurements for the GOES-14 Imager band-4 (10.7 µm)

Errors have been found in Table 4.11 (on page 40), in the daytime brightness temperature (Tb) biases between AIRS and IASI data and the double difference Tb value for GOES-14 Imager band-4 (10.7 µm). Corrections to the corresponding values are made in the following revised table (where updated values are shown in both ***bold and italic***).

Table 4.11: Brightness temperature (Tb) biases between GOES-14 Imager and AIRS/IASI for the daytime collocated pixels and the double difference between AIRS and IASI through GOES-14 Imager daytime collocation data using the GSICS-method. The Tb biases between GOES-14 and IASI over the night time (9:30pm) collocated pixels are also compared. The Tb biases were based on the collocated pixels acquired after 24 November 2009. Standard deviations are given in parentheses.

Band number	Central wavelength (µm)	Daytime (K)			Nighttime (K)
		GOES-AIRS	GOES-IASI	(GOES-AIRS) – (GOES-IASI)	GOES-IASI (9:30 pm)
2	3.9	-1.31 (±2.13)	-1.24 (±1.09)	-0.09 (±2.58)	-0.01 (±0.04)
3	6.5	0.99 (±0.12)	0.97 (±0.08)	-0.10 (±0.11)	0.77 (±0.11)
4	10.7	***0.17 (±0.18)***	***0.27 (±0.20)***	***-0.15 (±0.29)***	0.07 (±0.11)
6	13.3	-0.48 (±0.13)	-0.55 (±0.12)	-0.10 (±0.18)	-0.59 (±0.20)